INER-F1205 **INER-F1205**

出國報告（出國類別：實習）

赴日本東京工業大學研究風場評估與風機發電預測計算

服務機關：核能研究所
姓名職稱：林彥廷　副研究員
派赴國家：日本
出國期間：106 年 8 月 11 日~106 年 9 月 2 日
報告日期：106 年 9 月 25 日

摘 要

由於近年來台灣在再生能源與相關綠能政策上的支持，陸域與離岸風力發電之相關計畫已蓬勃發展。但由於風力發電的不穩定與季節變動影響，特別是以台灣或日本之的複雜地形及島嶼氣候，對於電網系統的建置與發電量造成重大影響。因此精確與可靠的風能評估與預報資料以提供風力發電預測是降低電網調度與電力衝擊之解決方法之一。在風力發電之電力系統中不同時間尺度的預報系統皆有不同領域的應用，極短期預報模式通常應用在電力負載追蹤與操作行為安排等；短期預報模式則應用於電力負載匹配調度等；中期預報模式可以安排風力機是否停機或是後備運轉；長期預報模式則可以安排歲修等維修保養工作。但根據過去的研究資料，台灣目前較無針對風機系統的風力預報與即時發電評估技術，故本次出國實習公差前往東京工業大學機械系學習風能評估與風力發電預報計算，主要指導成員為機械系 Feng Xiao 教授與 CEF(clean energy factory)工程師 Dr. Yuzhang Che。實習期間學習利用 WRF 氣象分析軟體分析日本淡路島風場風速分布，以及淡路島風機之發電預報，分析過程也導入卡爾曼濾波器(Kalman filter)與資料同化方法(Data assimilation)、並採用 CFD 分析驗證以獲得更準確預報資料。淡路島風力機風場位於淡路島西南方區域，共安裝 15 台 GE(General Electric GE)公司 2.5MW 水平軸風機，並由日本 CEF 公司負責運轉維護。安裝塔架為 80m 與風機旋轉直徑 84m，風速量測資料利用風機機艙上方的風速風向儀並採用 IEC61400 量測標準，以每 10 分鐘為平均完成風速風量資料收集。研究結果發現利用資料同化方法可以使原始 WRF 預報資料誤差在 ME、RMSE 與 IA 指標分別下降 34.6%、23.9%與 8.8%，而卡爾曼濾波器則可以分別降低 97%、22%與 10%誤差。因此相對於資料同化方法的電腦運算量，卡爾曼濾波器提供更加簡易且有效的預報結果。預報確認發電數據後，OpenFOAM 計算流體力學程式被使用於驗證以及分析淡路島流場細節，如風速與紊流程度。故在透過大尺度與微觀尺度的流場分析之後對於特定風場之風力發電量可更加準確與可靠的預測並安排相關風機運維為工作。最後此行程期間也實地見習東工大 GSIC-TSUBAME2.5 氣象分析之平行電腦並與研究人員研究交流，並介紹台灣核能研究所 150kW 風機實驗平台以尋求未來雙方的合作機會。

關鍵字：東京工業大學、WRF、淡路島、風力發電、風速預報

目　　次

摘　要…………………………………i
一、目　的………………………………1
二、過　程………………………………2
三、心　得………………………………20
四、建　議　事　項…………………………21
五、附　錄………………………………22

一、目　的

風能是再生能源之一，主要來源係透過太陽對空氣加熱而形成的空氣對流現象。風力發電系統由製造到發電過程皆有著對環境友善與可持續發展的優越特性，因此成為近年來發展最蓬勃的再生能源。依據世界風能協會(WWEA)資料顯示，截至 105 年底，全世界累積的風電裝置容量為 487GW，其中以中國大陸其累積的風電裝置容量為 169GW 居世界領先地位，而離岸風電的全世界累積容量則為 14.4GW，並以英國 5.2GW 離岸風力裝置容量為最多。此外，於 106 年 6 月底止，台灣大型風力機組亦已安裝建置 345 部，其中國營台電公司 169 部，其他民間企業 176 部，總裝置容量為 690MW，至 106 年 6 月之總發電量為 8 億 895 萬度。預計 114 年裝置容量達 9,952 MW。台灣政府於 106 年通過之離岸風力再生能源躉購電價也以每度 7.0622 新台幣達到最高收購價格。此外，政府也透過國內離岸風機設置之能源國家型計畫，並整合產官學研各界之科技研發資源，以協助相關技術的建立順利推動此國家重大的風力發電政策。

根據台電陸域風力發電機的發電歷史資料台灣陸域風能來源主要依賴秋季與冬季之東北季風，而在夏季則因為北回歸線的直射造成風力大減，且由於風機無法在颱風環境化操作，因此造成在台灣用電量最高的夏季而無法使用廉價的風電。更因為台灣島內人口稠密因此無法如同日本與歐洲，將陸域風電建設在內陸或丘陵地區，因此透過離岸風電的建置將風力機組建構在風能較佳的海域，既可遠離人群避免生活干擾亦可達到綠能減碳與促進產業發展。由於離岸風電建置位於海上，因此對於維修作業、運轉保養、發電併網規劃、天災預防與實驗驗證皆須透過穩定可靠的風力評估與發電預報技術。且對於未來離岸風電之發電量與電網或微電網調度匹配需要相應的操作策略，又因風力發電係依靠自然風力發電，故良好的風能預測與風機發電預報是建構與發展離岸風能產業的重要基礎。

此外，2015 年蘇迪勒颱風通過台灣台中地區也造成台中及石門共七座風力發電機倒塌，約造成 5 億元的投資損失，而此倒塌風機距離除役年限約還有 10 年之久。可歸咎於此次颱風因沒有透過風力預報針對此倒塌地區預測風速分布，以及該風速類型對運轉風機之結構計算，形成運轉廠家無法有效預防與確保而造成重大損失。因此局部風速預報與風機系統整合計算是台灣地區必須參與的研發課題。

核能研究所過去的風機研發主要以風機本體製作技術為基礎，經歷 400W、25 kW 及 150 kW 的中小型風機研製與設計評估技術，並於近 5 年專注於離岸風機支撐結構負載計算且與國外重要風力發電實驗室合作，是目前國內唯一具有設計及系統整合技術能力的國家級研究實驗室。因此為精進風機系統設計、分析、測試及運轉之機械系統整合工程技術能力，本次出國前往東京工業大學機械工程系實習，主要加入肖鋒教授之計算流體實驗室學習風能評估與風力發電預報技術，並透過肖教授的安排見習東工大 GSIC-TSUBAME 2.5 高速電腦中心並與 CEF 業界工程師討論風機運轉發電分析技術。亦透過實地的技術交流了解目前日本風電產業研發現況與發展方向，以希冀促成國際合作機會與強化本研究單位風機研發能量與競爭力，亦有助於核能研究所「中小型風機工程技術研發」計畫及「大型風機工程技術研發」計畫的執行及未來風能研發方向之規劃。

二、過　程

此行於 106 年 8 月 11 日由桃園機場搭機前往日本，本公差目的主要前往東京工業大學實習風能分析與風機發電預報分析技術，地理位置如圖 2-1。實習過程主要跟隨機械系肖鋒教授。肖教授在 Journal of Computational Physics 國際期刊上的數值方法論著 “The Constrained Interpolation Profile Method for Multiphase Analysis” 在 2017 年達到 842 次的論文引用次數，研究結果已成功應用於大氣現象、波浪行為、雙相流模擬與流故耦合模擬。肖鋒教授為計算物理與雙相流領域專家且為日本機械學會、日本氣象學會、日本數值流體力學會、日本流體力學會與日本計算工學會會員並擔任國際期刊 J. of Computational Physics 副編輯。肖教授也與國際知名研究單位共同合作，如中國科學院、中國氣象科學研究院、西安交通大學與 Johns Hopkins 大學等。

本次實習課程由肖教授傳授淡路島風場風能分析與風機發電預報分析技術，實習過程並與 CEF (CLEAN ENERGY FACTORY http://cef.co.jp/index.html)公司工程師 Dr. Yuzhang Che 學習風力發電機的實際發電監測方式與發電評估方法，並與該員技術交流。CEF 公司為日本風力發電場建設承包商與風電管理公司，其主要業務之風場管理涵蓋全日本 9 座風場共 107 台陸域大型風力機。故本次實習亦是學習 CEF 公司與東工大合作開發之風場評估與風機發電預報技術，課程期間也實地見習東工大 GSIC-TSUBAME2.5 平行電腦並與研究人員研究交流，實習期間也介紹台灣核研所 150kW 風機實驗平台以尋求未來雙方的合作機會。由於東工大在日本關東地區共有三個校區(圖 2-2)，校本部與高速電腦在大崗山(圖 2-3)，本次主要在橫濱分校區(圖 2-4)實習除前往校本部見習 GSIC-TSUBAME2.5 超級電腦。本次公差工作人員為核能研究所林彥廷副研究員，工作日期自 8 月 11 日至 9 月 2 日，為期共 23 天。

圖 2-1，日本東京出差行程地理位置圖

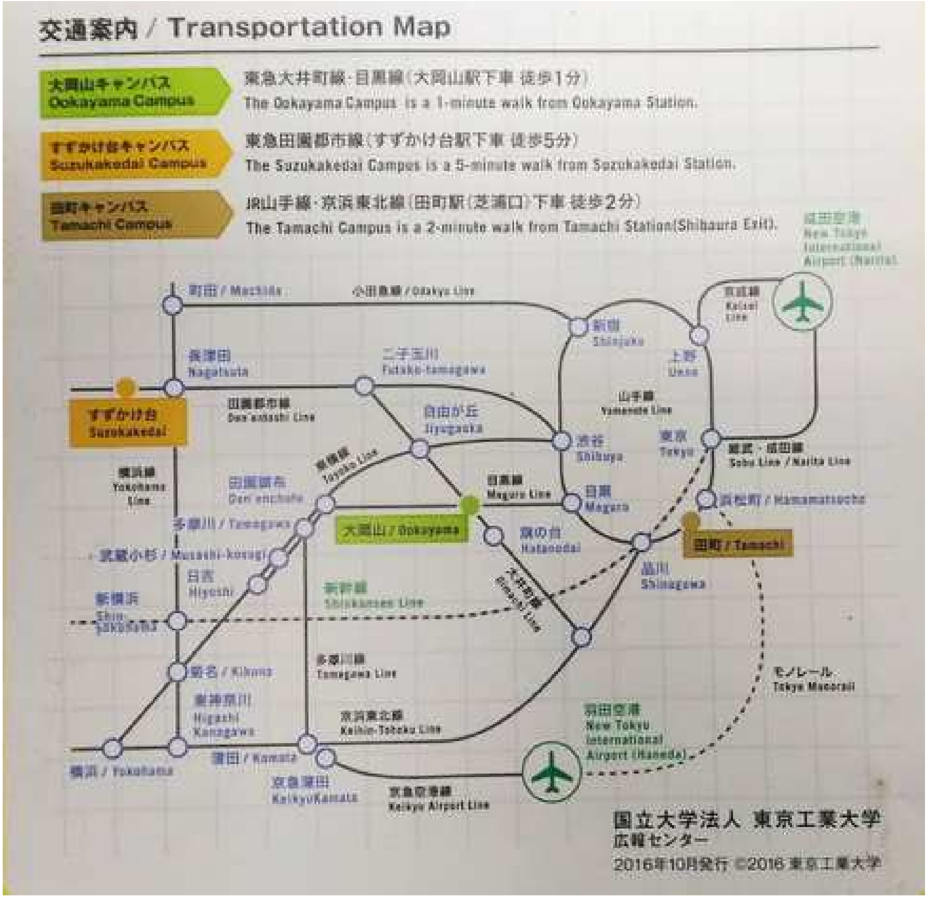

圖 2-2、東工大全部校區(引用東工大校園簡介資料)

圖 2-3、東工大大岡山校本部與高速電腦中心(引用東工大校園簡介資料)

圖 2-4、東工大橫濱校區(引用東工大校園簡介資料)

由於本次實習主要藉由肖鋒教授(Prof. Feng XIAO)與 CEF 公司車玉章博士(Dr. Yuzhang Che)的直接教學。由於肖教授與車博士皆為氣象物理與計算流體力學專家，因此訓練課程以氣象基本現象教導、分析工具介紹、分析軟體提供、分析軟體安裝教學、網路重要資源提供與分析軟體操作教學。之後經由車博士教導示範 CEF 公司在實際風機風力與發電數據收集與分析，最後利用理論修正精進預報結果。圖 2-5 為與東京工業大學機械系肖鋒教授(左)及 CEF 公司車玉章博士(右)於學校合影。圖 2-6 前往校本部見習東京工業大學 GSIC-TSUBAME2.5 高速電腦中心。

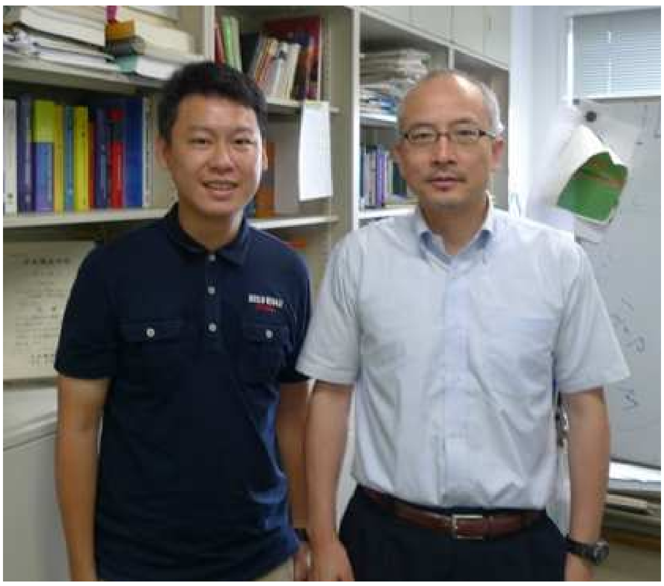 

圖 2-5、與東京工業大學機械系肖鋒教授(左)及 CEF 公司車玉章博士(右)合影

圖 2-6、見習東京工業大學 GSIC-TSUBAME2.5 高速電腦中心(引用附錄五-(三))

表 2-1、實習課程表

序列	課程名稱	課程內容
1	氣象介紹	風力來源、分類及其特性介紹
2	氣象預報分類與分析技術	氣象預報的分類對風機運維的影響及主要分析技術介紹
3	氣象分析軟體	氣象分析軟體介紹及市場簡介
4	氣象軟體安裝教學與軟體資源提供	氣象軟體安裝與操作教學，並提供關鍵軟體資源
5	風場風機介紹	介紹淡路島風機系統與 CEF 風場營運公司
6	風機發電分析	淡路島 2.5MW 風機系統發電與模式建立
7	平行電腦教學	東工大 TSUBAME 2.5 平行電腦介紹與連線操作教學
8	預報修正教學	學習卡爾曼濾波器(Kalman filter)與資料同化方法(Data assimilation)
9	預報評估教學	WRF 預報資料誤差 ME、RMSE 與 IA 指標教學
10	OpenFOAM-CFD 驗證	OpenFOAM-CFD 驗證與 WRF 驗證比較教學

以下章節將介紹本次實習所提供之教學內容大綱，詳細的論文資料將以附錄呈現。根據表 2-1 的課程順序，課程內容主要由大氣現象開始介紹，之後再依序介紹軟體以及實際操作與分析過程。

(二)-1 風的來源

風是空氣受不同大氣壓力而導致的移動現象，當大氣之間存在壓力差時則空氣將會由高壓區域流向低壓區域。風的強度或速度主要受以下兩要素影響。一為兩地區的壓力差異(pressure difference)的多寡，壓力的差異越大則風的速度越快，而大氣壓力則來自於太陽熱對空氣的加熱。另一為隧道效應(tunneling effect)，風速主要受到地形地貌的影響，如峽谷與大樓間隙等。因此，根據風的流動過程又可將風分類為四種，分別定義如下：

1. 行星風系(Planetary Winds)：忽略地形地貌影響之低層大氣之氣流，包含東北季風(North-East Trade Winds)、東南季風(North-East Trade Winds)、溫帶西風帶(Temperate Westerlies)

與極地東風帶(Polar Easterlies)。這些風況整年皆非常的平穩並受緯度壓力帶所控制。整體來說，行星風的理論有三個假設：地軸不傾斜，地表無海陸差異與地表無高度差異。因此地球整體皆受此行星風系影響。

2. 季候風系(Monsoon Winds)：陸地與海洋之間的溫度差異造成兩區域之間的氣壓分布差異，也形成兩區域之間在不同季節的大氣壓力變化。因此形成風向大致相反的季節性風系，稱為季候風。其主要為風向在夏季由海洋吹向陸地，冬季風向則由陸地吹向海洋。季候風以東南亞區域最為強盛，因此台灣也是季候風系的主要影響區域。
3. 氣旋與反氣旋風系(Cyclone and Anti-cyclone Winds)：氣旋是指圍繞著一個低壓中心而強烈旋轉的大氣風系系統，且由於內外大氣壓力差異大，四周的空氣快速流向低壓中心。氣旋通常會帶來不穩定且惡劣的天氣，如颱風與颶風。反氣旋則是指地區性的大氣系統其中心氣壓較高，四周氣壓較低造成高壓中心的大氣向外圍壓力降流動之現象。高壓區域內部空氣向下流動，形成晴朗而乾燥的天氣。
4. 局部風系(Local Winds)：局部地區的空氣受熱不均而產生小規模環流現象，包括焚風（fohn winds）、谷風、山風、龍捲風、海風和陸風等地方性風系。海風和陸風出現於沿海地區，受海面與陸地溫差造成的空氣壓力差異，日間風由海吹向陸地，夜間風由陸地吹向海面，如同季候風系。山風和谷風常見於山區，白天時，空氣受熱而上升，風從山谷吹向山頂爬升，稱為谷風；夜間時，空氣冷卻而沿山頂吹向山谷下沉，稱為山風。焚風則是乾燥而溫度較高的風系，當有風系吹過高山，由於迎風面的上升空氣導致凝結降雨，使得水汽減少，之後再沿背風面山坡下降，使空氣溫度增加而形成焚風風系。

除了上述風系，亦有其他受科式加速度與離心加速度等造成的相對穩定之壓力系統。但由於複雜的地球表面之地形地貌所造成的複雜大氣邊界層(Atmosphere boundary layer, ABL)，通常造成更加複雜的局部之不穩定大氣壓力系統。因此適當解析 ABL 是開發風能與預測風力機發電之重要步驟。

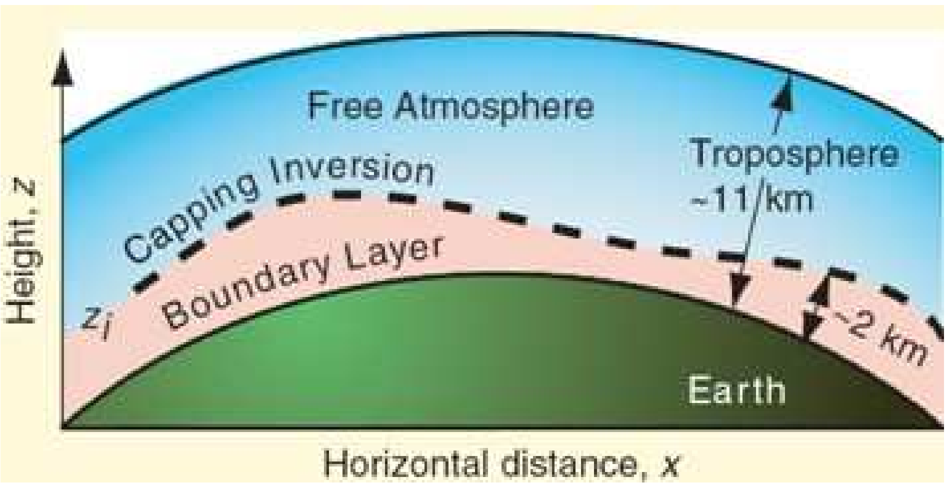

圖 2-2-1、地球大氣之對流層示意圖(引用 Atmospheric Science 2006,Wallace and Hobbs 圖 9.1)

(二)-2 大氣邊界層(Atmosphere boundary layer, ABL)

地球大氣之對流層可以粗略的分類成兩部分：第一為自由大氣層(free atmosphere, FA)與靠近表面的邊界層(boundary layer)，又稱大氣邊界層(Atmosphere boundary layer, ABL)，如圖 2-2-1 所示。此 ABL 在各類工程領域皆為重要的背景資料，如航空氣象學、空氣汙染、農業氣象、

水文學、氣象預測、氣候研究與風能研究。ABL 主要被定義在 1 個小時的尺度之內大氣與地球表面交互作用之氣流層。其垂直高度約在 10m 到 2km 之間，約占比對流層 10%到 20%。相比於自由大氣層 FA，其之間的差異列於表 2-2-1。大氣邊界層 ABL 與日照循環的結構繪製於圖 2-2-2。大氣邊界層 ABL 主要有三層結構，分別為混合層(mixed layer, ML)、滯留層(residual layer, RL)與穩定邊界層(stable boundary layer)。在靠近地球表面，有終日存在的薄邊界層(thin boundary layer)且垂直方向的紊流通量(turbulence fluxes)趨於常數。

表 2-2-1、自由大氣層(free atmosphere, FA)與大氣邊界層(Atmosphere boundary layer, ABL)

Property	free atmosphere, FA	Atmosphere boundary layer, ABL
Turbulence	Mostly laminar.	Almost continuously turbulent over its whole depth.
Friction	Small viscous dissipation.	Strong drag against the earth’ s surface. Large energy dissipation.
Dispersion	Small molecular diffusion.	Rapid turbulent mixing in the vertical and horizontal.
Winds	Winds nearly geostrophic.	Near logarithmic wind speed profile in the surface layer. Sub geostrophic, cross-isobaric flow common.
Vertical Transport	Mean wind dominates.	Turbulence dominates.
Thickness	Less variable 8-18Km. Small time variations.	Varies between 100m to 3km in time and space. Diurnal oscillations over land.

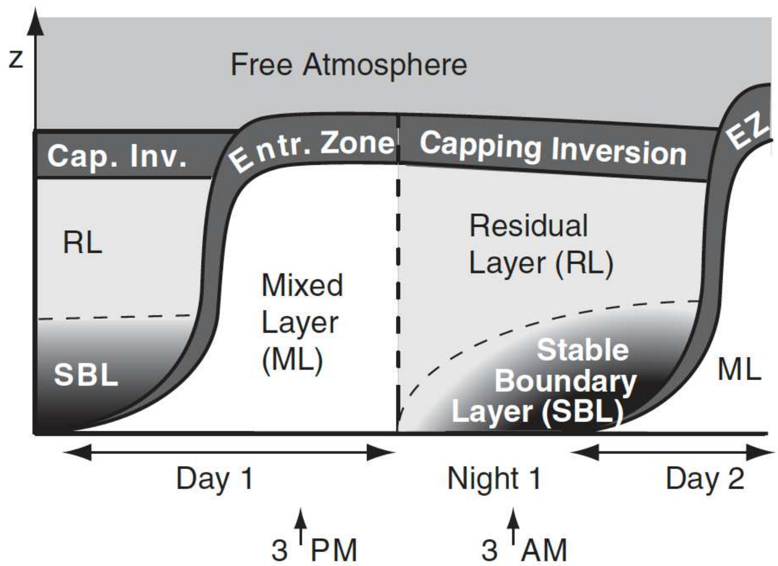

圖 2-2-2、大氣邊界層 ABL 與日照循環的結構示意圖

(引用 Stull, R. (2010). Meteorology for Scientists and Engineers, third edition)

(二)-3 複雜地貌的流動現象

在日本陸域風場的風機通常是位於複雜山脈區域，因此地形所造成的影響(如紊流)將影響

風場評估位置的風速與風向，並間接造成風資源與風場評估的難度。為了解地形地貌對風場的影響，實地量測驗證是直接有效的方法，但通常受限於地形問題造成量測困難。因此透過有限的實驗量測驗證與數值分析是目前風場評估最被推薦的方法。風洞模型與實驗是研究特定地形地貌最常用的方法，其關鍵是利用特定比例模型重建真實地形並在風洞中實驗量測。Meroney(Meroney, RN. 1980. Wind-tunnel simulation of the flow over hills and complex terrain. J. of wind engineering and industrial aerodynamics, 5(3-4):297-321)與 Neal 及 Stevenson 等人(Neal, D., Stevenson, D., and Lindley, D. 1981. A wind tunnel boundary layer simulation of wind flow over complex terrain: Effect of terrain and model construction. Boundary-layer meteorology, 21(3):271-293)分別利用 1/5000 與 1/4000 比例模型研究紐西蘭山脈風速。Bowen 學者(Bowen, A. 2003. Modeling of strong wind flows over complex terrain at small geometric scales. J. of wind engineering and industrial aerodynamics, 91(12):1859-1871)則建議最低為 1/6000 比例的模型才有較佳實驗結果，亦有其他學者提出相關研究。但由於風洞的設備維持與實驗方法複雜，以及難以模擬地球之大氣邊界層(Atmosphere boundary layer, ABL)現象，故有效模擬地球大氣邊界層的數值方法則可能提供更精確且更有效率的風能評估方法。

近年來利用計算流體力學方法(computational fluid dynamics, CFD)是廣泛使用於評估複雜地形之風能評估方法。目前被廣泛使用的數值方法則有 Reynolds-averaged Navier-Stokes(RANS), Large-eddy Simulations 與 Detached-eddy simulation 等方法。RANS 已被廣泛使用於複雜流場，但由於其基本架構是採用平均值與變動量的計算，因此對於大小不一的渦流並無法適當的分析與重建。也因此近年來 LES 方法被廣泛地用於 RANS 數值分析所無法分析的問題並獲得更準確的結果。但是由於 LES 之邊界條件的重建、地形幾何建立與 LES 的紊流區域網格細緻化設定難度皆遠大於 RANS，因此 RANS 依然是執行風能計算與評估的經濟選擇。

(二)-4 風能預報模式

由於地球風系行為的混沌特性，因此正確預測其風場未來風速與方向趨勢依然是重要研究課題，以期能達到與電網發電操作匹配與電力儲存之預備。一般來說，風能預測主要希望能預測風力機發電量，且其通常利用一種以上的風力預報模式以完成該項任務。風力預測模式主要可以區分為以下四類：

1. 極短期預報(Very-short-term forecasting)：由幾分鐘到 1 小時以內。
2. 短期預報(Short-term forecasting)：由 1 小時到數小時之間。
3. 中期預報(Medium-term forecasting)：由數小時到 1 週以內。
4. 長期預報(Long-term forecasting)：由 1 週到一年以上。

表 2-4-1 繪製出各個時間尺度預測模式在風力發電產業的應用。在電力系統中不同時間尺度的預報系統皆有不同領域的應用，極短期預報模式通常應用在電力負載追蹤與操作行為安排等；短期預報模式則應用於電力負載匹配調度等；中期預報模式可以安排風力機是否停機或是後備運轉；長期預報模式則可以安排歲修等維修保養工作。整理如下：

表 2-4-1、各個時間尺度預測模式在電力產業的應用

Time-scale	Range	Applications
Very-short-term	Few minutes to 1hour ahead	Electricity market clearing

		Real-time grid operations Regulation actions
Short-term	1 hour to several hours ahead	Economic load dispatch planning Load reasonable decisions Operational security in electricity market
Medium-term	Several hours to 1 week ahead	Unit commitment decisions Reserve requirement decisions Generator online or offline decisions
Long-term	1 week to 1 year or more ahead	Maintenance planning Operation management Optimal operating cost Feasibility study for design of the wind farm

(二)-5 風能預報技術

風能預報模式技術是利用現有的風力資訊或是過去一段時間的風力資訊再耦合各類數值分析軟體達到預測未來風能資訊，目前主要採用的方法有守恆法(persistence method)、物理近似法(physical approach)、統計法(statistical technique)與混合法(hybrid method) 四種，介紹如下。

1. 守恆法(persistence method)

此方法利用當下的風速預測未來的風速，其數值方法需建立在極微小的時間步長，因此及計算時間較長但數值技術簡單。其優點是在 Very-short-term 與 Short-term 預報上比物理近似法(physical approach)、統計法(statistical technique)準確。

2. 物理近似法(physical approach)

此方法係建構在數值氣象預報模式(numerical weather prediction model, NWP)，其是利用已知的物理公式搭配當下真實的氣候資訊去預測未來氣象，並可以獲得數小時到數天的精確且可靠的預估。NWP 是透過複雜的數學公式與考慮溫度、風速、風向、壓力與表面粗糙度等條件達到氣候預報目的。各類衍生的 NWP 技術如 WRF(Weather research and forecasting)、RAMS(regional atmosphere modeling system)與 MM5(Fifth-Generation Penn state/NCAR mesoscale model)等皆已被大量地使用於風能預報與評估技術。

3. 統計法(statistical technique)

相對於 NWP 方法，統計法則提供更加精簡與簡易的氣象預測，特色是只須少許電腦運算資源即可達到精確的短期預報。其核心理論主要運用於過去風速氣象等歷史資料去預測未來數小時的氣象資料，主要技術可以區分為時間序列模式(time-series based models)與神經網路法(neural network based models, NN)。以時間序列模式(time-series based models)建構的預報方法則有自動回歸移動平均模式(auto regressive moving average, ARMA)與其他衍生模式，如自動回歸積分移動平均模式(auto regressive integrated moving average, ARIMA)、季節-自動回歸移動平均模式(seasonal-ARMA)、分段自動回歸移動平均模式(fractional - ARMA)與含外加資料自動回歸移動平均模式(ARMA with exogenous input, ARMAX or ARX)。以及有其他時間序列模式如：線性預測(linear predictions)、灰色預測(grey predictors)與指數平滑(exponential smoothing)。ARMA 方法

已被 Torres 學者等人文獻證明其 10 小時預報結果比 persistence method 減少約 20%誤差。

神經網路法(NN)利用過去一段週期的氣象資料學習風速輸入與輸出的關係，其方法並不需要氣象流體力學等基礎公式運算，只要是利用神經網路學習達到資料輸入與輸出的關聯模式即可完成預測要求。但如同 ARMA，當預測的時間過長時則 NN 的準確度也快速下降。NN 法亦有其他衍生模式，如供給向前神經網路法(feed-forward neural networks, FNNs)、多層感控法(multi-layer perceptron, MLP)、迴圈神經網路法(recurrent neural networks, RNNs)、逕向基本函數(radial basis function, RBF)與 Adaline networks 神經網路法。

除了上述的方法，有些統計法持續被開發中，如：fuzzy logic model、wavelet transform、spacial correlation、ensemble forecasts 與 entropy based training 等。

4. 混合法(hybrid method)

混合法顧名思義即是利用前述 3 種主要技術達到氣象與風力預測目的，主要綜合各個方法的優點達到最佳化預測目的。如 ANFIS 法即是結合 ANN 與 fuzzy logic 的方法，並成功運用於短期風力預報。此外亦有學者成功利用 NN 結合 NWP 或是 spacial correlation 的預測方法。此方法是目前學者們所努力的方向。

(二)-6 NWP 數值氣象預報模式

NWP 預報技術主要是利用空氣流動的控制方程式完成預測分析，其主要可以分為資料收集(data collection)、資料同化(data assimilation)、預報、後處理(post-processing)與發佈資料(distribution)。前兩項為預測核心程式，研究開發主要著重於此以建立更精確的起始資料與數值方法。根據運算區域分類，亦可區分為兩類，一為全體地球計算，另一為局部區域細部計算，如圖 2-6-1 所示。目前商業與科學研究主要採用的 NWP 技術軟體如表 2-6-1 所示。這些軟體已被廣泛使用於氣象預報，如洪水、強降雨與颱風等，因此本次於東京工業大學機械系實習主要也是以 NWP 技術為主，並用於風速預測與風力機發電量評估。

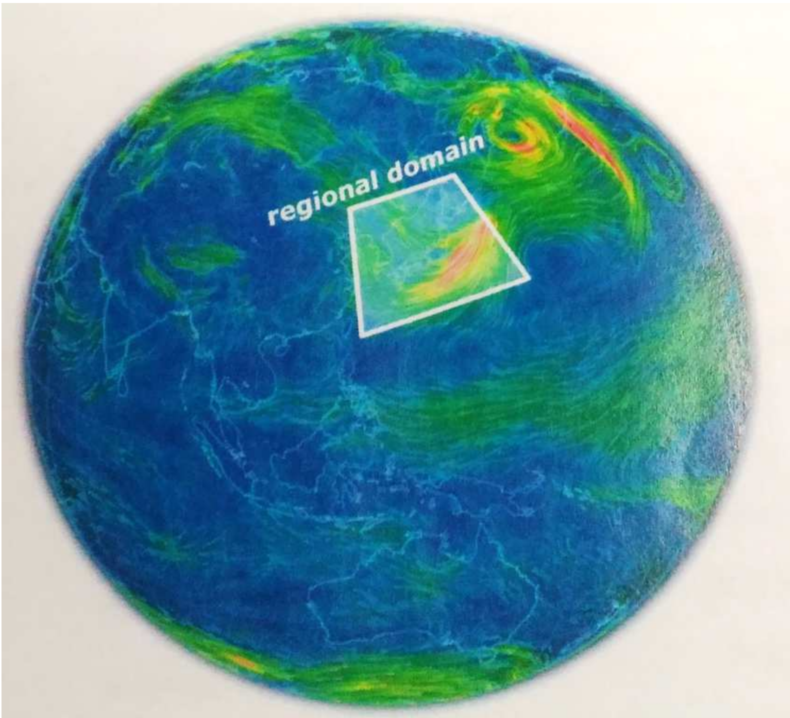

圖 2-6-1、日本列島局部區域細部計算示意圖(引用附錄五-(一)與(二))

表 2-6-1、目前市場主要 NWP 軟體列表

Model name	Hydrostatic or Non-hydrostatic	Global or Regional model	Owner
ECMWF	Non-hydrostatic	Global	European union
GEM	Hydrostatic	Global	Canada
UKMET	Non-hydrostatic	Global/Regional	United kingdom
NOGAPS	Non-hydrostatic	Global	Navy
T639	Non-hydrostatic	Global	China
MM5	Non-hydrostatic	Global	PSU
MSM	Non-hydrostatic	Global	Japan
GSM	Non-hydrostatic	Global	Japan
NAM	Non-hydrostatic	Global	NCEP
WRF	Non-hydrostatic	Global	NCEP
GFS	Non-hydrostatic	Global	NCEP

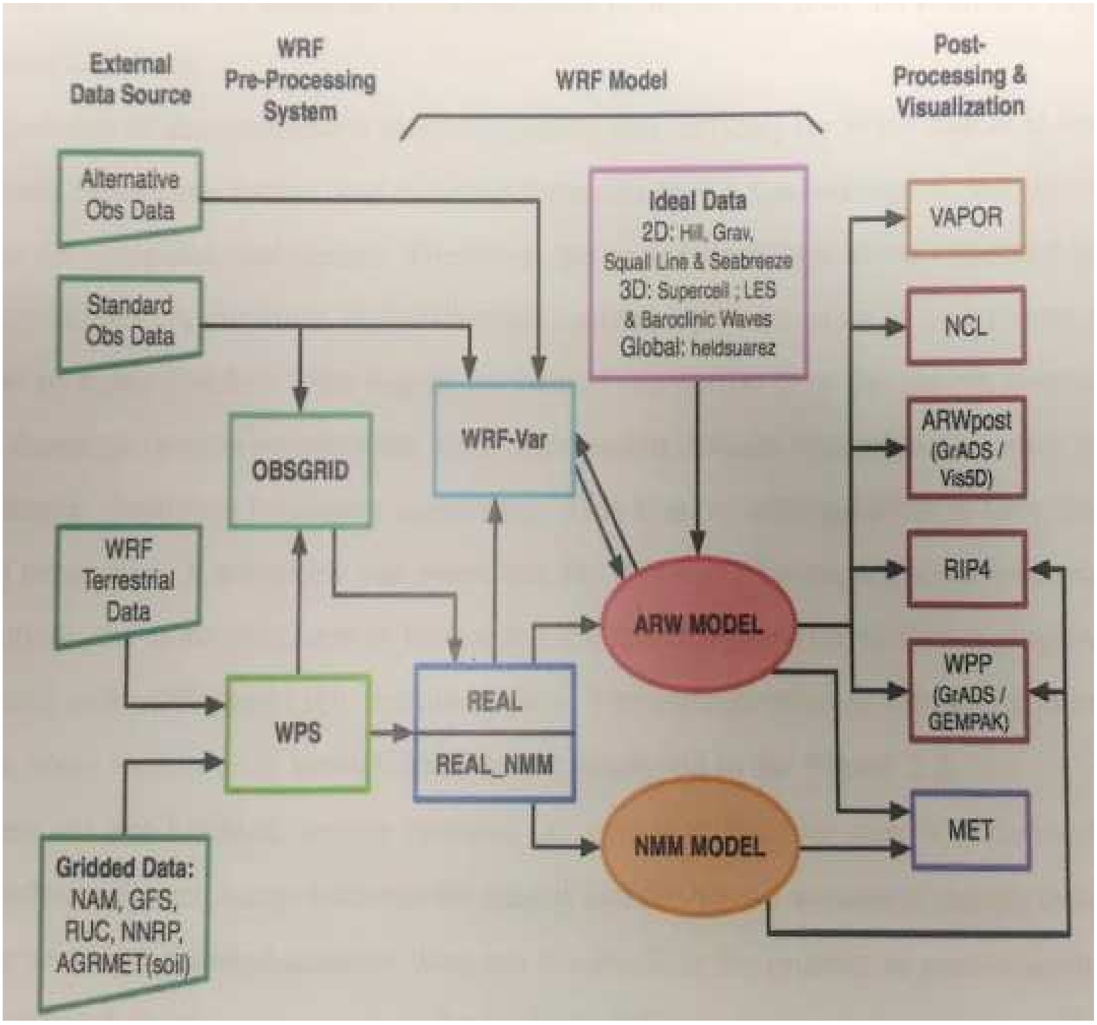

圖 2-7-1、WRF 計算流程架構示意圖(引用 http://www2.mmm.ucar.edu/wrf/users/supports/tutorial.html)

(二)-7 WRF 氣象預報軟體架構

Weather Research and Forecasting Model 軟體功能主要分為三組架構，分別為前處理

pre-processing system、核心處理器 WRF model 與後處理 post-processing。其各功能之間的連結如圖 2-7-1 所示。圖中顯示出 WRF 整體架構有兩套運算核心，分別為 advanced research WRF(ARW)另一套為 non-hydrostatic mesoscale model (NMM)，本次實習主要採用前一套核心。此外 WRF 計算資料主要提供理論風場計算與預測真實風場資料之預報，本分析選擇後者。WRF 預報的真實風場之起始資料設定步驟如下：

1. 讀取 WRF 前處理所生成之資料。
2. 計算乾燥地形表面壓力、模型階層與垂直差補資料。
3. 計算參考溫度曲線。
4. 準備土壤地表參數。
5. 檢查地表土壤類別、土地使用、土地遮蔽、地表土壤溫度、海面溫度皆互相符合季節特性。
6. 輸入時間週期以產生橫向邊界條件(lateral boundary conditions)。
7. 定義三維邊界條件，如溫度、速度、熱量與溼度等資料與地圖網格耦合。

此外，在實際運算 WRF 之前，其前處理主要是劃分計算區域與設定相應邊界條件，因此適當設定邊界與區域可以獲得準確的預報資料且消耗較低的運算資源。故分析通常採用巢式迴圈的運算區域，主要利用較大的網格運算區域預先算出周邊區域，再於此範圍更加的局部細化所需要的風場資料，如此經由父子區域的巢式運算可以獲得最佳的預報結果，巢式迴圈的運算區域示意圖如圖 2-7-2 所示。因此巢式運算則可根據運算資源與風場條件規劃為單向資料傳遞之 one-way 計算或是父子網格相互傳遞與修正之 two-way 計算。鑒於風場特性與運算資源，日本淡路島風場風力發電計算採用 one-way 巢式計算。

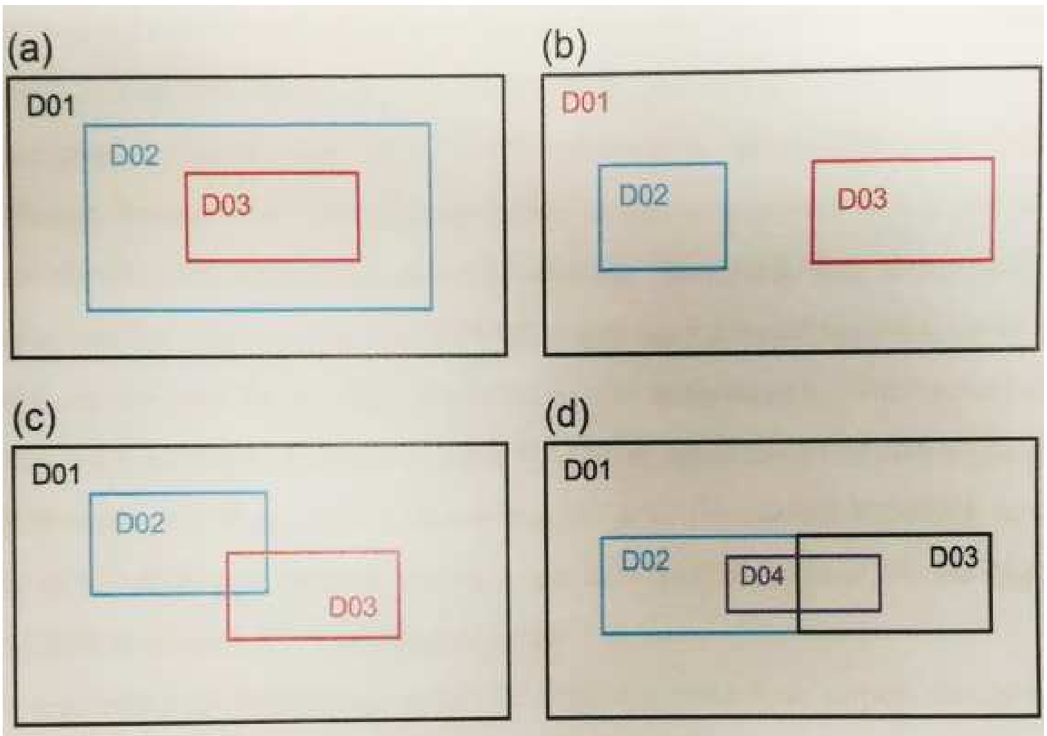

圖 2-7-2、WRF 計算區域之巢式結構示意圖

(引用 http://www2.mmm.ucar.edu/wrf/users/supports/tutorial.html)

(二)-8 WRF 氣象預報模式處理器

WRF 核心處理係利用全可壓縮、Euler non-hydrostatic 與 hydrostatic 模式，並使用 2 階與 3 階 Runge-Kutta 時間積分算則，在垂直與水平方向的空間離散可由 2 階定義到 6 階對流算則。網格計算採用 Arakawa C-grid 錯離網格(staggering grid)。氣象物理條件則又區分為幾類副程式分析氣象特性，分類如下：

1. 微物理模組(Microphysics)：主要計算水蒸氣、雲以及降雨過程。
2. 積雲參數化模組(Cumulus parameterization)：主要計算積雲現象。
3. 地表層模組(Surface layer)與 land-=surface model：計算地表之摩擦速度、交換係數(Exchange coefficient)、熱量與濕度。
4. 行星邊界層模組(Planetary boundary layer)：提供大氣之溫度、空氣動量與濕度趨勢計算。
5. 大氣輻射(Atmospheric radiation)：計算大氣與地表吸收與放射太陽輻射，以計算大氣溫度變化。

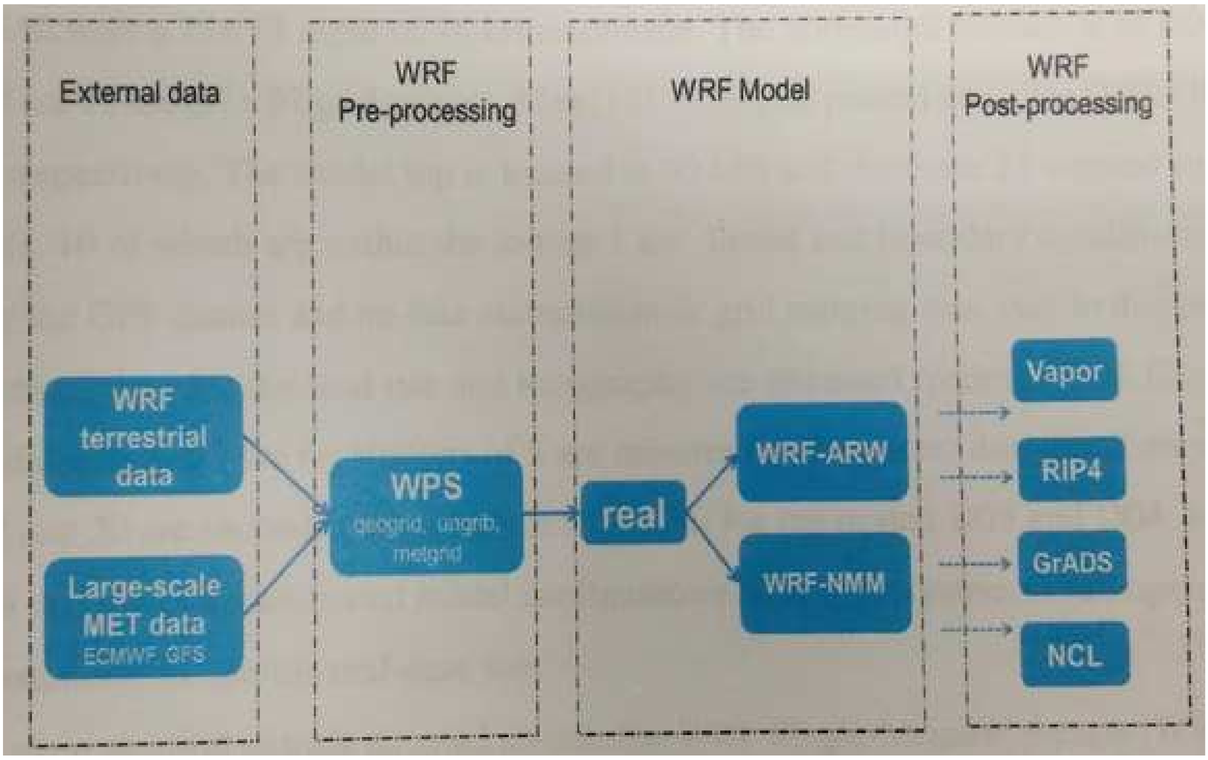

圖 2-9-1、WRF 計算分析流程

(引用 http://www2.mmm.ucar.edu/wrf/users/supports/tutorial.html)

(二)-9 WRF 氣象預報後處理

WRF 核心處理程式計算完成之後主要以 NETCDF 的格式輸出，之後通常採用 NCL(NCAR Command Language)軟體完成計算數據的後處理與可視化。該軟體亦支援各類氣象分析數據輸出格式，如 NETCDF、HDF4、HDF4-EOS、GRIB、binary 與 ASCII 格式。另一套後處理採用 RIP4(Read/Interpolate/Plot4)軟體，該軟體係採用 fortran 格式操作之可視化與氣象資料網格化軟體。整體的 WRF 操作軟體分類如圖 2-9-1 所示。

(二)-10 日本淡路島風場模擬設定

本次實習主要了解第2類技術之NWP方法的風力預測技術，其採用的分析工具為Weather Research and Forecasting Model (WRF)分析軟體，並用於分析日本淡路島風場(Awaji wind farm)的風力預測與發電資料。淡路島氣象分析採用Warnar學者提出的巢式分析模式，採用一個父計算區域與三個子計算區域並使用one-way計算方式。父區域位於北緯34.65度與東經134.635度且為75x73計算網格之78公里解析度。子計算區域分別為97x97之12km網格、101x109之3km網格與103x109之1km網格。背景氣象條件為50hPa並採用GFS(Global Forecast System)氣象資料作為邊界條件，以及採用U.S. Geological Survey的地形資料並分別套用在父系統與三個子系統解析度為5弧分(Arc minute)、2弧分、30弧秒(Arc second)與30弧秒。

淡路島模型風機發電量預報時間訂為2013年8月1日到2014年1月31日並採用1小時週期預報輸出。每一次的預報時間都必須要利用歷史資料的前12小時並加上6小時的計算穩定時間以達到最適當24小時預報分析。因此在持續預報資料分析需先累績前18小時的歷史資料以達到分析驗證。詳細的淡路島模型解析如下圖2-10-1與圖2-10-2。

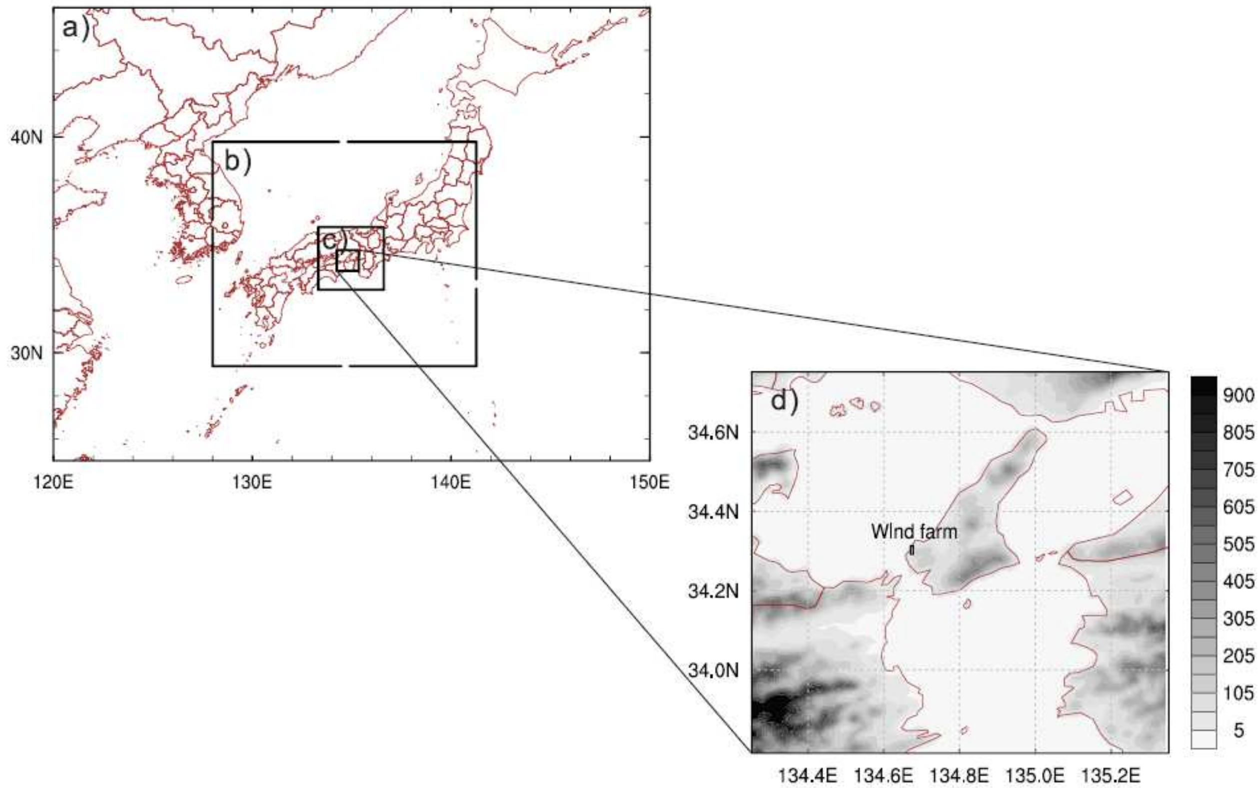

圖2-10-1、WRF預報分析之地理幾何規劃示意圖(引用附錄五-(一)與(二))

淡路島風力機風場位於淡路島西南方區域，共安裝15台GE(General Electric GE)公司2.5MW水平軸風機，並由日本CEF公司負責運轉維護。安裝塔架為80m與風機旋轉直徑84m。根據本次預報分析，量測資料利用風機機艙上方的風速風向儀並採用IEC61400量測標準，以每10分鐘為平均完成風速風量資料收集。2.5MW風機之運轉資料如圖2-10-3所示。但由於為了數值解析方便，將風機的功率曲線採用多項式擬合以利數值計算，係數如下(根據附錄五-(一)與(二))：

風能理論輸出	$Power(w) = \frac{1}{2} C_p \rho A V^3$
實際發電輸出	$Power(w) = a_{10} \cdot V^{10} + a_9 \cdot V^9 + a_8 \cdot V^8 + \cdots \ldots a_1 \cdot V + a_0$
相關係數	a_{10}=2.23e-06，a_9=-0.002，a_8=0.0061，a_7=-0.1125 a_6=1.2089，a_5=-7.8032，a_4=29.3869，a_3=-55.9710 a_2=48.3195，a_1=-16.7577，a_0=2.0053

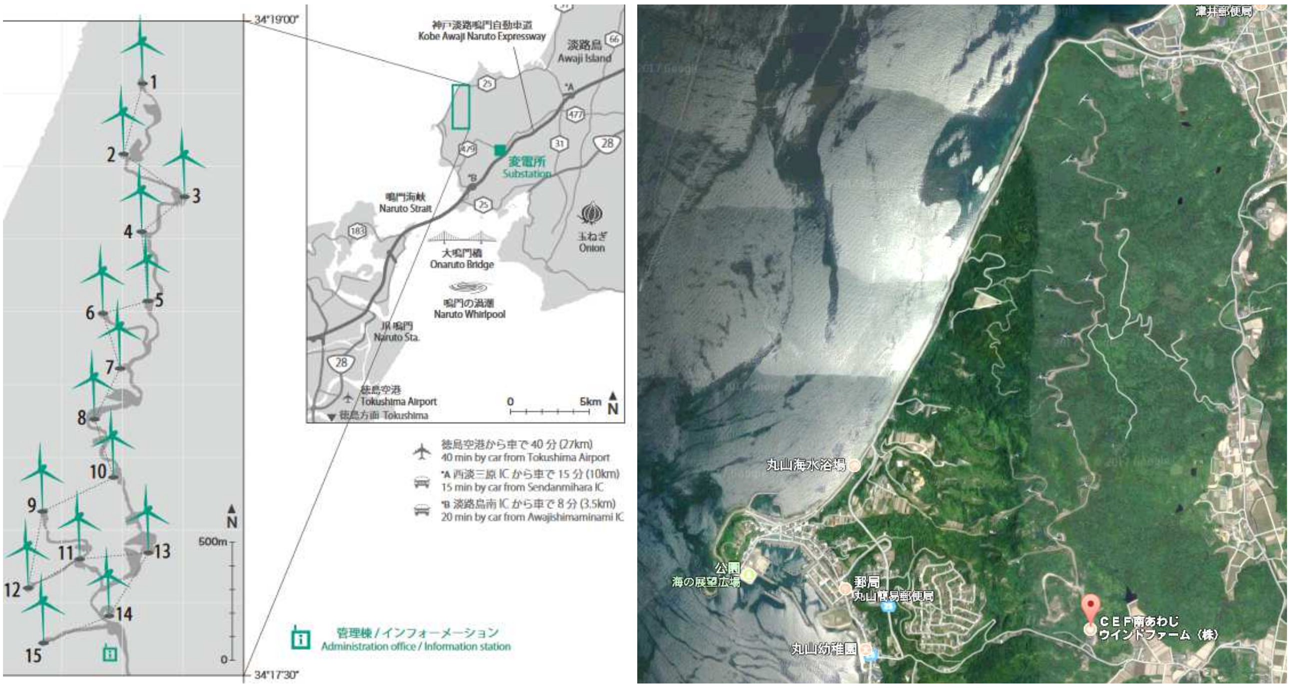

圖 2-10-2、淡路島陸域風場高度與空照圖(引用 CEF 公司官網 http://cef.co.jp/)

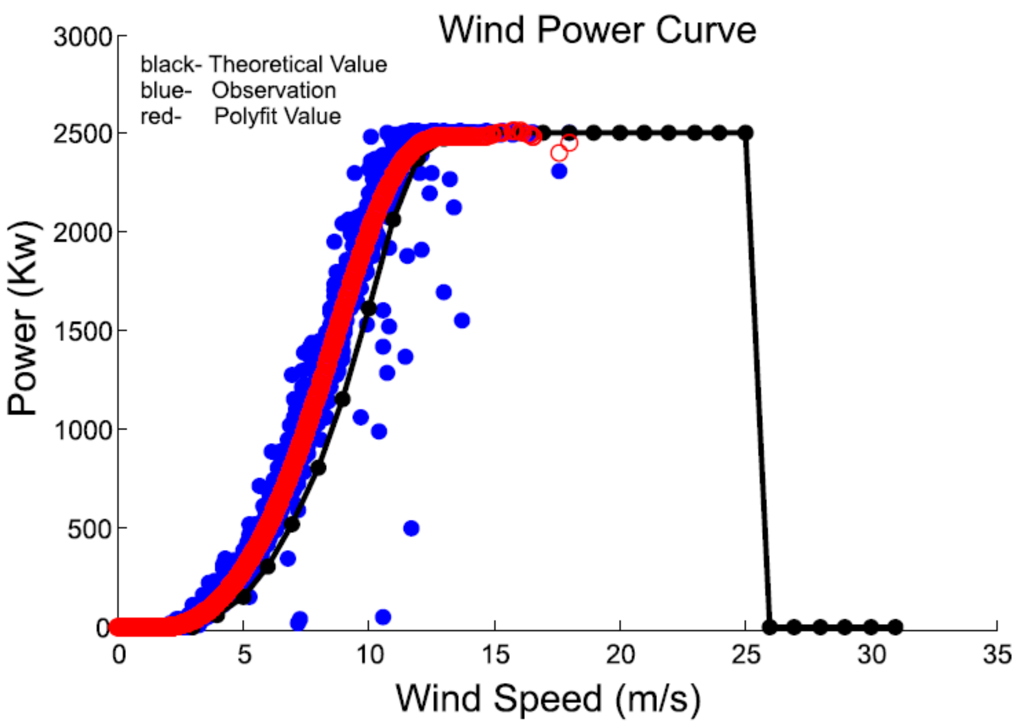

圖 2-10-3、GE2.5MW 實際運轉與理論數據比較圖(引用附錄五-(一)與(二))

(二)-11 Kalman filter 卡爾曼濾波器與 Data assimilation 資料同化方法

本次實習亦討論NWP方法的風力預測技術與卡爾曼濾波器及Data assimilation資料同化方法對發電預測的改善。卡爾曼濾波器是由 150 年前 Rudolf E. Kalman 所發展，其採用遞迴操作在連續的資料中運算出統計上的最佳輸出。此方法的優點在於容易調控、遞迴運算、最佳化特徵與最小電腦運算量。因此淡路島風場的發電預報則採用卡爾曼濾波器降低 WRF 預報的誤差以獲得更精確的預測。

卡爾曼濾波器的導入通常可分為兩步驟，第一為時間更新(time update)，主要利用現有的誤差去投影下一時間的誤差。第二步驟為量測更新(measurement update)，採用實際量測資料以修正過去的預測資料，再更正未來的預報。詳細的運算過程可參考卡爾曼濾波器相關文獻。

Data assimilation 資料同化則是採用三類主要分析方法：1.採用優先資訊(prior information)的動態系統。2.連續性的真實數據資料收集。3.數值模式的選用。詳細的背景理論可參閱附件資料。

(二)-12 預報準確度評估方法

淡路島風機再經由 WRF 預報軟體運算後，再利用卡爾曼濾波器的修正以達到最佳的預報結果，其準確度評估方法可利用三種計算方式，分別為平均誤差(mean error, ME)、均方根誤差(root mean square error, RMSE)、Pearson 修正係數(Pearson product moment correlation coefficient, CC)與重合指數(index of agreement, IA)，定義如下(根據附錄五-(一)與(二)):

$$ME = \frac{1}{N}\sum_{i=1}^{N}(fore_i - obs_i),$$

$$RMSE = \sqrt{\frac{\sum_{i=1}^{N}(fore_i - obs_i)^2}{N}},$$

$$CC = \frac{\sum_{i=1}^{N}\left(fore_i - \overline{fore}\right)\left(obs_i - \overline{obs}\right)}{\left[\sum_{i=1}^{N}\left(fore_i - \overline{fore}\right)^2 \sum_{i=1}^{N}\left(obs_i - \overline{obs}\right)^2\right]^{1/2}}$$

$$IA = 1 - \frac{\sum_{i=1}^{N}(fore_i - obs_i)^2}{\sum_{i=1}^{N}\left(|fore_i - \overline{obs}| + |obs_i - \overline{obs}|\right)^2}$$

(二)-13 WRF 氣象分析與淡路島發電量預報分析結果

本次實習主要學習整體的風機風場發電預報技術，主要利用 WRF 計算後再透過卡爾曼濾波器修正以即資料同化方法等修正預測風速以達到準確預報發電量。整體的計算流程與相關技術的導入如圖 2-13-1 所示。透過已知的氣象與地形資料搭配 WRF 並選擇適當的算則與數值方法，之後搭配卡爾曼濾波器與淡路島風機的實際發電量與風速完成風機的發電量預測。

根據圖 2-13-2 與圖 2-13-3 之計算結果，預報趨勢分布可確定透過 WRF 以及 Kalman filter 卡爾曼濾波器與 Data assimilation 資料同化方法可準確預估風機發電量，且有效降低傳統 WRF 預報愈差。其結果也顯示 Kalman filter 卡爾曼濾波器與 Data assimilation 資料同化方法有相同的誤差改善效果。研究結果發現利用資料同化方法可以使原始 WRF 預報資料誤差在 ME、RMSE 與 IA 指標分別下降 34.6%、23.9%與 8.8%，而卡爾曼濾波器則可以分別降低 97%、22%與 10%誤差。因此相對於資料同化方法的電腦運算量，卡爾曼濾波器提供更加簡易且有效的預報結果，故卡爾曼濾波器是較佳的 WRF 改善策略。預報確認發電數據後，OpenFOAM 計算流體力學程式被使用於驗證以及分析流場細節，如風速與紊流程度。故在透過大尺度與微觀尺度的流場分析之後對於特定風場之風力發電量可更加準確與可靠的預測並安排相關風機運維工作。

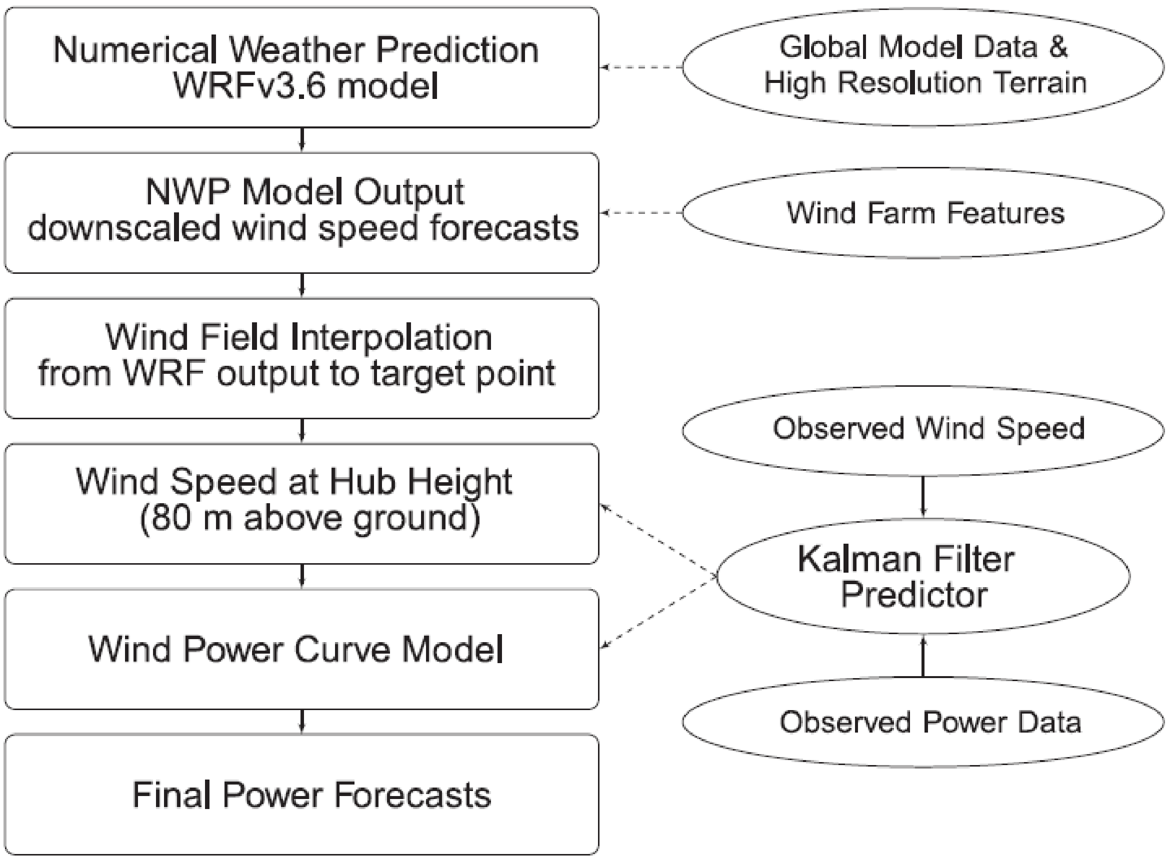

圖 2-13-1、計算流程與相關技術的導入示意圖

(引用附錄五-(一)與(二)及 http://www2.mmm.ucar.edu/wrf/users/supports/tutorial.html)
)

Experiment	Case1	Case2	Case3	Case4
WRF	+	+	+	+
GSI_DA		+		+
KF			+	+

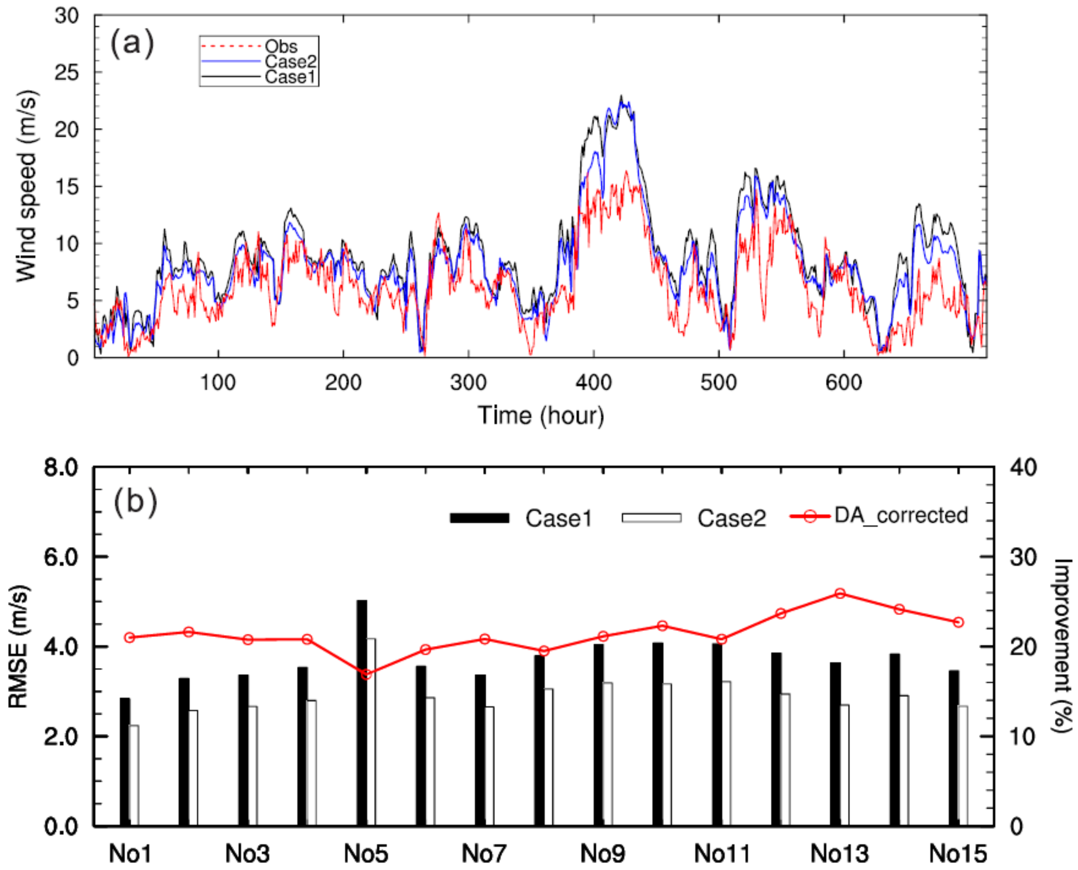

圖 2-13-2、WRF 預報與資料同化方法結果比較圖

(引用附錄五-(一)與(二))

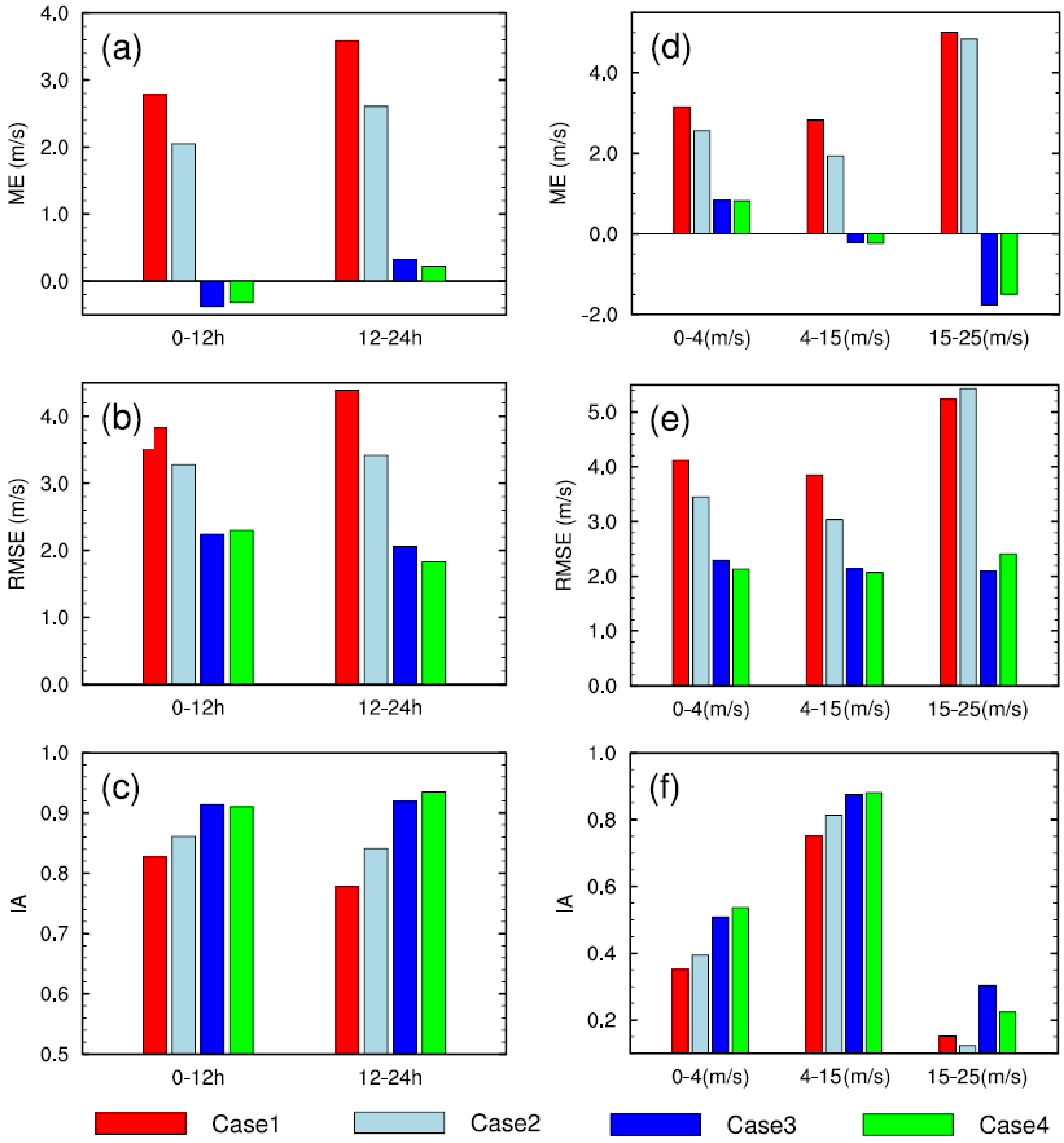

圖 2-13-3、WRF 預報、卡爾曼濾波器與資料同化方法結果比較圖
(引用附錄五-(一)與(二))

三、心　得

由於風力發電機的潔淨與、可持續性與再生能源特性，自 1990 年全球風能安裝容量約為每四年達到倍數成長。但根據日本市場統計，2016 年風能在日本全國發電只占比約 0.6%，其發展遲緩原因約可歸納於複雜地理環境、人口密度與政府政策。其中複雜的地理環境容易造成複雜的空氣對流而形成較大的發電量變動，進而造成區域電網整併困難。有效的解決方案即是在併網之前補充穩定風力發電量來源。此外為了最佳化操作策略，精確的預測風場與風力機之風速與發電量是最為關鍵的技術。但不論是台灣或是日本，風電公司對於預報發電系統開發皆較為缺乏。

因此，本次的實習主要是因為 CEF 公司遇見此預報系統的重要性而委託東京工業大學機械系執行此預報系統開發，並開發中尺度氣象 WRF 模式之發電預報。此研發成果已利用日本淡路島複雜地形風場之 15 台風機完成 WRF 驗證。在將近 6 個月實驗期間裡利用預報結果與風機機艙風速的量測比較後，已確認 WRF 的發電預報系統可提供相對可靠的操作控制預測。但由於量測數據的不確定性易造成數據判斷誤差與預報錯誤，因此透過導入 Kalman filter 濾波器與 data assimilation 資料同化法應用於後處理資料的重製，亦被確認有效降低風速預報誤差與發電量之量測不確定性。且 data assimilation 資料同化法更可優於 Kalman filter 濾波器在降低亂數誤差之功效，但其電腦運算量亦遠大於後者。

由於 WRF 預報計算之解析度為 500m 為單位之計算，因此更加複雜的地形亦會降低 WRF 之預報結果，也限制 WRF 之預報只能用於中尺度的地形幾何，故實習課程亦討論利用 CFD 技術以彌補次預報上的缺陷。CFD 的特點是可以建立多尺度的預報系統，不論地形的複雜程度皆可在運算系統獲得解析。故針對本次實習提出未來精進方案：(一)、CFD 之流體紊流模式、算則與網格結構需要更進一步修正以獲得更準確與改進目前之預報系統。(二)、紊流模式之不穩定係數可採用 Ensemble Kalman filter(EnKF)方法以了解對發電機預報的影響。(三)、在資料同化分析中，運算過程比較需要高品質的數據來源，但商業風機通常採用 IEC61400 量測標準，故數據只有 10 分鐘一筆。未來可以透過合作以獲得較佳的 WRF 起始運算資料。

日本風機市場與台灣市場類似，皆較歐洲起步較晚。其早期的風力機大多數來自國外，但近期已開始有自製風機或是合資公司。其風機管理公司大多是外包給民間公司長期管理，並且亦有與學校與研究機構的研究開發案，此點比台灣進步且已達到市場開放。日本東京工業大學與其研究單位亦與業界緊密結合，通常企業會派駐資深員工研讀博士班並提供相關計畫投資學校以達到投資-研究-合作相輔相成。

東京工業大學之 GSIC-TSUBAME 高速電腦中心在日本系採用聯盟營運方式，其合作方式有收費、優待與免費使用方式。最便宜的合作方式提供企業與其他單位無償使用，但其研究成果必須無償提供給學校與日本政府。優待方式則可用較便宜的方式輔導中小企業研發並保有研發機密。

最後感謝行政院原子能委員會核能研究所提供此次出國實習公差，藉由此機會得以學習未來執行業務時所需之專業知識，期許將此次所學充分運用於發展研究上，使專業更為精進，並透過此次交流得以拓展與推廣所內風能相關計畫研發成果，以提升本所於國際間更多相關計畫合作之機會。

四、建　議　事　項

(一) 日本 CEF 公司為風力發電運維公司(http://cef.co.jp/index.html)，其主要業務為風場開發、風機建設、運轉維護與發電監控。目前該公司擁有 9 座風場共 107 台風機之管理業務，並依其公司需求尋求東京工業大學等研究單位技術開發。建議核能研究所亦可依此經驗，尋找台灣類似於 CEF 之相關風機管理公司，輔導研究升級，亦可獲得業界運轉數據。

(二)以WRF軟體評估風能評估與風力發電預報技術已被確定可行且有效幫助電網電力調度。但目前台灣風力預測停留在較長期的風力預報，對於短期間預測，如數小時的預報資訊較缺乏，且對於局部區域的預測也缺乏此類評估單位。建議核研所成立相關研究小組。

(三) 東工大肖鋒教授建議核研所應積極與日本學術界或各研究單位合作，以精進風機技術與離岸風能工程分析技術。因台灣特殊且嚴苛的地形與氣候條件與日本類似，傳統國際上IEC61400標準無法滿足國內設計要求，台灣應積極開發自主分析軟體與程序以掌握開發離岸風電與風機技術。

(四) 日本東京工業大學之GSIC高速電腦中心，有提供免費合作計畫但其研究成果需歸於學校與日本政府。因此建議所內亦可在計畫範圍內利用此機制擴大與業界合作機會，並鼓勵中小企業參與研發。

(五) 日本風機發展與台灣雷同，皆比歐洲或是中國大陸起步較晚，故其風機大多來自國外機組，如美商 GE 公司。但日本依然透過國營企業積極開發自製風機與支撐結構組件，並開發相關安裝機具以完整佈建風機運維供應鏈。建議台灣相關單位亦可尋求此模式或參與日本相關產業建立合作模式。

五、附　錄

檢附相關研究論文兩篇、GSIC 見習資料與核研所交流資料

(一) An integrated wind-forecast system based on the weather research and forecasting model, Kalman filter, and data assimilation with nacelle-wind observation

(二) A wind power forecasting system based on the weather research and forecasting model and Kalman filtering over a wind-farm in Japan

(三) 東京工業大學 GSIC-TSUBAME2.5 資料

(四) 與日本東京工業大學交流簡報-Wind energy research in INER

An integrated wind-forecast system based on the weather research and forecasting model, Kalman filter, and data assimilation with nacelle-wind observation

Yuzhang Che and Feng Xiao

Citation: J. Renewable Sustainable Energy **8**, 053308 (2016); doi: 10.1063/1.4966693
View online: http://dx.doi.org/10.1063/1.4966693
View Table of Contents: http://aip.scitation.org/toc/rse/8/5
Published by the American Institute of Physics

JOURNAL OF RENEWABLE AND SUSTAINABLE ENERGY **8**, 053308 (2016)

An integrated wind-forecast system based on the weather research and forecasting model, Kalman filter, and data assimilation with nacelle-wind observation

Yuzhang Che and Feng Xiao[a)]
Department of Energy Sciences, Tokyo Institute of Technology, 4259 Nagatsuta Midori-ku, Yokohama 226-8502, Japan

(Received 16 May 2016; accepted 18 October 2016; published online 27 October 2016)

To forecast wind speed at hub-height is a challenging task for wind energy application, especially in Japan where the terrain feature is very complex and large fluctuations are observed in surface wind field. In this study, an integrated system to predict the hub-height wind speed has been developed by combining data assimilation and Kalman filter with the high resolution Weather Research and Forecasting (WRF) model. Assimilating the nacelle wind data (quality-controlled) and the Kalman filter algorithm effectively improves accuracy of the WRF model forecast by optimizing initial condition and post-processing the model output, respectively. It is found that the WRF model forecasts can be markedly improved after assimilating the nacelle wind data through the Gridpoint Statistical Interpolation analysis system, with the relative improvements of 34.3%, 23.9%, and 8.8% in ME (mean error), RMSE (root mean square error), and IA (index of agreement), respectively. The implementation of the Kalman filter can significantly reduce ME and RMSE while increases the value of IA as well. Further improvement can be achieved if the Kalman filter and nacelle wind data assimilation are implemented simultaneously. It is observed that the role of the Kalman filter is more dominant for the wind band of rated out speeds, while data assimilation is effective in reducing the random errors and becomes more important in rare or extreme weather conditions. Both data assimilation and Kalman filter modules apply the nacelle wind data which is routinely available, so the system can be easily adopted in different wind farm sites for operational use. *Published by AIP Publishing.* [http://dx.doi.org/10.1063/1.4966693]

I. INTRODUCTION

The short-term wind energy estimation relies heavily on the low-level wind forecasts derived from the numerical weather prediction (NWP) model. As documented by Landberg and Watson,[1] Costa *et al.*,[2] recent progresses in forecast skills of NWP models make it possible to provide more reliable predictions of surface wind field which is essential for wind energy management. However, the current NWP models are still far from a mature stage and particularly large errors are found in the prediction of the surface wind forecasts, which has motivated continuous efforts to improve the NWP models themselves.[3,4] The encouraging results in these works suggest that more reliable forecasts can be made by using more advanced and sophisticated numerical models which are generally believed to possess dynamic cores with less assumptions and accurate numerics, refined parameterization packages for physical processes that directly affect the phenomena of interests. Unfortunately, other factors beside the model inaccuracy, such as the uncertainties in observations and the chaotic nature of atmosphere, also prevent the outputs of deterministic NWP models being directly usable to many applications. Thus, other approaches are found to be more effective in improving the forecasts of the given

[a)]Author to whom correspondence should be addressed. Electronic mail: xiao@es.titech.ac.jp

numerical models. For example, efforts have been made to use the available observations which are always regarded as the more reliable representation of the real atmosphere.

Some existing studies[5–7] indicate that post-processing statistical methods that evaluate and correct the model outputs against the observations, for example, Model Output Statistics (MOS) and Kalman filter, are very effective and demonstrate significant capability of reducing errors in the outputs of numerical models. Another effective method is data assimilation (DA) to generate the initial conditions (known as the "analysis") as close as possible to the real atmosphere[8] for the NWP models in use to improve their forecasting skill. In this work, we develop and evaluate a DA component for a forecast system of local surface wind field,[9] which is based on the Weather Forecasting and Research (WRF) model and Kalman filter.

For operational wind farms, the conventional observations include upwind meteorological (MET) tower measurement and nacelle wind data. In general, the measurements from an MET tower at a wind farm site cannot accurately reflect the real wind field around the turbines which are located at different locations away from the MET tower, particularly when the terrain of a wind farm is complex. Instead, the nacelle-mounted anemometer which is placed on the top of nacelle behind the rotor can provide the routine data of wind speed and direction for each turbine. Although the wind observation of the nacelle-mounted anemometer is always affected by the design/shape of the wind turbine and nacelle, as well as the operation condition of the turbine,[10,11] some studies still show that nacelle-based wind speed observation, after proper calibration and data quality control, is more representative to the wind behavior (e.g., wind disturbance) experienced by the wind turbines in a wind farm than that from an upwind MET tower.[12,13] In this study, we have developed and evaluated a DA module to assimilate the nacelle-based wind data for a surface wind forecast system we developed previously.[9] The DA module has been constructed by using the WRF model and the Gridpoint Statistical Interpolation (GSI) analysis system developed by the National Centers for Environmental Prediction (NCEP) Environmental Modeling Center (EMC).

Being a continuation of our existing work[9] to establish a practical prediction system of surface wind and power generation for wind farms in Japan, we have developed the data assimilation module as another key technique and integrated it to the WRF model in addition to the Kalman filter post-processing tool. Both DA and Kalman filter make use of the nacelle-based wind data which are available for common wind farms, and thus the system can be easily adopted for operations on different sites.

The rest of the paper is organized as follows: the details of methodology, data, and experiment design are described in Section II. The performance of the DA technique based on the nacelle wind data and Kalman filter is presented in Section III. Section IV summarizes the results and provides several concluding remarks.

II. METHODOLOGY AND DATA

A. The forecasting model and GSI assimilation system

The Advanced Research WRF (ARW) model version 3.6, which is a limited-area mesoscale model based on a fully compressible and non-hydrostatic dynamic core,[14] is used in this study. The initial and boundary conditions used to drive the WRF model are taken from the NCEP Global Forecast System (GFS) real-time forecasts, which are gridded to a horizontal resolution of $0.5 \times 0.5°$.

The domain configuration of the WRF model which follows the steps recommended by Warner *et al.*[15] is shown in Figure 1, including a parent domain (D01) and three nested domains (D02, D03, and D04) with horizontal resolution of 24.0 km, 6.0 km, 1.5 km, and 0.5 km, respectively. There are 35 vertically stretched eta levels, 10 of which are within the lowest 1 km used for all domains and the top level is located at 50 hPa. The topographic data are obtained from the U.S. Geological Survey (USGS) global 30 arc-s elevation (GTOPO30) dataset for all domains except that the topography height of D04 is replaced with a 50 m resolution data obtained from the Geospatial Information Authority of Japan to furnish the local real observation information during the GSI DA processing. The longwave and shortwave

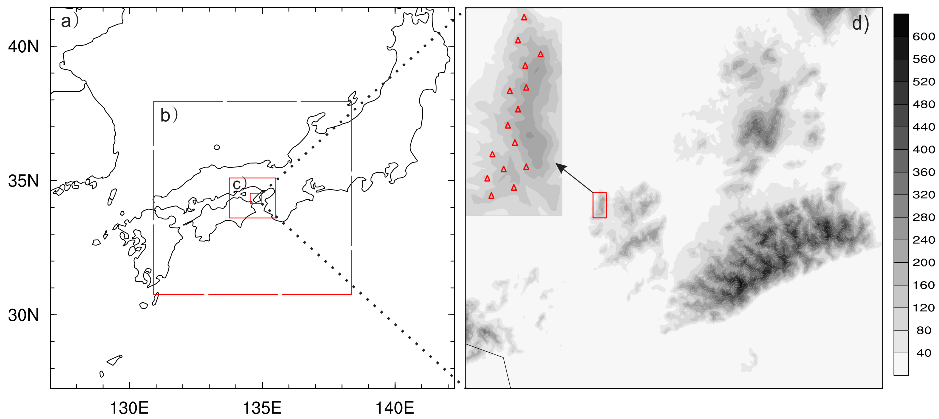

FIG. 1. Four nested domains (a) D01, (b) D02, (c) D03, and (d) D04 and model topography. The detailed terrain height (shaded with the gray bar in meter) of the D04 is shown in panel (d). The red triangles indicate the locations of the 15 turbines in a wind farm in south Awaji Island, Japan. Wind speed and direction are measured on the nacelle top of each turbine.

radiation schemes are based on the studies of Mlawer *et al.*[16] and Dudhia,[17] respectively. The WRF Single-Moment 6-class (WSM6) microphysics parameterization scheme,[18] the Kain-Fritsch convective parameterization scheme,[19] and the Noah land surface model (LSM)[20] are used in the four domains. With respect to the planetary boundary layer (PBL) scheme, the Asymmetric Convective Model version 2 (ACM2)[21] is adopted based on the sensitivity experiments in our previous study.[9]

One of the biggest limitations of WRF wind forecasts at hub-height is the difficulty in obtaining accurate information on the current state of the atmosphere, which can be partly solved by using the DA technique based on the available observations. In this study, the GSI analysis system, which is capable of assimilating a diverse set of observations, is integrated with the WRF-ARW mesoscale system. More specifically, this paper will implement the GSI 3DVar (three-dimensional variational data assimilation) system using the nacelle wind data to improve the hub-height wind forecasts.

The underlying idea of 3DVar data assimilation is to find the analysis increment x' of physical variable x by minimizing the cost function that measures the distance between the background forecast and observation.[8] The cost function $J(x')$ is defined by

$$J(x') = \frac{1}{2}(x')^T B_f^{-1}(x') + \frac{1}{2}\left(Hx' - y'\right)^T R^{-1}\left(Hx' - y'\right), \tag{1}$$

where B_f and R are the static background and observation error covariance matrices, respectively; y' is the innovation vector; and H is the linearized observation operator. More detailed description and information of the GSI system can be found on the GSI website (http://www.dtcenter.org/com-GSI/users).

B. Observational data

Same as in our previous work, the target region (shown in Figure 1) is the wind farm located in south Awaji Island, Japan, where 15 wind turbines (see in Figure 1(d)) have been installed. All wind turbines (General Electric GE2.5) have a rated capacity of 2.5 MW and the power curve is displayed in Figure 7. The rotor diameter of the turbines is 84 m and the tower height is 80 m. The nacelle wind for each turbine is measured by the anemometers placed on the top of the nacelle behind the rotor. After the conventional quality control, the observed wind data are input into the GSI DA system for wind prediction and used to evaluate the forecast results as well. The wind data (speed and direction) are available every 10 min for one month period from 1 January to 31 January 2016.

In general, the nacelle-based wind data are always used by wind farm operators directly for the turbine control (e.g., to determine the cut-in/cut-out speeds). Nevertheless, the quality of the nacelle wind observations needs to be evaluated before assimilating the data into the NWP models, so as to avoid the degradation of forecasting skill due to the assimilation of a few bad data points, which might even outweigh the benefits of assimilating many other good data points. Thus, we, in this study, implement the standards addressed in the technical report of National Oceanic and Atmospheric Administration (NOAA) Earth Systems Research Laboratory (ESRL)[22] to flag out the unreasonable data points for each turbine separately.

C. The Kalman filter algorithm

The primary Kalman filter is a recursive algorithm to estimate a signal from noisy measurements. In this study the Kalman filter is used in predictor mode, to reduce the uncertainties in wind speed forecasts at hub-height by using the information of the most recent forecasts and observations. Though a number of studies have already demonstrated that the Kalman filter can improve the raw forecasts of the NWP model, we still intend to understand its performance in eliminating the errors in high resolution (i.e., 500 m for D04 of the WRF model in the present configuration) wind speed forecasts at hub-height and then to investigate whether it has advantages to the DA technique. Here, only the main equations are given as below and the more detailed description of the Kalman filter algorithm can be found in Refs. 6 and 23.

Considering the state of the unknown process at time t, the bias between the forecasts and the true (unknown) is related to the state at previous time $t - \delta t$

$$x_{t|t-\delta t} = x_{t-\delta t|t-2\delta t} + \eta_{t-\delta t}, \tag{2}$$

where δt is a time lag, x_t is the true forecasting bias at time t, $x_{t|t-\delta t}$ is the *a priori* state estimate at time t, η is the white noise that has zero-mean, and the variance ($\sigma^2_{\eta,t}$) uncorrected in time. Then the forecasting errors y_t can be written as

$$y_t = x_t + \varepsilon_t = x_{t|t-\delta t} + \eta_t + \varepsilon_t, \tag{3}$$

where a random error ε_t is normally distributed with zero-mean and variance $\sigma^2_{\varepsilon,t}$. The uncertainties and errors in numerical models and inaccuracy in initial and boundary conditions are the main sources of ε_t.

Given a reasonable initial guess of the expected mean square error p and Kalman gain K (i.e., p_0 and K_0), the Kalman filter can recursively generate an estimate of forecast bias x at $t + \delta t$ through the equations shown below

$$\begin{cases} \hat{x}_{t+\delta t|t} = \hat{x}_{t|t-\delta t} + K_t\left(y_t - \hat{x}_{t|t-\delta t}\right) \\ K_t = \dfrac{p_{t-\delta t} + \sigma^2_{\eta,t}}{p_{t-\delta t} + \sigma^2_{\eta,t} + \sigma^2_{\varepsilon,t}} \\ p_t = (p_{t-\delta t} + \sigma^2_{\eta,t})(1 - K_t), \end{cases} \tag{4}$$

where the hat (ˆ) notation indicates the estimation of the variable. The white noise, $\sigma^2_{\eta,t}$ and $\sigma^2_{\varepsilon,t}$, which are crucial to the implementation of the Kalman filter procedure, are calculated via the same procedure by Delle Monache *et al.*[6]

D. Experiment design

Four experiments (shown in Table I) were carried out to investigate how assimilating the nacelle wind data and using the Kalman filter algorithm influence the performance of WRF wind forecasts at hub-height, and to understand the priority of those two procedures. In the first experiment (Case1), only GFS data were used to obtain the raw wind speed forecasts by re-initializing the WRF model as a "cold-start" at 12:00 UTC each day. In each re-initialization runs for 30 h,

TABLE I. The four sets of experiments for evaluating the impact of data assimilation and Kalman filer. The "WRF," "GSI_DA," and "KF" with "+" represent the use of WRF model, GSI analysis system, and Kalman filter, respectively.

Experiment	Case1	Case2	Case3	Case4
WRF	+	+	+	+
GSI_DA		+		+
KF			+	+

the initial 6 h (spin-up time) were excluded from the forecasting data series. The second experiment (Case2) was conducted to evaluate the impact of assimilating the nacelle wind data with cyclic mode, in comparison with the results of Case1. As displayed schematically in Figure 2, the final analysis field at 18:00 UTC each day was cyclically assimilated three times with a 6-h interval. Using this analysis field as initial condition, the wind speed forecasts of continued 24 h were obtained. We designed the experiment of Case3 to evaluate the contribution of the Kalman filter algorithm for improving the raw forecasts of Case1 based on the available nacelle wind speed observations. Finally, the experiment of Case4 was carried out to compare the contributions of the DA technique and the Kalman filter algorithm in improving the wind speed forecasts.

To compare the difference in these experiments quantitatively, the following set of statistical metrics is used.

Mean error (ME):

$$ME = \frac{1}{N}\sum_{i=1}^{N}(fore_i - obs_i), \tag{5}$$

where i is the time point and N is the total number of verification time points. *fore* and *obs* represent the predicted and observed values, respectively.

Root mean square error (RMSE):

$$RMSE = \sqrt{\frac{\sum_{i=1}^{N}(fore_i - obs_i)^2}{N}}. \tag{6}$$

Index of agreement (IA):

$$IA = 1 - \frac{\sum_{i=1}^{N}(fore_i - obs_i)^2}{\sum_{i=1}^{N}\left(|fore_i - \overline{obs}| + |obs_i - \overline{obs}|\right)^2}, \tag{7}$$

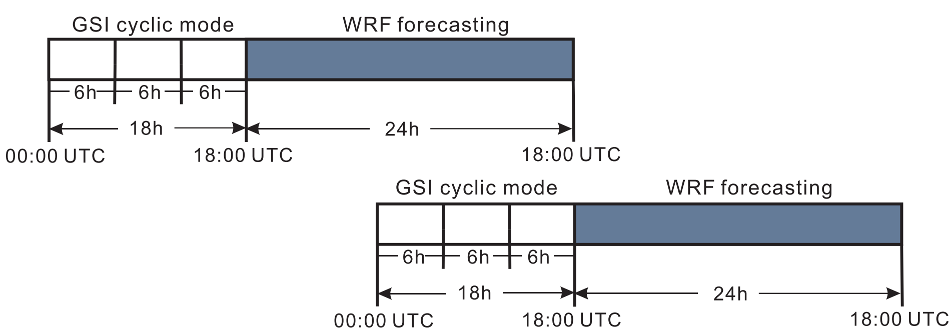

FIG. 2. The schematic of implementing GSI system in cyclic mode. The white boxes stand for the total assimilation time of 18 h with an interval of 6 h, while the gray boxes represent the forecasting length (24 h) of WRF model after assimilating the nacelle wind data.

where $\overline{obs}$ denotes the mean of observations. The value of IA, which indicates the agreement between the observations and forecasts, ranges from 0 to 1. A larger IA value means better agreement.

Pearson product-moment correlation coefficient (CC):

$$CC = \frac{\sum_{i=1}^{N}\left(fore_i - \overline{fore}\right)\left(obs_i - \overline{obs}\right)}{\left[\sum_{i=1}^{N}\left(fore_i - \overline{fore}\right)^2 \sum_{i=1}^{N}\left(obs_i - \overline{obs}\right)^2\right]^{1/2}}, \tag{8}$$

where $\overline{fore}$ indicates the average of forecasts.

III. RESULTS

In this section, first the overall result of comparison between the raw wind speed forecasts of the WRF model and the forecasts with DA is presented based on the statistical parameters introduced in Section II. Then the role of the DA technique and the Kalman filter algorithm in improving the raw wind speed forecasts of the WRF model will be investigated. It is noted that all of the statistics and discussions are based on the 15-turbine averaged data unless otherwise specifically stated.

A. Impact of assimilation on the hub-height wind forecasts for the experiment period

Figure 3(a) illustrates the comparison between raw forecasts (black), observations (red) and the forecasts with DA (blue) of wind speed, which are represented with "Case1," "Obs," and

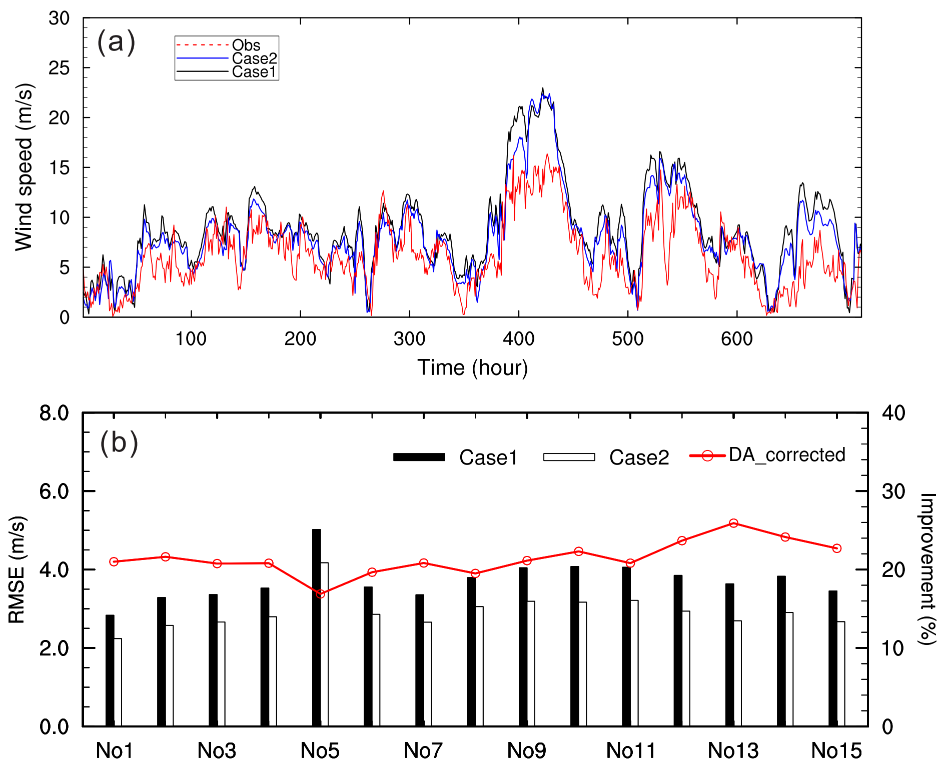

FIG. 3. (a) One month series of the raw wind speed forecasts (black), the forecasts with assimilation (blue), and the corresponding observations (red). (b) The comparison of the RMSE of wind speed using data assimilation (solid white bar) with respect to the raw forecasts (solid black bar) for the 15 turbines individually. The marked red line stands for the relative improvement due to the data assimilation. The period is from 18:00 UTC 1 January to 23:00 UTC 31 January 2016.

"Case2," respectively, during the experiment period from 18:00 UTC 2 January to 23:00 UTC 31 January 2016. It can be seen that the raw wind speed forecasts (Case1) reproduces the observation with relatively good accuracy, though there are occasional large errors, especially when the observed wind speed is larger than $15\,\mathrm{ms}^{-1}$. It is also easy to find that the blue line lies closer to the red line than the black one during almost the whole period, which implies that the forecasts of wind speed with DA are remarkably improved in comparison with the forecasts without DA (Case1). Obviously, the evidence from Figure 3(a) also shows that the forecasting skill of wind ridge is largely increased after assimilating the nacelle wind data, though the contribution of DA for other periods is relatively slighter or even not clear in some cases. This might be attributed to the WRF model itself whose forecasting ability of large wind speed at hub-height is inferior to that of regular wind speed (e.g., ranging from $4\,\mathrm{ms}^{-1}$ to $15\,\mathrm{ms}^{-1}$). It reveals that implementing DA with the nacelle wind data can significantly improve the forecasting skill of the WRF model in extreme weather conditions. The values of ME, RMSE, IA, and CC are listed in Table II to quantify the effects of assimilating nacelle wind data into the WRF model, in comparison with the raw forecasts. Examining the second column, the positive values of ME indicate that both cases overestimate the wind speed in the whole period (nearly one month). Compared to the raw forecasts (Case1), the ME in case 2 is reduced by 34.3% where the nacelle wind data is assimilated. Regarding RMSE, the value of Case2 is much smaller compared to Case1, with a relative error reduction of 23.9%. Similarly, both IA and CC are increased when assimilation is implemented.

In addition to the 15-turbine average results shown above, we also examined the impact of the data assimilation on each individual turbine. Figure 3(b) illustrates the comparison of the RMSE between the raw wind speed forecasts and the forecasts with data assimilation for 15 turbines separately. It is found that forecasting skills of wind speed are improved by assimilating the nacelle wind data for all 15 turbines. The relative improvement in RMSE varies from 19.5% to 25.9% with an average of 21.5%.

Figure 4 displays the 30-case mean (30 days) forecasts of Case1, Case2 and observations during the 24-h forecasting length. Apparently, the overestimation of wind speed is found no matter whether the nacelle wind data is assimilated or not. However, this systematic discrepancy has been significantly corrected by using the DA technique. The relative decrease of RMSE (36.4%) further demonstrates the large impact of assimilating the nacelle wind data in reduction of the systematic bias in WRF model.

From the above discussions, we may conclude that assimilating the nacelle wind data can substantially improve the accuracy of WRF model in forecasting the hub-height wind field in the target wind farm site of interest.

B. Verification of Kalman filter and the difference compared to DA

Having confirmed the effect of assimilating the nacelle wind data on improving the raw wind forecasts at hub-height, we further evaluated the integrated forecasting system which uses the Kalman filter as another key technique to improve the prediction. To this end, we conducted other two experiments, i.e., Case3 and Case4, to include the Kalman filter as another module. In order to implement the Kalman filter properly, the first 15 days are chosen as a training period and thus the following discussions are all based on the forecasts and corresponding observations of the second half 15 days. Figure 5 displays the statistical parameters that quantify the performance of the integrated prediction system and the contributions of its different components in forecasting the hub-height wind under configurations of the four test cases.

TABLE II. The monthly mean ME, RMSE, and CC calculated with the forecasts (with or without assimilating the nacelle wind data) and the corresponding observations of wind speed at hub-height.

Experiment	ME (ms^{-1})	RMSE (ms^{-1})	IA	CC
Case1	2.54	3.51	0.80	0.83
Case2	1.67	2.67	0.87	0.84

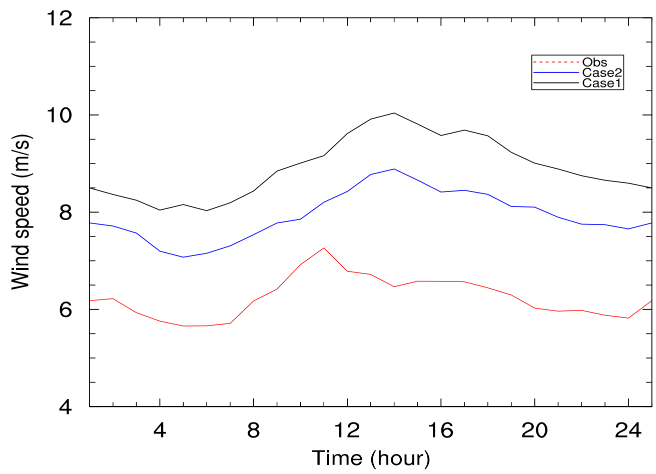

FIG. 4. Comparison between the hub-height wind speed forecasts with (blue) and without (black) assimilating the nacelle wind data based on the corresponding observations (red), during the 24 h forecasting period (30-day averaged).

As observed above, the ME and RMSE of Case2 are largely reduced compared to Case1, while the values of IA and CC are increased, which shows the large improvement due to assimilating the nacelle wind data.

The effects of implementing the Kalman filter to the raw forecasts of the WRF model are also examined by comparing the results of Case1 and Case3 in Figure 5. It seems that the bias (Figure 5(a)) in the raw forecasts can be largely revised and meanwhile the random errors (Figure 5(b)) can be partly reduced as well. Furthermore, the values of IA and CC of Case3

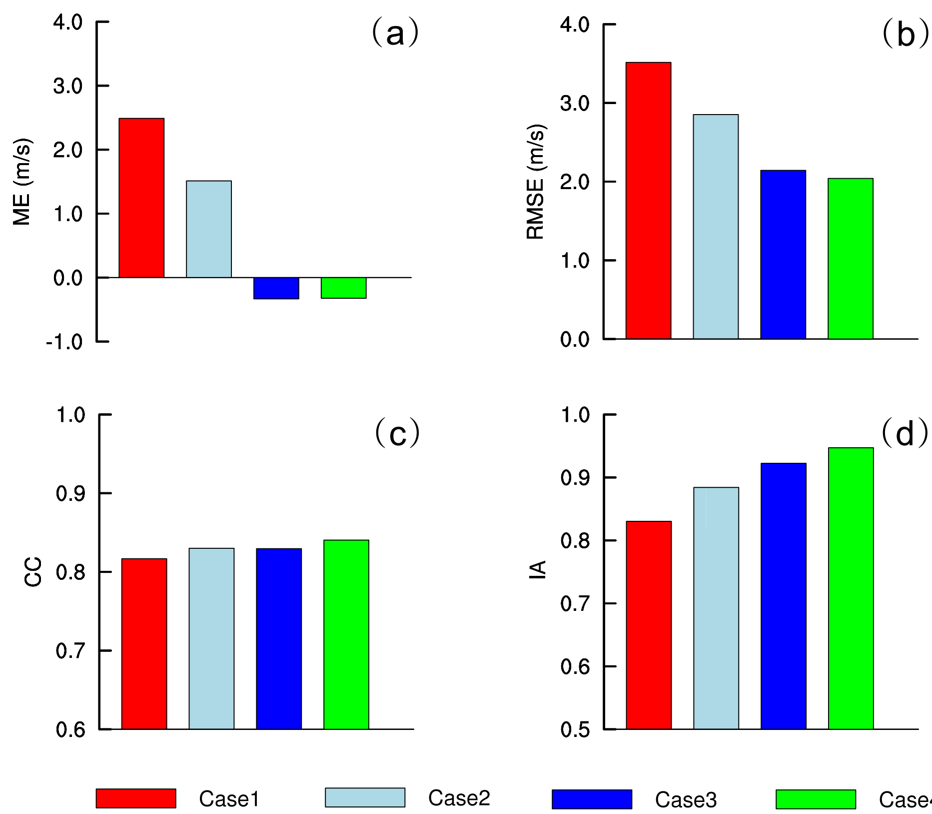

FIG. 5. The ME (a), RMSE (b), CC (c) and IA (d) of four cases described in Table I. All results are based on data series of the second half 15 days (16–31 January 2016 with 1 h interval).

become larger after using the Kalman filter compared to those of Case1. All of these results demonstrate that the Kalman filter as a post-processing method can significantly improve the forecasting skill of hub-height wind speed.

Figure 5 also illustrates the difference between DA and Kalman filter when one compares among the results of Case2, Case3, and Case4. For Case4, in which the DA is used to improve the initial condition and then the Kalman filter is adopted to post-process the forecasts, the RMSE is further reduced and the values of IA and CC are larger than both Case 2 and Case3, while the value of ME is nearly same. This implies that combining the Kalman filter and the nacelle wind data assimilation can provide the best forecasts and the role of the Kalman filter is more important in calibrating the systematic bias. On the contrary, comparing the RMSE and IA of Case3 and Case4 suggests that assimilation of nacelle wind data shows better performance against the Kalman filter in revising random uncertainties. However, if we consider the differences represented by all four statistic parameters of Case2 and Case3 synthetically, the Kalman filer shows the priority over DA for wind speed forecasts at hub-height.

To further evaluate the improvements of assimilating the nacelle wind data and Kalman filter, we show in Figures 6(a)–6(c) the ME, RMSE, and IA at different forecasting periods (i.e., 0–12 h and 12–24 h). In regard to the raw forecasts (Case1), the forecasting skill at period of

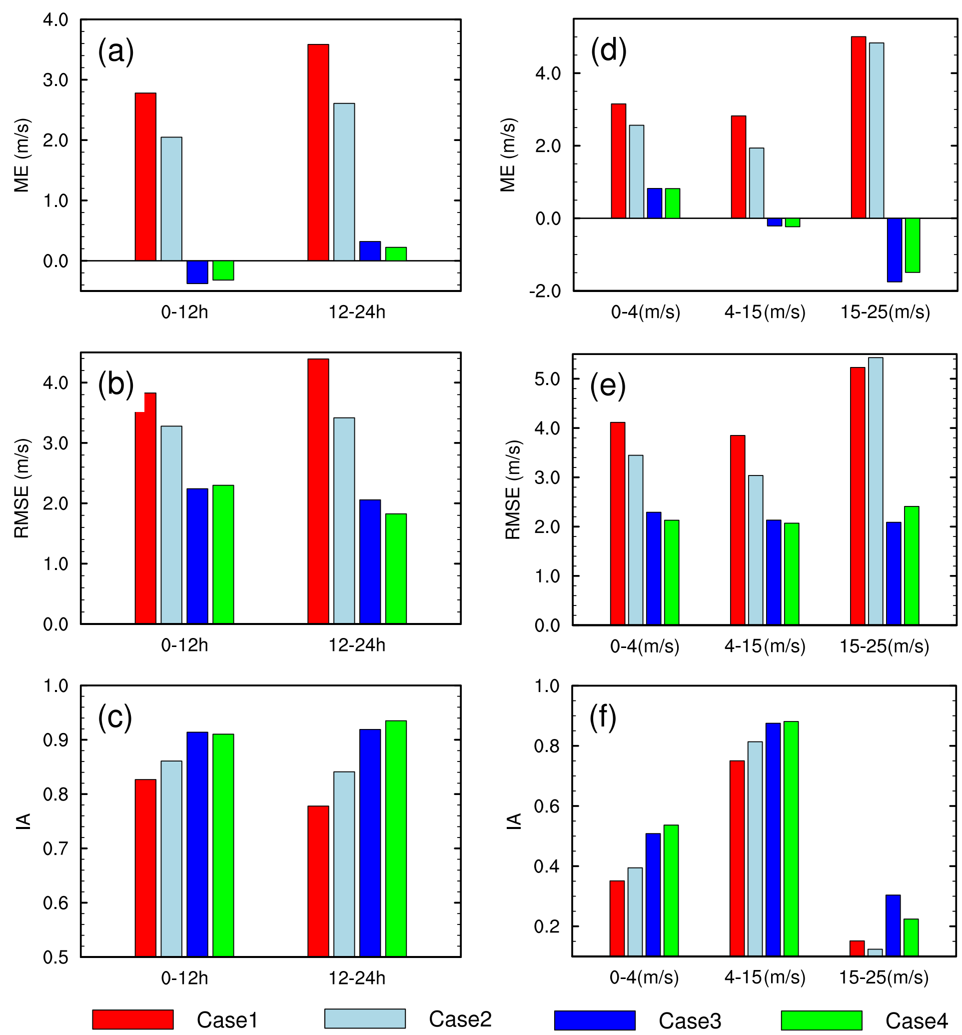

FIG. 6. The statistical parameters of the hub-height wind speed forecasts for four cases in different forecasting periods ((a)–(c)) and different wind speed bands ((d)–(f)). Same as in Figure 5, the evaluation period is 15 days from 16 to 31 January 2016.

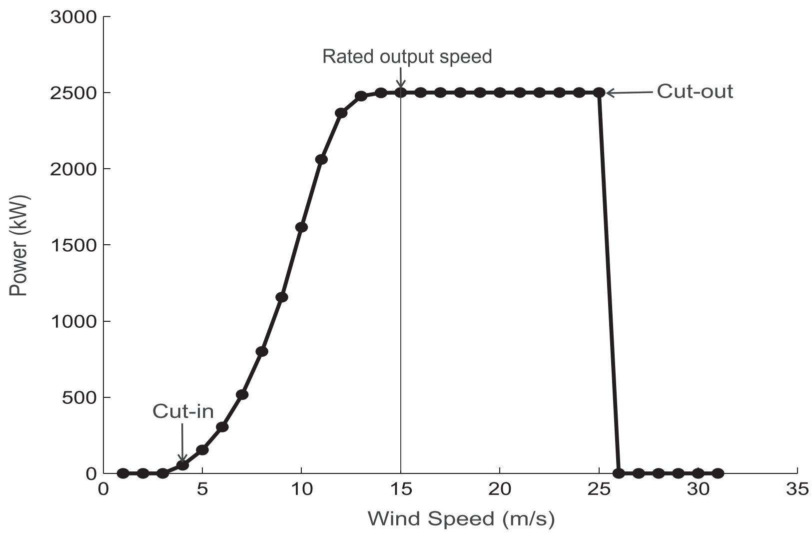

FIG. 7. The theoretical wind power curve for a 2.5 MW turbine used in this study and the corresponding cut-in, rated output and cut-out speed.

0–12 h is slightly higher than the period of 12–24 h. The same conclusion can be drawn for the forecasts with data assimilation (Case2) where the errors in the raw forecasts have been largely reduced after assimilating the nacelle wind data. As same as shown in the Figures 5(a), 5(b), and 5(d), the Kalman filter (Case3 and Case4) can significantly improve the model forecasts under the situations with or without DA for different forecasting periods. Comparing the values of ME, RMSE and IA of Case3 and Case4 during different periods, we observe that the impact of DA is more apparent compared to the Kalman filter in the period of 12–24 h, due to the difference between Case3 and Case4 during 12–24 h is larger than that in the period of 0–12 h.

In practice, the simplest way to obtain the wind energy forecasts of a specific turbine is to use the designed (or theoretical) power curve provided by the turbine manufacturer, which is usually a function of the mean hub-height wind speed. In this study, the target wind farm consists of 15 2.5 MW horizontal-axis turbines and the corresponding power curve is shown in Figure 7. As displayed, the value of cut-in ($4\,\mathrm{ms}^{-1}$), rated output ($15\,\mathrm{ms}^{-1}$) and cut-out speed ($25\,\mathrm{ms}^{-1}$) is crucial to power management in routine operations. Therefore, the forecasts of 0–4, 4–15 and 15–25 ms^{-1} wind speed bands are further validated. The results are displayed in Figures 6(d)–6(f). Apparently, almost all of the ME and RMSE of the raw forecasts (Case1) are reduced by applying both DA and the Kalman filter, meanwhile the value of IA is increased. In addition, the smallest value of ME and RMSE and the largest IA in the band of 4–15 ms^{-1} indicate that it is easier to obtain relatively accurate hub-height wind speed forecasts in the interval of 4–15 ms^{-1} compared to other wind speed bands. When the wind speed is larger than $15\,\mathrm{ms}^{-1}$ which is the rare case in the experiment period, the performance of the system becomes worse (with small IA), and DA shows more significant effect in comparison with the Kalman filter. It suggests that the DA technique can be more effective in correcting the forecast under rare or extreme weather conditions.

Overall, the forecasts are remarkably improved after assimilating the nacelle wind data (Case2) or using the Kalman filer (Case3). The largest improvement is found when the two techniques are combined (Case4). It seems that the role of the Kalman filter is more dominated as the difference between Case3 and Case4 is much smaller than that between Case1 and Case2, while DA becomes more important in rare or extreme weather conditions.

IV. SUMMARY

We have developed a practical forecasting system for surface wind and power output by integrating data assimilation and Kalman filter into the WRF model. Both data assimilation and

Kalman filter modules make use the nacelle wind data which is routinely available, so the system can be easily adopted in different wind farm sites for operational use. Due to the complex topographic features, the surface wind field in Japan region is significantly fluctuating and more difficult to predict, the present system employs data assimilation and Kalman filter to eliminate the uncertainties from two aspects, i.e., the data assimilation improves the accuracy in initial conditions and Kalman filter provides a posterior correction to the raw model output, and thus can be expected as a promising tool in real-case operations.

The system has been validated using the data of a wind farm in Awaji Island, Japan. The wind speed forecasts at hub-height have been substantially improved by data assimilation to refine the initial wind field for WRF model, i.e., the ME and RMSE errors in WRF prediction were reduced by 34.3% and 23.9%, respectively, while IA has been improved by 8.8% due to the DA technique. On the other hand, the Kalman filter, as a post-processing method, is able to provide more reliable wind forecasts with a short training period (15-day in this study). By using both Kalman filter and nacelle wind data assimilation, the raw forecasts can be further improved. Detailed evaluation indicates that the role of the Kalman filter is more dominant for the wind band of rated out speeds, while data assimilation becomes more important in rare or extreme weather conditions.

[1] L. Landberg and S. J. Watson, "Short-term prediction of local wind conditions," Boundary-Layer Meteorol. **70**, 171–195 (1994).
[2] A. Costa, A. Crespo, J. Navarro, G. Lizcano, H. Madsen, and E. Feitosa, "A review on the young history of the wind power short-term prediction," Renewable Sustainable Energy Rev. **12**, 1725–1744 (2008).
[3] T. Davies, M. Cullen, A. Malcolm, M. Mawson, A. Staniforth, A. White, and N. Wood, "A new dynamical core for the Met Office's global and regional modelling of the atmosphere," Q. J. R. Meteorol. Soc. **131**, 1759–1782 (2005).
[4] A. Simmons and A. Hollingsworth, "Some aspects of the improvement in skill of numerical weather prediction," Q. J. R. Meteorol. Soc. **128**, 647–677 (2002).
[5] H. R. Glahn and D. A. Lowry, "The use of model output statistics (MOS) in objective weather forecasting," J. Appl. Meteorol. **11**, 1203–1211 (1972).
[6] L. Delle Monache, T. Nipen, X. Deng, Y. Zhou, and R. Stull, "Ozone ensemble forecasts: 2. A Kalman filter predictor bias correction," J. Geophys. Res.: Atmos. **111**, D05308 (2006).
[7] P. Louka, G. Galanis, N. Siebert, G. Kariniotakis, P. Katsafados, I. Pytharoulis, and G. Kallos, "Improvements in wind speed forecasts for wind power prediction purposes using Kalman filtering," J. Wind Eng. Ind. Aerodyn. **96**, 2348–2362 (2008).
[8] E. Kalnay, *Atmospheric Modeling, Data Assimilation and Predictability* (Cambridge University Press, 2003), pp. 115–116.
[9] Y. Che, X. Peng, L. Delle Monache, T. Kawaguchi, and F. Xiao, "A wind power forecasting system based on the weather research and forecasting model and Kalman filtering over a wind-farm in Japan," J. Renewable Sustainable Energy **8**, 013302 (2016).
[10] F. Zahle and N. N. Sørensen, "Characterization of the unsteady flow in the nacelle region of a modern wind turbine," Wind Energy **14**, 271–283 (2011).
[11] A. Smaïli and C. Masson, "On the rotor effects upon nacelle anemometry for wind turbines," Wind Eng. **28**, 695–714 (2004).
[12] B. Smith, H. Link, G. Randall, and T. McCoy, "Applicability of nacelle anemometer measurements for use in turbine power performance tests," in Proceedings of the American Wind Energy Association (AWEA) WINDPOWER 2002 (2002).
[13] N. J. Cutler, H. R. Outhred, and I. F. MacGill, "Using nacelle-based wind speed observations to improve power curve modeling for wind power forecasting," Wind Energy **15**, 245–258 (2012).
[14] W. Wang, C. Bruyere, M. Duda, J. Dudhia, D. Gill, H. Lin, J. Michalakes, S. Rizvi, X. Zhang, J. Beezley *et al.*, see http://www.mmm. ucar. edu/wrf/users/docs/user_guide_V3/ARWUsersGuideV3. pdf for "ARW version 3 modeling system user's guide," Mesoscale & Miscroscale Meteorology Division, National Center for Atmospheric Research (2010).
[15] T. T. Warner, R. A. Peterson, and R. E. Treadon, "A tutorial on lateral boundary conditions as a basic and potentially serious limitation to regional numerical weather prediction," Bull. Am. Meteorol. Soc. **78**, 2599–2617 (1997).
[16] E. J. Mlawer, S. J. Taubman, P. D. Brown, M. J. Iacono, and S. A. Clough, "Radiative transfer for inhomogeneous atmospheres: RRTM, a validated correlated-k model for the longwave," J. Geophys. Res.: Atmos. **102**, 16663–16682, doi:10.1029/97JD00237 (1997).
[17] J. Dudhia, "Numerical study of convection observed during the winter monsoon experiment using a mesoscale two-dimensional model," J. Atmos. Sci. **46**, 3077–3107 (1989).
[18] S.-Y. Hong, Y. Noh, and J. Dudhia, "A new vertical diffusion package with an explicit treatment of entrainment processes," Mon. Weather Rev. **134**, 2318–2341 (2006).
[19] J. S. Kain, "The Kain-Fritsch convective parameterization: An update," J. Appl. Meteorol. **43**, 170–181 (2004).
[20] F. Chen and J. Dudhia, "Coupling an advanced land surface-hydrology model with the Penn State-NCAR MM5 modeling system. Part I: Model implementation and sensitivity," Mon. Weather Rev. **129**, 569–585 (2001).
[21] J. E. Pleim, "A combined local and nonlocal closure model for the atmospheric boundary layer. Part I: Model description and testing," J. Appl. Meteorol. Climatol. **46**, 1383–1395 (2007).

[22]J. M. Freedman, J. Manobianco, J. Schroeder, B. Ancell, K. Brewster, S. Basu, V. Banunarayanan, B.-M. Hodge, and I. Flores, "The Wind Forecast Improvement Project (WFIP): A public/private partnership for improving short term wind energy forecasts and quantifying the benefits of utility operations. The Southern Study Area, Final Report," Technical Report (AWS Truepower, LLC, Albany, NY (United States), 2014), pp. 22–31.
[23]R. E. Kalman, "A new approach to linear filtering and prediction problems," J. Fluids Eng. **82**, 35–45 (1960).

JOURNAL OF RENEWABLE AND SUSTAINABLE ENERGY **8**, 013302 (2016)

A wind power forecasting system based on the weather research and forecasting model and Kalman filtering over a wind-farm in Japan

Yuzhang Che,[1] Xindong Peng,[2] Luca Delle Monache,[3] Takayuki Kawaguchi,[4] and Feng Xiao[1,a)]

[1]*Department of Energy Sciences, Tokyo Institute of Technology, 4259 Nagatsuta, Midori-ku, Yokohama 226-8502, Japan*

[2]*State Key Laboratory of Severe Weather, Chinese Academy of Meteorological Sciences, Beijing 100081, China*

[3]*National Center for Atmospheric Research, Research Applications Laboratory, PO Box 3000, Boulder, Colorado 80307, USA*

[4]*Clean Energy Factory Co., Ltd., 1-7-14 Hirakawacho, Chiyoda-ku, Tokyo 102-0093, Japan*

(Received 10 July 2015; accepted 4 January 2016; published online 21 January 2016)

The rapid development of wind energy in Japan and the associated high uncertainties and fluctuations in power generation present a big challenge for both wind power generators and electric grids. Accurate and reliable wind power predictions are necessary to optimize the integration of wind power into existing electrical systems. In this study, a hybrid forecasting system of wind power generation was developed by integrating the Kalman filter (KF) with the high resolution Weather Research and Forecasting (WRF) model as well as an empirical formula of wind power output (power curve). The system has been validated with observations including wind speed and power output over a six-month period for 15 turbine sites at a wind farm in Awaji-island, Japan. The results show that the tuned WRF model is able to provide hub-height wind speed prediction for the target area with reliability to some extent. The predicted wind field can be substantially improved by the Kalman filter as a post-processing procedure. The 15-turbine averaged improvements of mean error, root mean square error, and correlation coefficient are 97%, 22%, and 10%, respectively. Meanwhile, the Kalman filter also demonstrates a promising capability of reducing the uncertainties in the power curve model. Systematic validations regarding both wind speed and power output were carried out against the observations for the target wind farm, which show that the hybrid power forecasting system presented in this paper can be an effective and practical tool for short-term predictions of wind speed and power output in Japan area. *© 2016 AIP Publishing LLC*. [http://dx.doi.org/10.1063/1.4940208]

I. INTRODUCTION

The recent assessments of the World Energy Council have reported the difficulties that Japan is facing in lieu of the shortage of energy caused by the complete shutdown of nuclear plants after the Fukushima accident.[1] In order to compensate for the loss of the nuclear power generation, extra fossil resources are currently imported, which has led to the rise of electricity cost and to an increase of the fossil fuel emissions. As an alternative to the traditional fossil-energy resources, renewable energy has been the focus of recent developments as a long-term and sustainable solution. In particular, wind energy has shown tremendous potential in terms of economic and environmental effects.

Global wind energy capacity has been doubling nearly every three and a half years since 1990, due to its clean, renewable, and sustainable characteristics. However, wind makes up

[a)]Author to whom correspondence should be addressed. Electronic mail: xiao@es.titech.ac.jp

only 0.44% of the total power supply in Japan[2] where the development of wind energy is limited by a number of factors, such as complex geographic features, high population density, and the government policy.[3] Among them, the topographical complexity may be an important reason that complicates wind flow, and thus causes greater fluctuation in power output, which makes the integration of wind power into the electric power grids more challenging than for other regions. An effective solution to stabilize the wind power output is to make use of supplementary electric sources/sinks through active operations before delivering the power to the grid systems. In order to optimize the operation plan, accurate predictions of both the wind speed and wind power for the targeted turbines and wind farms are of crucial importance.[4]

A number of studies have proposed several methods and models to predict wind speed, which can be grouped into two broad categories:[5] statistical and physical. Statistical approaches explore relationships between future and current state (observed data), and include techniques as artificial neural network[6,7] and auto-regressive moving average.[8] They can provide accurate wind speed forecasts over short time scales with limited computational requirements. However, the forecasting skill of these techniques degrades quickly with increasing forecasting lead time.[9] Physical-based models, often based on numerical weather prediction (NWP), on the other hand do not have this drawback. NWP models project the real atmosphere state based on an approximation of known physical laws, and result in more accurate and reliable estimates for longer time horizons (from hours to several days). Different limited-area NWP models, such as Weather Research and Forecasting (WRF), Regional Atmospheric Modeling System (RAMS), and Fifth-Generation Penn State/NCAR Mesoscale Model (MM5), have been used for wind energy resource assessment by various researchers.[10,11] However, to a large extent the wind forecasts derived from NWP models are affected by errors stemming from uncertainties in initial/boundary conditions, simplifications in physics, and numerical approximations.[12] Great efforts have been devoted to reduce these uncertainties by improving data quality[13] and developing more accurate numerical models with improved dynamic cores and more sophisticated physical parameterizations.[14,15]

Although efforts to improve NWP models have led to substantial progress in the accuracy of deterministic predictions, it cannot be expected to eliminate all uncertainties in real-case applications, which result in deviations between the NWP output and the real atmospheric state. An effective way to reduce the uncertainties of the NWP models is by implementing post-processing methods to revise or correct the NWP model outputs based on their past performances. Typical and widely used post-processing methods include Model Output Statistics (MOS)[16] and Kalman Filter (KF).[17–19] The Kalman filter is a popular algorithm due to the simplicity of the algorithm, the moderate computational costs, and the short training period required. It has been applied successfully for wind energy modeling to produce more accurate predictions. The works by Louka *et al*.[20] and Al-Hamadi and Soliman[21] clearly demonstrated that the forecasting errors of both wind power and electric load can be effectively reduced with the Kalman filter. They have shown that combining NWP models and statistical post-processing into a tuned prediction system can further improve wind speed and power forecasts. Unfortunately, to the best knowledge of the authors, there is no report in literature on any practice to establish such a prediction system for wind farm sites in Japan.

The purpose of this study is to develop a wind power prediction system for the Awaji-island wind farm in Japan as an effort to facilitate the short-term wind power forecast in Japan area. The system is mainly based on the high resolution WRF model and the Kalman filter. The power curve model adopted in this system is constructed based on a polynomial fit technique using the historical data of the observed wind speed at hub-height and power output. We first evaluate the forecasting ability of the WRF and power curve model separately as the basic components of the hybrid prediction system, to show that they are able to provide reasonably reliable forecasting results in the target site which has complex geographic environment very typical in Japan. Then the forecasting skill of the hybrid system has been further improved by implementing the Kalman filter to the WRF model and the power curve model. The capability of the system for predicting the real-case wind power outputs in the target farm has been validated over a four-month period.

The rest of the paper is organized as follows: the details of datasets and methodology are described in Section II. Section III mainly analyzes the performance of the hybrid approach for the predictions of wind speed and power. The paper ends with concluding remarks in Section IV.

II. DATA AND METHODOLOGY

A. Global forecast system (GFS) data and observations

Six-month (2013/08/01–2014/01/31) GFS forecasting products from the National Center for Environmental Prediction (NCEP) were used as the initial and boundary conditions for the WRF model with a 6-h interval. The horizontal resolution of all variables is 1.0×1.0 deg, with 27 levels ranging from 1000 to 10 hPa.

The anemometers which are placed on the top of the nacelle behind the rotor are used for collection of the wind data. The effects of the rotating blades and nacelle on the observed wind can be taken into account by adjusting the relationship between the nacelle-based observations and the measurements from the upwind meteorological tower.[22] This would increase the cost and is not widely adopted in practice. Alternatively, the study in Ref. 23 suggests that the nacelle-based wind speed observation is a more reliable estimation to the target turbine site than the measurement obtained from the meteorological tower with a distance away. Therefore, in this study, the nacelle-based wind speed from 15 turbines (see in Figure 1) at hub-height (80 m above ground) is utilized to validate the performance of the WRF model for the prediction of hub-height wind speed at the wind farm in Awaji island, Japan. In addition, observations of power output are also used to evaluate the reliability of the power prediction proposed in this study. Both wind speed and power observational data are available every 10 min for the six-month period from 1 August 2013 to 31 January 2014.

B. WRF model configurations

The meteorological model adopted in this work is the Advanced Research WRF (ARW) model version 3.6 (WRFv3.6 hereafter), which is based on a fully compressible and non-hydrostatic dynamic core.[24] The WRFv3.6 is a limited-area mesoscale model, with a terrain-following hydrostatic-pressure vertical coordinate, designed for operational forecasting as well as research. The WRFv3.6 used in this study is the latest available version of WRF model which has been

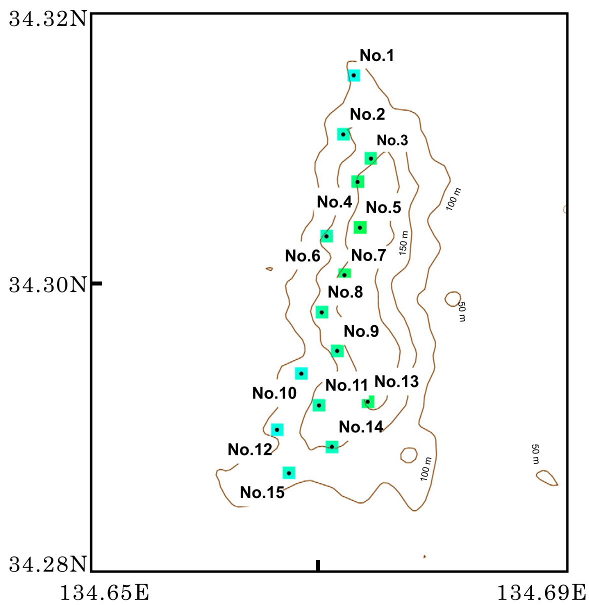

FIG. 1. The network of observational sites for wind speed at Awaji island wind farm. Contours stand for the terrain elevation.

continuously developed by a broad community of researchers across the world. Nevertheless, to our knowledge there are very limited studies of WRF model for the applications of wind power forecasting in Japan.

In this study, the domain configuration of WRFv3.6 which follows the steps recommended by Warner *et al.*[25,26] includes a parent domain (D01) and three nested domains (D02, D03, and D04) (Figure 2) with one-way interaction. The D01 is centered at 34.65°N and 134.635°E with a 75×73 mesh of 48 km resolution. The horizontal resolution of D02, D03, and D04 are 12 km (97×97 grid points), 3 km (101×109 grid points), and 1 km (103×109 grid points), respectively. The model top is located at 50 hPa and there are 35 vertical stretched eta levels, 10 of which are within the lowest 1 km. Initial and boundary conditions are all given by the GFS dataset and no data assimilation or grid nudging was used in this study. The geographical data for the land use and topography are obtained from the U.S. Geological Survey datasets and have resolutions of 5 arc min for the parent domain, 2 arc min for D02, and 30 arc s (about 925 m $\times$ 925 m) for the nested D03 and D04. It should be noted that the aforementioned model configuration allows the system to run operationally on workstations for routine real-case use.

The main physical options adopted include the WRF Single-Moment 6-class (WSM6) microphysics parameterization,[27] the Rapid Radiative Transfer Model (RRTM) scheme[28] for long-wave radiation with Dudhia's scheme[29] for shortwave radiation, the Kain-Fritsch convective parameterization,[30] and the Noah land surface model (LSM).[31] The specific information of the planetary boundary layer (PBL) scheme we selected is discussed in Section III D.

The model prediction period is from 1 August to 31 January 2014 and the numerical results are output at a 1 h interval. We re-initialize WRFv3.6 as a "cold-start" at 18:00 UTC each day and each re-initialization runs for 30 h. Due to the cold start, there is typically a spin-up time period of 6-h as recommended by Wang *et al.*[24] before the model turns to a stable state. Therefore, the forecasts during the initial 6 h of each run are excluded from the forecasting data series used to compute the performance metrics.

C. The Kalman filter algorithm and 7-day running mean method

1. The Kalman filter algorithm

The Kalman filter is an estimation algorithm that operates recursively on streams of input data (containing random variations) to produce a statistically optimal estimate of the underlying

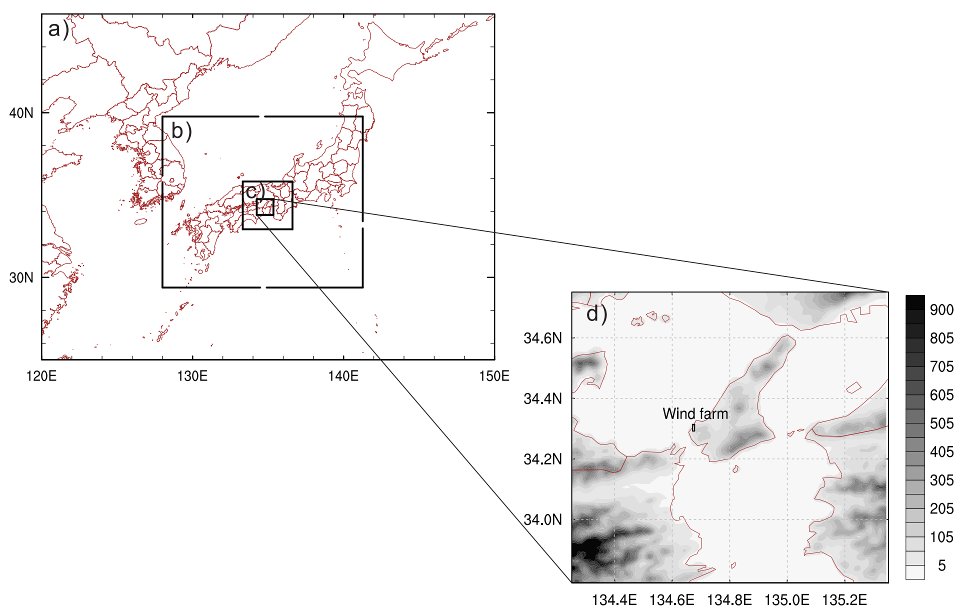

FIG. 2. WRF domains and model topography: (a) D01, (b) D02, (c) D03, and (d) D04 are indicated by black frames. The detailed terrain height (shaded with the gray bar in meter) of the D04 is shown in the panel (d).

system state. It is widely used in various fields from radar and computer vision to meteorological applications due to its adaptive, recursive, and optimal characteristics. The specific set of mathematical equations can be found in Refs. 17, 19, and 32.

The implementation of the Kalman filter can be divided into two main steps: one is "time update," aiming to project forward the bias of the current state to estimate the forecasting bias at the next time step; the other part is a "measurement update," namely, incorporating a new observation into the previous estimation to obtain a corrected estimate of the forecasting bias.

In general, the forecasting bias between the forecasts and measurements of a variable at time t is related to the state at previous time $t - \delta t$

$$x_{t|t-\delta t} = x_{t-\delta t|t-2\delta t} + \eta_{t-\delta t}, \tag{1}$$

where x_t is the true forecasting bias at time t, δt is a time lag, $x_{t|t-\delta t}$ is the priori state estimate at time t, η is the white noise that has zero-mean, and the variance ($\sigma^2_{\eta,t}$) is uncorrected in time. Although the real forecasting bias is unknown, it has certain relationships with the forecasting errors (also called measurement bias) y_t. That is, the forecasting errors consist of the forecasting bias and a random error ϵ_t

$$y_t = x_t + \epsilon_t = x_{t|t-\delta t} + \eta_t + \epsilon_t, \tag{2}$$

where ϵ_t is normally distributed with zero-mean and variance $\sigma^2_{\epsilon,t}$. The source of random errors ϵ_t comes mainly from uncertainties and errors in numerical models, as well as inaccuracy in initial and boundary conditions.

The Kalman filter gives the recursive estimation of the unknown forecasting bias x_t based on the bias estimation at previous time and the historical forecasting errors y

$$\hat{x}_{t+\delta t|t} = \hat{x}_{t|t-\delta t} + K_t(y_t - \hat{x}_{t|t-\delta t}), \tag{3}$$

where the hat ($\hat{}$) notation indicates the estimation of the variable. K_t is the Kalman gain, which is recursively calculated as follows:

$$K_t = \frac{p_{t-\delta t} + \sigma^2_{\eta,t}}{p_{t-\delta t} + \sigma^2_{\eta,t} + \sigma^2_{\epsilon,t}}, \tag{4}$$

where p is the expected mean square error

$$p_t = (p_{t-\delta t} + \sigma^2_{\eta,t})(1 - K_t). \tag{5}$$

Given a reasonable initial guess of p_0 and K_0, as well as the model forecast M_t and observation time series, the Kalman Filter can recursively generate an estimate of forecast bias x at $t + \delta t$ through Eqs. (1)–(5). Then, the model forecast can be corrected as follows:

$$M_{kf_{t+\delta t}} = M_{t+\delta t} - \hat{x}_{t+\delta t|t}. \tag{6}$$

It is worthwhile to note that the calculation of white noise $\sigma^2_{\eta,t}$ and $\sigma^2_{\epsilon,t}$ is crucial to the implementation of Kalman filter procedure. According to Refs. 19 and 33, $\sigma^2_{\epsilon,t}$ is a time-varying quantity which can be calculated with the Kalman algorithm itself using Eqs. (3)–(5). The estimation of $\sigma^2_{\eta,t}$ is derived from the estimation of $\sigma^2_{\epsilon,t}$ with a ratio r

$$\sigma^2_{\eta,t} = r\sigma^2_{\epsilon,t}. \tag{7}$$

The ratio r is a parameter reflecting the relative weighting of observation and forecasts. As r is somewhat sensitive to different models and predicted variables, several tests have been carried out to find the best values of $r = 0.6$ for wind speed and $r = 0.15$ for wind power forecasting, respectively, in present study.

2. 7-day running mean method

Stensrud and Skindlov[34] showed that a simple bias correction method using the previous 7-day mean bias correction can improve the direct model forecast of maximum temperature. This method is easy to implement, and meanwhile has the ability of improving the raw predictions. Therefore, it is chosen as a reference to validate the performance of Kalman filter algorithm for correcting the raw prediction of wind speed in this study.

D. Power curve model

From the fluid mechanical definition, the power output P of a wind turbine is a non-linear function of the wind speed and can be expressed as follows:

$$P = \frac{1}{2} C_p \rho A v^3, \tag{8}$$

where P is the power, C_p is the turbine coefficient of performance, and ρ is the air density which depends on air pressure and temperature. A is the swept area of a turbine blade and v represents the wind speed at the turbine site. The theoretical power curve of turbine No. 3, which is a 2.5 MW horizontal-axis wind turbine (HAWT) with three blades, is shown in Figure 3 (black line and points). In Figure 3, the blue points represent the observed electrical power output obtained for turbine No. 3 measured from routine operation. It is easily found that although the overall trend shows an agreement with the theoretical manufacture power curve, there are remarkable uncertainties and deviations from it. This is not surprising considering that there are still other factors that affect the power output, such as the unresolvable sub-scale fluctuations, wake effects, wind direction, as well as operation control.[35] Consequently, the manufacturer power curve cannot be directly used to predict wind power in real cases, and the approach followed in this study is to build the empirical power model for each turbine based on 2-month (from 1 August 2013 to 30 September 2013 with a 10-min interval) observed wind speed and power data using a polynomial fit technique. The empirical power curve is expressed by

$$P' = a_{10} v^{10} + a_9 v^9 + \cdots + a_1 v + a_0, \tag{9}$$

where v is the wind speed, P' is the prediction of wind power, and $a_0, a_1, \cdots, a_{10}$ are the coefficients separately generated for different turbines. The empirical power curve of No. 3 turbine is plotted in Figure 3 (red circles), which looks noticeably different from the manufacturer power curve. It is also seen that there is an uncertainty between the observed wind speed and power

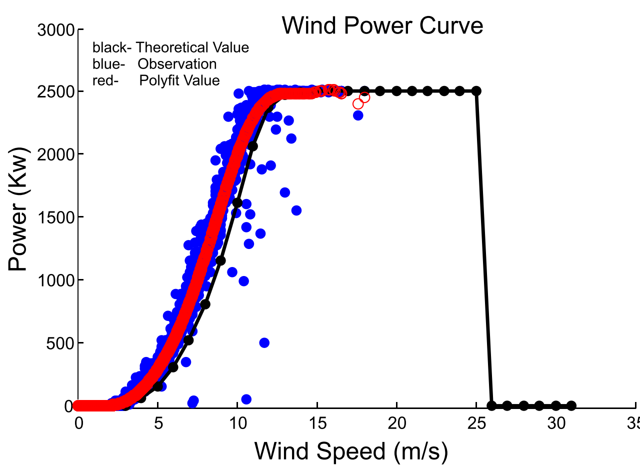

FIG. 3. The theoretical (black line and points), observed (blue point), and the tenth-order polynomial (red point) wind power curve of No. 3 turbine.

output, which might be attributed to other factors, such as variations of wind direction, air temperature, as well as the effects of mechanical and operation control systems. Our main interest in this study is to generate a power output prediction system as a function of wind speed.

E. System overview

We summarize the hybrid wind power prediction system described in Figure 4. The numerical procedure mainly involves two steps, i.e., the surface wind prediction from the WRF model and the post-processing of Kalman filter.

Given the large scale forecasting data and topographic information, the wind held prediction over the target wind farm can be derived from the WRF model forecasts. After considering the local geographic information, the forecasts of wind speed at hub height can be obtained by linearly interpolating the WRF model outputs from the two nearest levels. The Kalman filter is then generated based on the observations of wind speed and power output at the turbine sites, which is used to correct the systematic bias and uncertainties in both WRFv3.6 and power curve models, and thus to obtain an optimal prediction of power production.

III. RESULTS AND DISCUSSION

The statistical parameters introduced in Section III A will be used to evaluate the performance of the predicting system described in Sec. II. We have tuned the WRF model for the surface wind prediction in the target region via a set of sensitivity tests of PBL parameterization schemes in Section III B. The overall forecasting skill of WRFv3.6 model for predicting wind speed is verified in Section III C. Finally, the performance of Kalman filtered wind speed and power prediction is discussed in Section III D.

A. Verification metrics

Evaluation of the forecasting skills of the proposed model is conducted quantitatively with various statistical verification metrics. In this study, the mean error (ME), root mean square error (RMSE), and the Pearson product-moment correlation coefficient (CC) are adopted, which are defined, respectively, as follows:

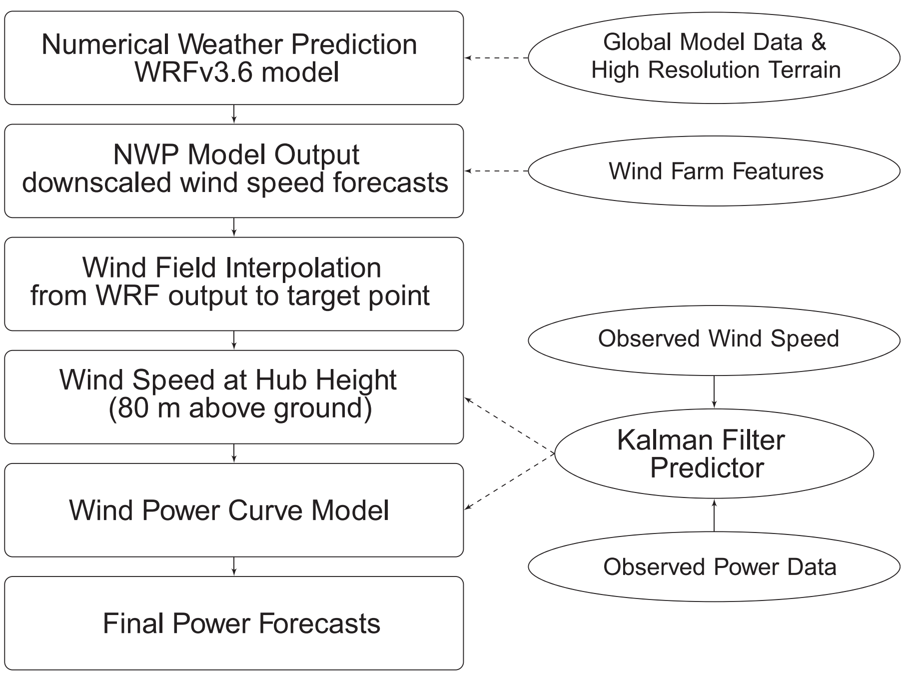

FIG. 4. A schematic diagram of the hybrid wind power forecasting system.

$$ME = \frac{1}{N}\sum_{i=1}^{N}(fore_i - obs_i), \tag{10}$$

$$RMSE = \sqrt{\frac{\sum_{i=1}^{N}(fore_i - obs_i)^2}{N}}, \tag{11}$$

$$CC = \frac{\sum_{i=1}^{N}\left(fore_i - \overline{fore}\right)\left(obs_i - \overline{obs}\right)}{\left[\sum_{i=1}^{N}\left(fore_i - \overline{fore}\right)^2 \sum_{i=1}^{N}\left(obs_i - \overline{obs}\right)^2\right]^{1/2}}, \tag{12}$$

where i presents time point, N is the total number of verification time points, and *fore* and *obs* are the predicted and observed values, respectively. In Eq. (12), the bar denotes the mean of the corresponding variable.

B. Sensitivity experiments of PBL schemes

The PBL is the lowest part of the atmosphere in which turbulent motions dominate the atmospheric flow. In atmospheric models, the turbulent effects are taken into account by PBL parameterizations. The current WRFv3.6 model has 12 PBL schemes that might exhibit different performances even for the same simulation region.[36,37] Therefore, prior to applying the WRFv3.6 model to the target wind farm, it is worthwhile to examine the prediction skills of different PBL schemes for the low-level wind field. To this end, the sensitivity of five PBL schemes, i.e., the Quasi-Normal Scale Elimination (QNSE),[38] the Asymmetric Convective Model version 2 (ACM2),[39] the Mellor-Yamada-Janjic (MYJ),[40] the Mellor-Yamada-Nakanishi-Niino (MYNN),[41] and the Yonsei University Scheme (YSU),[42] is tested over 15-day (from 1 October to 15 October 2013) for predictions of wind speed. The setup of the numerical experiments for this inter-comparison of PBL schemes is summarized in Table I.

Figure 5(a) illustrates the predicted diurnal variations of the predicted wind speed of No. 3 turbine at 80 m from the five sets of experiments with different PBL parameterization schemes, referred to as QNSE, ACM2, MYJ, MYNN, and YSU, and the corresponding observations. All the experimental runs capture the wind speed variations well and the sensitivity of PBL schemes is more apparent in period 09:00–23:00 UTC than in period 00:00–08:00 UTC. The forecasts from all experiments overestimate the wind speed during the whole period. The largest bias (0.94 ms^{-1}, shown in the third row of Table II) at No. 3 turbine site is observed in the QNSE experiment, while the smallest bias (0.63 ms^{-1}) is seen in the ACM2 prediction. The RMSEs also indicate that the performances of the ACM2, MYJ, MYNN, and YSU schemes are better than that of the QNSE scheme, and ACM2 has the smallest RMSE of 0.87 ms^{-1}.

The correlation and normalized standard deviation (NSD) of each experiment are calculated and summarized in a Taylor diagram,[43] which provides a synthetically visual comparison in terms of centered RMSE, correlation, and NSD. From Figure 5(b), although the NSD difference among

TABLE I. The five sets of numerical experiments for the inter-comparison of PBL schemes.

Experiment	PBL scheme	Land surface model	Surface-layer scheme
QNSE	Quasi-normal scale elimination	Unified Noah LSM	QNSE
ACM2	Asymmetric convective model	Pleim-Xu	Pleim-Xu
MYJ	Mellor-Yamada-Janjic	Unified Noah LSM	Eta similarity
MYNN	Mellor-Yamada-Nakanishi-Niino	Unified Noah LSM	MYNN
YSU	Yonsei University Scheme	Unified Noah LSM	Monin Obukhov

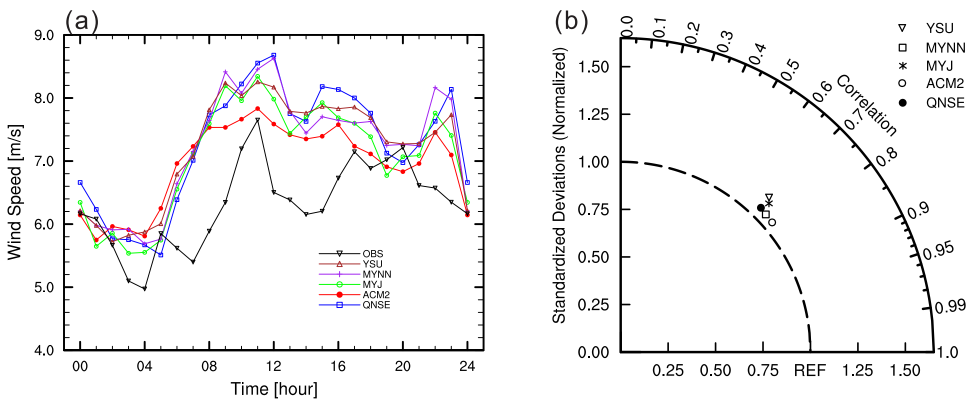

FIG. 5. Comparisons of observations and forecasts of five sensitivity experiments shown in Table I at No. 3 turbine site. (a) The diurnal variation of 15-day (1–15 October 2013) averaged wind speed at hub-height. The black line depicts the series corresponding to the observations, whereas the colored lines correspond to the forecasts with different experimental setups. (b) Taylor diagram shows normalized standard derivation and correlation of wind speed at hub-height for five experiments referred to observation (REF). The number of samples is 360 (1 h interval from 1 October to 15 October 2013).

five experiments is probably not significant, advantage of ACM2 is still observed. Moreover, regarding both NSD and correlation, the ACM2 prediction is the one closest to the observations. Thus, the ACM2 scheme is chosen as the optimum PBL scheme for the prediction of wind speed at the wind farm site of interest. We further substantiated this conclusion by examining the values of ME and RMSE for other two turbines, i.e., No. 7 and No. 14 in Table II, which show that the ACM2 scheme gives the best forecast for the local wind field of the target area.

C. Overall performance of WRFv3.6 model

Although the performance of WRFv3.6 does not appear highly sensitive to the PBL schemes tested, the results of the experiments above partly demonstrate that the configuration including the ACM2 PBL scheme with Pleim-Xu land surface model and Pleim-Xu surface-layer scheme works best for the wind speed prediction at the wind farm site analyzed in this study. With this configuration of the WRFv3.6 model, a six-month time series (i.e., from 00:00 UTC 2 August 2013 to 23:00 UTC 31 January 2014) of the low-level wind speed prediction was generated following the procedure described in Section II B. In this section, No. 3 turbine is first chosen as an example to show that the WRFv3.6 model is able to predict the wind speed at hub-height for the target area with reasonably good accuracy. The conclusion is then confirmed by the consistent results obtained from other 14 turbines.

Figure 6 shows the comparison between predicted (black), observed (red), and bias (green) of wind speed at No. 3 turbine site during the period from 00:00 UTC 2 August 2013 to 23:00 UTC 31 January 2014. The green dotted curve which lies close to the zero reference line reveals that the predicted raw wind speed reproduces the observation with good accuracy.

TABLE II. Error statistics of diurnal variation between WRFv3.6 forecasts and observations of wind speed at hub-height for different experiments. The verification metrics are computed over the 1–15 October 2013 period at No. 3, No. 7, and No. 14 wind turbine sites. The smallest values of ME and RMSE for each turbine are in boldface.

Experiment	QNSE		ACM2		MYJ		MYNN		YSU	
Errors / Turbine	ME	RMSE	ME	RMSE	ME	RMSE	ME	RMSE	ME	RMSE
No. 3	0.94	1.16	**0.63**	**0.87**	0.75	0.99	0.90	1.13	0.88	1.09
No. 7	0.58	0.98	**0.20**	**0.79**	0.39	0.88	0.53	0.96	0.55	0.93
No. 14	1.42	1.68	**1.08**	**1.30**	1.21	1.49	1.33	1.62	1.38	1.60

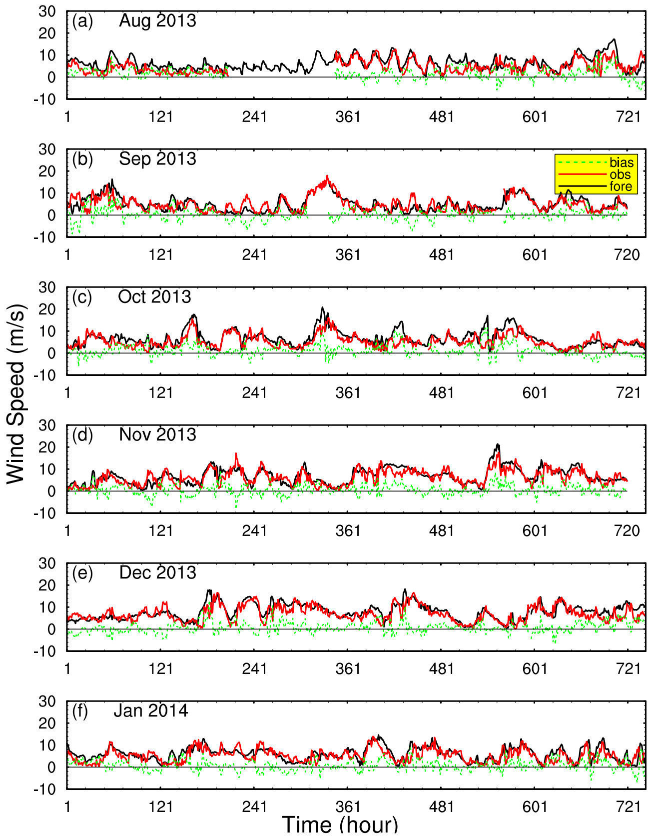

FIG. 6. Six-month series of the predicted raw (black) and observed (red) wind speed (ms^{-1}) at hub-height and bias (green) of No. 3 turbine. Panels from (a) to (f) stand for August, September, October, November, December 2013, and January 2014, respectively.

Although there are occasional large errors, in general the predicted wind speed coincides well with the observation through all six months. Similar conclusions characterized by small value of ME ($\leq$1.23) and RMSE ($\leq$2.84), as well as relatively large value of CC ($\geq$0.62) can be drawn from the statistics listed in Table III (column 5).

Table III also exhibits error statistics for other 14 turbines to ensure that the reasonable prediction for No. 3 turbine is not a success by chance. This table shows that only 3 out of 90 CC are smaller than 0.60, which indicates that the trend of predictions is in good accordance with observations. For most of turbines, the ME varies from $-1.45\,ms^{-1}$ to $2.00\,ms^{-1}$, and the smallest ME ($0.03\,ms^{-1}$) is found in December for No. 1 turbine. All predictions overestimate the wind speed. Except for a few large values (bold in Table III), the RMSE retains a relatively small value and does not change much through the six months for all turbines. All these results substantiate that the WRFv3.6 model has reasonably good forecasting skill in predicting low-level wind speed for the Awaji-island wind farm. However, the relatively large variation in MEs and RMSEs still shows the possibility to further improve the prediction of wind speed by using the Kalman filter as a post-processing approach.

D. Kalman filtered prediction

The Kalman filter procedure is applied independently to every prediction lead time. For instance, WRFv3.6 raw predictions at 00:00 UTC are revised by the Kalman filter that is updated by using the predictions and observations at the same time on the previous days ($dt = 24$ h). The first 60 days (August and September) are chosen as a training period for implementing the Kalman filter. The following discussions are all based on the statistic metrics computed over the 4-month prediction period (from October 2013 to January 2014).

TABLE III. The monthly ME, RMSE, and CC calculated with the predictions and corresponding observations of wind speed at hub-height of 15 turbines. The values of ME $\geq$ 2.00, RMSE $\geq$ 3.50, and CC < 0.60 are bold.

Month	Statistics	No. 1	No. 2	No. 3	No. 4	No. 5	No. 6	No. 7	No. 8	No. 9	No. 10	No.11	No. 12	No. 13	No. 14	No. 15
August	ME	0.89	1.39	0.51	1.06	1.05	−1.45	1.00	0.94	1.89	1.07	1.15	1.24	1.28	1.31	0.54
	RMSE	2.43	2.51	2.35	2.37	2.76	3.20	2.78	2.83	3.06	2.90	2.54	2.84	2.45	2.60	2.53
	CC	0.70	0.62	0.71	0.68	0.68	**0.54**	0.66	0.68	0.64	0.67	0.61	0.65	0.67	0.70	0.73
September	ME	0.68	0.82	0.25	0.66	0.24	1.19	0.46	0.80	1.05	1.11	1.04	0.72	0.70	0.76	0.49
	RMSE	2.70	2.76	2.63	2.91	2.90	2.72	2.93	2.70	2.77	2.84	2.68	2.71	2.70	2.77	2.48
	CC	0.71	0.72	0.73	**0.58**	0.68	0.67	0.68	0.70	0.69	0.72	0.73	0.73	0.70	0.68	**0.52**
October	ME	1.10	0.91	1.23	1.43	0.93	1.71	1.37	1.68	1.97	**2.36**	**2.17**	1.35	1.34	**2.01**	1.38
	RMSE	2.83	2.91	2.84	3.14	2.83	3.12	3.11	3.33	2.77	**3.72**	**3.90**	**3.45**	3.02	**3.59**	3.28
	CC	0.72	0.71	0.74	0.67	0.74	0.68	0.67	0.65	0.74	0.63	0.60	0.75	0.72	0.63	0.66
November	ME	0.54	0.68	0.62	0.79	1.01	1.27	0.35	0.99	1.14	1.28	1.12	0.92	0.89	1.04	0.45
	RMSE	2.75	2.67	2.74	2.42	2.64	2.65	2.22	2.51	2.52	2.60	2.60	2.34	2.54	2.47	2.41
	CC	0.70	0.74	0.68	0.78	0.75	0.78	0.81	0.78	0.79	0.77	0.85	0.80	0.78	0.80	0.78
December	ME	0.03	0.47	0.87	0.79	1.28	1.78	0.77	1.05	1.42	1.24	1.16	1.06	1.15	1.45	0.88
	RMSE	2.59	2.59	2.67	2.51	2.65	**3.54**	2.57	2.86	3.05	3.02	2.98	2.80	2.79	3.17	3.03
	CC	0.72	0.73	0.72	0.75	0.75	0.66	0.75	0.70	0.68	0.70	0.70	0.70	0.72	0.71	0.74
January	ME	0.34	0.61	0.84	0.80	0.89	1.63	1.23	1.14	1.37	1.60	1.47	1.05	1.14	1.53	0.71
	RMSE	2.49	2.45	2.58	2.34	2.44	2.77	2.58	2.57	2.75	2.74	2.74	2.54	2.58	2.82	2.52
	CC	0.72	0.71	0.66	0.74	0.70	0.70	0.69	0.72	0.69	0.70	0.72	0.76	0.70	0.70	0.71

Sections III D.1 and III D.2 present and discuss the improvement of the Kalman filter predictions for both wind speed and power in terms of the error quantifications, such as ME, RMSE, and CC. Additionally, the results of the 7-day running mean (7-day hereafter) method are also included for comparison.

1. Wind speed

A comparison of the 7-day method and the Kalman filter to correct the WRF prediction is depicted in Figure 7. It presents hourly model raw forecasts (black line) and observed wind speed at 80-m of No. 3 turbine (red line) as well as the corrected predictions using the Kalman filter (blue line) and 7-day method (green line) for the 10-day period, from 00:00 UTC 14 to 23:00 UTC 23 October 2013. Again, the WRFv3.6 model demonstrates the capability of predicting the local wind speed. Moreover, both the Kalman filter and 7-day method are able to significantly improve the raw prediction of the WRF model; particularly, the systematic bias has been largely reduced.

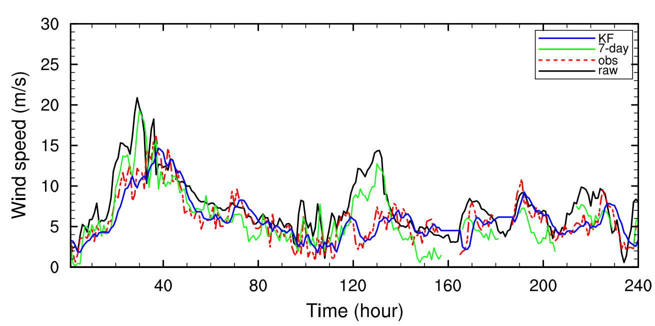

FIG. 7. Hourly WRFv3.6 model raw forecasts (black) and corresponding observations (red) of wind speed at hub-height of No. 3 turbine for the 10-day period from 00:00 UTC 14 October to 23:00 UTC 23 October 2013. The blue and green line present the predictions corrected by the Kalman filter and 7-day method, respectively.

TABLE IV. Averaged ME, RMSE, and CC of No. 3 turbine over a 10-day period of 00:00 UTC 14–23:00 UTC 23 October, 2013.

Statistic quantity / Approach / Predicted variable	ME			RMSE			CC (%)		
	Raw	KF	7-day	Raw	KF	7-day	Raw	KF	7-day
Wind speed (ms^{-1})	1.79	−0.02	0.05	2.97	1.58	2.62	69.21	85.42	71.11
Wind power (kW)	371.19	−62.43	—	762.94	443.27	—	64.26	75.53	—

When comparing the correction results of Kalman filter and the 7-day method, we see the remarkable advantage of the Kalman filter in reducing the forecasting errors. This advantage is further illustrated by the statistic parameters in Table IV. Compared to the 7-day method, the Kalman filter shows much smaller RMSE and larger CC. This may be due in part to the fact that the current Kalman filter can not only correct the systematical error but also part of stochastic uncertainties, while the 7-day method has an effect barely on the systematic bias.

The ME, RMSE, and CC of the Kalman filter and 7-day method predictions with respect to the raw WRFv3.6 prediction are shown in Figure 8 for the total 15 turbines in the Awaji-island

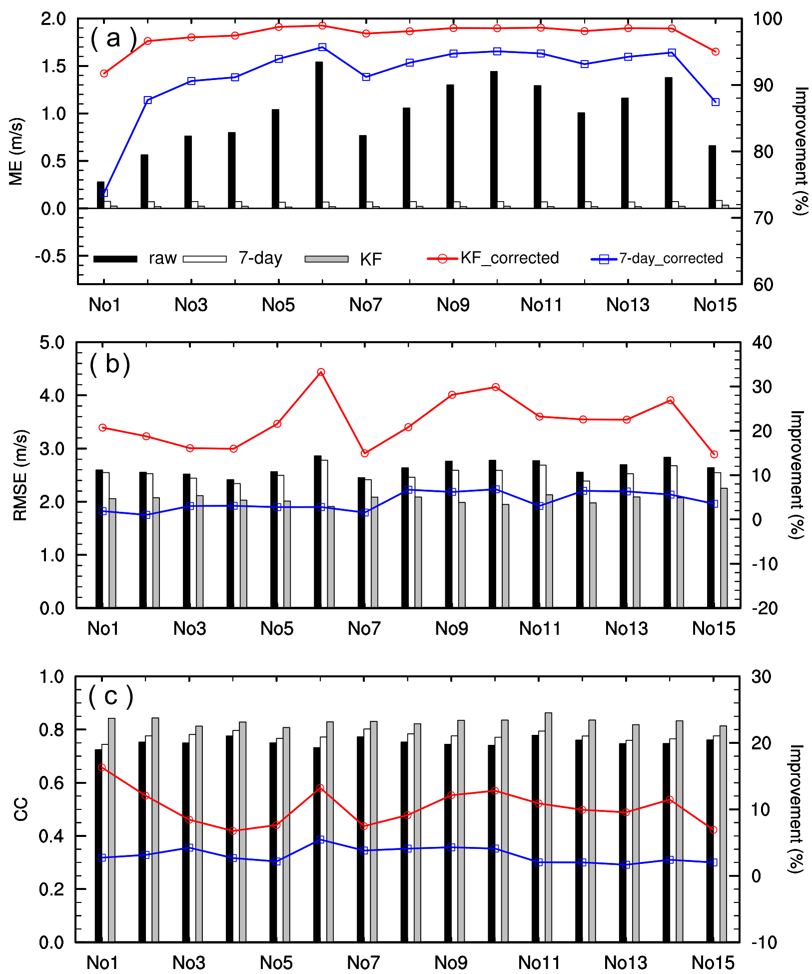

FIG. 8. A comparison of the ME (a), RMSE (b), and CC (c) for wind speed at hub-height of the Kalman filter (solid gray bar) and 7-day method (solid white bar) predictions with respect to the raw WRFv3.6 prediction (solid black bar) for the 15 turbines of the Awaji-island wind farm. The marked lines stand for the relative improvement of the Kalman filter (red) and 7-day method (blue) against the raw forecasts of WRFv3.6 model.

wind farm. From Figure 8(a), it can be seen that most of the ME of raw forecast range from 0.28 ms^{-1} to 1.54 ms^{-1}. Although the ME looks different for each turbine, both the Kalman filter and 7-day method can largely alleviate the systematic error tendency in the raw forecast of the wind speed. The reduction of ME from the Kalman filter correction ranges from 92% to 99%, while that of the 7-day method ranges from 74% to 96%. The comparison of RMSE is given in Figure 8(b). As expected, the Kalman filter reduces the 15-turbine mean RMSE by 22% which is much more significant compared to that of 7-day method (4%). Consistent to RMSE, the CC displayed in Figure 8(c) further demonstrates that the Kalman filter algorithm is superior than the 7-day method in improving wind speed forecast.

From the validations discussed above, we may conclude that (1) the raw forecasts of WRFv3.6 model with a tuned PBL package are able to produce reasonably good prediction for the wind speed at the hub height in Awaji-island wind farm site which is characterized by complex topography, and (2) the Kalman filter, as a better post-processing method against 7-day method, can significantly improve the forecasting skill for the surface wind at the target turbine site considered in this study.

2. Wind power

In this section, the power curve model described in Section II D is first tested with the dataset of No. 3 turbine over a 10-day period from 00:00 UTC 14 to 23:00 UTC 23, 2013. Then the Kalman filtered wind speed is used as an input of the power curve model to investigate whether improvement can be seen in the power output by using the corrected wind speed. The results are concluded in Table IV and Figure 9.

Figure 9 shows a 10-day example for comparing the performances of raw forecast and the Kalman filter prediction of wind power. The Kalman filter significantly improves the power output prediction. The systematic overestimation of the raw wind power forecasts is consistently reduced during the whole period. From Table IV, it can be seen that the power output from the raw wind forecast is overestimated with an ME of 371.19 kW, which has been effectively reduced down to −62.43 kW by using the Kalman filtered wind speed. Other two statistic quantities, RMSE and CC, show consistent results revealing that the Kalman filtered wind field effectively improves the power prediction. These results also indicate that given reliable wind prediction the power curve model constructed from the historic data provides reasonable projection for wind power.

Furthermore, three-month datasets (November, December 2013, and January 2014) of the total 15 turbines were used to validate the performance of Kalman filter in predicting the power output for the whole farm site. Figure 10 shows ME, RMSE, and CC of the power predictions with both raw wind speed and the Kalman filter corrected wind speed as the input of the power curve model for each turbine. It is found that the Kalman filter predictions (Figure 10(a)) improved the power output predictions for all turbines. We also show the relative improvement for each case (the right vertical axis in percentage), which reveals that the improvement brought by the Kalman filter to each turbine is different from one another. The relative improvement in

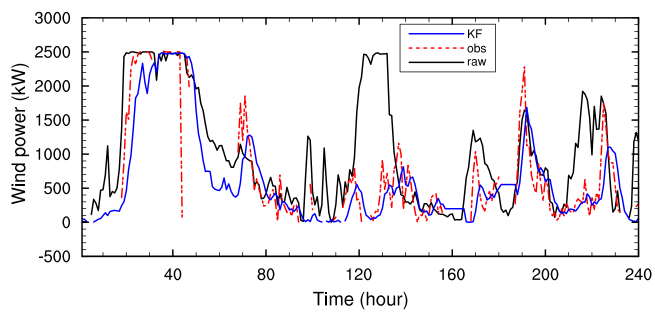

FIG. 9. A comparison of the raw wind power forecast (black) and the Kalman filter corrected prediction (blue) against the observed power output (red) for No. 3 turbine over the period from 00:00 UTC 14 to 23:00 UTC 23 October 2013.

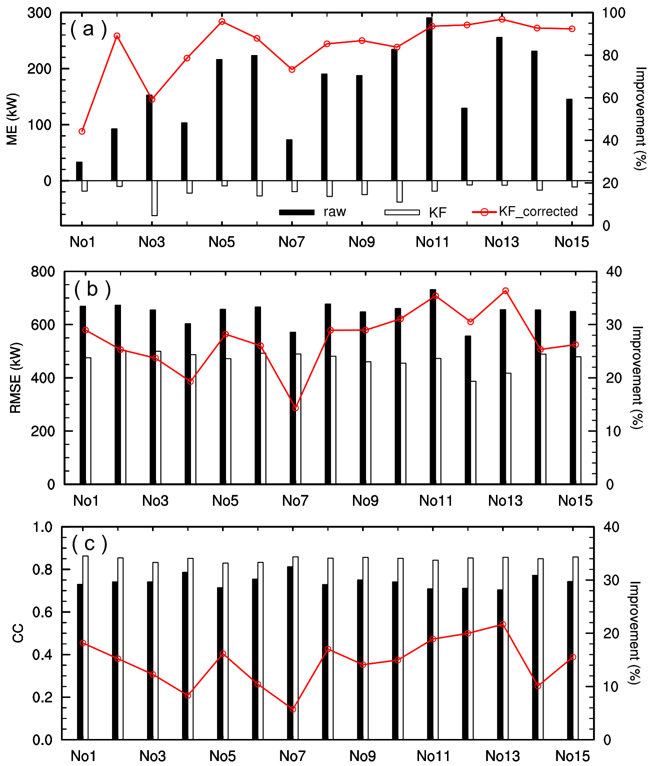

FIG. 10. A comparison of the ME (a), RMSE (b), and CC (c) of the Kalman filter (solid white bar) and the raw power forecasts (solid black bar) for the 15 turbines of the Awaji-island wind farm. The red line stands for the relative improvement of the Kalman filter against the raw forecasts of the power curve model.

ME varies from 44% to 97% with an average of 83%. As shown in Figure 10(b), the RMSE of the power forecasts for all 15 turbines is largely reduced by Kalman filter, with No. 13 being the best, having the value of relative improvement over 36%. Regarding the CC parameter displayed in Figure 10(c), the Kalman filtered wind speed leads to an averaged improvement of 15% for all 15 turbines.

From all results shown above, it can be concluded that the accuracy of power output prediction can be significantly improved when the Kalman filtered wind speed is used as the input of power curve model Eq. (9).

In the power predictions discussed above, the Kalman filter is implemented to reduce the systematical and random errors in the wind prediction of the WRFv3.6 model, which exhibit significant improvement in power prediction. However, uncertainties still remain in the power curve model as mentioned before. It motivates us to implement the Kalman filter further to reduce the uncertainties in the power curve. To this end, we carried out four experiments to evaluate the impact of Kalman filter for both wind speed prediction and power curve model as follows.

- Baseline: We use it as a controlled case, where the raw forecasts of wind speed from the WRF model are directly used to calculate the power output by Eq. (9). The Kalman filter is not used to correct either wind speed or power curve model by Eq. (9).
- KF-speed: The Kalman filter is used to correct the wind speed from the WRF model, and the corrected wind speed is used to calculate the wind power by Eq. (9).
- KF-power: The raw forecast of wind speed of the WRF model is used as the input for the power curve model by Eq. (9) and the Kalman filter is only applied to the power output.
- KF-speed and power: The Kalman filter is applied to the predictions of both wind speed and the power curve model.

The results of the four cases are shown in Table V. The larger positive value of ME for controlled case (baseline) indicates the overestimation of wind power. Having implemented the

TABLE V. The ME, RMSE, and CC of inter-comparison among four experiments with different configurations of implementing the Kalman filter. Shown are the average results for total 15 turbines.

Case	Baseline	KF-power	Improvement (%)	KF-speed	Improvement (%)	KF-speed & power	Improvement (%)
ME (kW)	142.79	−65.52	54	−21.42	85	−11.27	92
RMSE (kW)	648.43	500.64	23	470.57	27	431.32	33
CC (%)	74.24	76.37	3	84.94	14	85.46	15

Kalman filter, the ME is largely reduced, especially for cases KF-speed, and KF-speed and power showing 85% and 92% reductions in bias, respectively. Furthermore, case KF-speed and power has got the most significant reduction in RMSE and improvement in CC. Compared with the baseline case, the KF-power case demonstrates that the Kalman filter indeed makes significant positive impact on error correction of wind power curve model. This conclusion is further validated by the differences between the case KF-speed, and KF-speed and power presented in Table V.

IV. SUMMARY

In this study, we have established a hybrid forecasting system for wind power prediction, based on the mesoscale meteorological model WRFV3.6 and a Kalman filter post-processing method. The system has been validated for the targeted wind farm in Awaji-island, Japan, which is characterized by complex topographic features.

The global-scale GFS dataset is adopted as both initial and boundary conditions for the regional-scale and high resolution WRFV3.6 model through a 4-level nesting refining the horizontal grid resolution down to 1 km $\times$ 1 km for the target region. The model has been tuned, and the ACM2 PBL and the corresponding parameterization schemes were chosen for predicting the wind speed at hub height (80 m above ground) in the wind farm site. Compared to the observed wind speed of 15 turbines in the target wind farm, from 1 August 2013 to 31 January 2014, the WRFV3.6 model shows good performance in forecasting the surface wind field.

The Kalman filter presented in this study is a linear and adaptive algorithm which can minimize both the systematical and random errors by recursively combining direct model outputs with the most updated observations. It demonstrates the ability to improve the ME, RMSE, and CC in both wind speed and power predictions based on the WRFv3.6 NWP model and the empirical power curve model. As shown in Table V, Kalman filter significantly improves the raw model prediction of power by 92%, 33%, and 15% in ME, RMSE, and CC, respectively. Compared with other post-processing methods, such as MOS and 7-day method, Kalman filter is able to provide more reliable prediction with a short training period and is more flexible to adapt to any target prediction with available observation and forecasting model. However, as other statistical correction methods, Kalman filter has limited ability to predict the sudden changes in forecasting error.[44] It should be also noted that extra initial tests are always needed to successfully implement the Kalman filter presented in this study, since the correction effect depends on the ratio r $(\sigma^2_{\eta,t}/\sigma^2_{\epsilon,t})$ which is somewhat sensitive to different models and predicted variables.

In spite of these, the wind power forecasting system presented in the paper can be expected as an effective tool for short-term operational control for both single turbine and whole wind farm in a target site. Having validated the system as a hybrid wind power forecasting system of practical significance for the Awaji-island wind farm site, we are planning to adopt it to other wind farm sites in Japan.

The present research has shown the promising performance of the proposed hybrid model for wind power prediction under complex topographic conditions which feature almost all land-based wind farms in Japan. It also indicates some new directions worthy of further investigations, for example, a computational fluid dynamic model with finer grid resolution coupled with the WRF model to directly resolve the topographic effects on the surface wind field, and more reliable power curve models that include more factors and are thus able to remove the uncertainties due to the processes not reflected in the current model.

ACKNOWLEDGMENTS

This work was supported in part by Clean Energy Factory Co., Ltd., Japan.

[1]World Energy Council, see http://www.worldenergy.org/publications/2015/world-energy-issues-monitor-2015/ for 2015 World Energy Issues Monitor, 2015.
[2]Japan for Sustainability, see http://www.japanfs.org/en/news/archives/news_id035124.html/ for current status of renewable energy in Japan, 2014.
[3]W.-M. Chen, H. Kim, and H. Yamaguchi, "Renewable energy in eastern Asia: Renewable energy policy review and comparative {SWOT} analysis for promoting renewable energy in Japan, South Korea, and Taiwan," Energy Policy **74**, 319–329 (2014).
[4]M. Kay and I. MacGill, "Improving weather forecasts for wind energy applications," in *IOP Conference Series: Earth and Environmental Science* (IOP Publishing, 2010), Vol. 11, p. 012009.
[5]A. Costa, A. Crespo, J. Navarro, G. Lizcano, H. Madsen, and E. Feitosa, "A review on the young history of the wind power short-term prediction," Renewable Sustainable Energy Rev. **12**, 1725–1744 (2008).
[6]G. A. Dutton, G. Kariniotakis, J. A. Halliday, E. Nogaret *et al*., "Load and wind power forecasting methods for the optimal management of isolated power systems with high wind penetration," Wind Eng. **23**, 69–87 (1999).
[7]S. Pourmousavi Kani and M. Ardehali, "Very short-term wind speed prediction: A new artificial neural network-Markov chain model," Energy Convers. Manage. **52**, 738–745 (2011).
[8]E. Erdem and J. Shi, "ARMA based approaches for forecasting the tuple of wind speed and direction," Appl. Energy **88**, 1405–1414 (2011).
[9]A. S. Hering and M. G. Genton, "Powering up with space-time wind forecasting," J. Am. Stat. Assoc. **105**, 92–104 (2010).
[10]S. Shimada, T. Ohsawa, and K. Yatsu, "A study on the ability of mesoscale model MM5 for offshore wind resource assessment in Japanese coastal waters," in European Wind Energy Conference (EWEC) (2009), Vol. 2009.
[11]H. Sukegawa, T. Ishihara, A. Yamaguchi, Y. Fukumoto, A. Yamaguchi, T. Ishihara, and Y. Fujino, "An assessment of offshore wind energy potential using mesoscale model," in Proceedings of the European Wind Energy Conference (CD-ROM), Athens, 2006.
[12]S. Al-Yahyai, Y. Charabi, and A. Gastli, "Review of the use of numerical weather prediction (NWP) models for wind energy assessment," Renewable Sustainable Energy Rev. **14**, 3192–3198 (2010).
[13]G. J. DiMego, "The national meteorological center regional analysis system," Mon. Weather Rev. **116**, 977–1000 (1988).
[14]S. Marras, J. F. Kelly, M. Moragues, A. Müller, M. A. Kopera, M. Vázquez, F. X. Giraldo, G. Houzeaux, and O. Jorba, "A review of element-based Galerkin methods for numerical weather prediction: Finite elements, spectral elements, and discontinuous Galerkin," Arch. Comput. Methods Eng. (published online 2015).
[15]R. McTaggart-Cowan and A. Zadra, "Representing Richardson number hysteresis in the NWP boundary layer," Mon. Weather Rev. **143**, 1232–1258 (2015).
[16]H. R. Glahn and D. A. Lowry, "The use of model output statistics (MOS) in objective weather forecasting," J. Appl. Meteorol. **11**, 1203–1211 (1972).
[17]R. E. Kalman, "A new approach to linear filtering and prediction problems," J. Fluids Eng. **82**, 35–45 (1960).
[18]G. Galanis, P. Louka, P. Katsafados, I. Pytharoulis, and G. Kallos, "Applications of Kalman filters based on non-linear functions to numerical weather predictions," *Annales Geophysicae* (Copernicus GmbH, 2006), Vol. 24, pp. 2451–2460.
[19]L. Delle Monache, T. Nipen, X. Deng, Y. Zhou, and R. Stull, "Ozone ensemble forecasts: 2. A Kalman filter predictor bias correction," J. Geophys. Res. **111**, D05308, doi:10.1029/2005JD006311 (2006).
[20]P. Louka, G. Galanis, N. Siebert, G. Kariniotakis, P. Katsafados, I. Pytharoulis, and G. Kallos, "Improvements in wind speed forecasts for wind power prediction purposes using Kalman filtering," J. Wind Eng. Ind. Aerodyn. **96**, 2348–2362 (2008).
[21]H. Al-Hamadi and S. Soliman, "Short-term electric load forecasting based on Kalman filtering algorithm with moving window weather and load model," Electr. Power Syst. Res. **68**, 47–59 (2004).
[22]B. Smith, H. Link, G. Randall, and T. McCoy, "Applicability of nacelle anemometer measurements for use in turbine power performance tests," in Proceedings of the American Wind Energy Association (AWEA) WINDPOWER 2002 (2002).
[23]N. J. Cutler, H. R. Outhred, and I. F. MacGill, "Using nacelle-based wind speed observations to improve power curve modeling for wind power forecasting," Wind Energy **15**, 245–258 (2012).
[24]W. Wang, C. Bruyere, M. Duda, J. Dudhia, D. Gill, H. Lin, J. Michalakes, S. Rizvi, X. Zhang, J. Beezley *et al*., *ARW Version 3 Modeling System User's Guide* (Mesoscale & Microscale Meteorology Division, National Center for Atmospheric Research, 2010), see http://www.mmm.ucar.edu/wrf/users/docs/user_guide_V3/ARWUsersGuideV3.pdf
[25]T. T. Warner, R. A. Peterson, and R. E. Treadon, "A tutorial on lateral boundary conditions as a basic and potentially serious limitation to regional numerical weather prediction," Bull. Am. Meteorol. Soc. **78**, 2599–2617 (1997).
[26]T. T. Warner, "Quality assurance in atmospheric modeling," Bull. Am. Meteorol. Soc. **92**, 1601–1610 (2011).
[27]S.-Y. Hong and J.-O. J. Lim, "The WRF single-moment 6-class microphysics scheme (WS-M6)," Asia-Pac. J. Atmos. Sci. **42**, 129–151 (2006).
[28]E. J. Mlawer, S. J. Taubman, P. D. Brown, M. J. Iacono, and S. A. Clough, "Radiative transfer for inhomogeneous atmospheres: RRTM, a validated correlated-k model for the longwave," J. Geophys. Res.: Atmos. **102**, 16663–16682 (1997).
[29]J. Dudhia, "Numerical study of convection observed during the winter monsoon experiment using a mesoscale two-dimensional model," J. Atmos. Sci. **46**, 3077–3107 (1989).

[30]J. S. Kain, "The Kain-Fritsch convective parameterization: An update," J. Appl. Meteorol. **43**, 170–181 (2004).
[31]F. Chen and J. Dudhia, "Coupling an advanced land surface-hydrology model with the Penn State-NCAR MM5 modeling system. Part I: Model implementation and sensitivity," Mon. Weather Rev. **129**, 569–585 (2001).
[32]G. Welch and G. Bishop, "An introduction to the Kalman filter," in Proceedings of the Siggraph Course, Los Angeles (2001).
[33]L. Delle Monache, J. Wilczak, S. Mckeen, G. Grell, M. Pagowski, S. Peckham, R. Stull, J. Mchenry, and J. Mcqueen, "A Kalman-filter bias correction method applied to deterministic, ensemble averaged and probabilistic forecasts of surface ozone," Tellus B **60**, 238–249 (2008).
[34]D. J. Stensrud and J. A. Skindlov, "Gridpoint predictions of high temperature from a mesoscale model," Weather Forecasting **11**, 103–110 (1996).
[35]V. Bulaevskaya, S. Wharton, A. Clifton, G. Qualley, and W. Miller, "Wind power curve modeling in complex terrain using statistical models," J. Renewable Sustainable Energy **7**, 013103 (2015).
[36]H. H. Shin and S.-Y. Hong, "Intercomparison of planetary boundary-layer parametrizations in the WRF model for a single day from CASES-99," Boundary-Layer Meteorol. **139**, 261–281 (2011).
[37]C. Draxl, A. N. Hahmann, A. Peña, and G. Giebel, "Evaluating winds and vertical wind shear from weather research and forecasting model forecasts using seven planetary boundary layer schemes," Wind Energy **17**, 39–55 (2014).
[38]S. Sukoriansky, B. Galperin, and V. Perov, "A quasi-normal scale elimination model of turbulence and its application to stably stratified flows," Nonlinear Processes Geophys. **13**, 9–22 (2006).
[39]J. E. Pleim, "A combined local and nonlocal closure model for the atmospheric boundary layer. Part I: Model description and testing," J. Appl. Meteorol. Climatol. **46**, 1383–1395 (2007).
[40]G. L. Mellor and T. Yamada, "Development of a turbulence closure model for geophysical fluid problems," Rev. Geophys. **20**, 851–875, doi:10.1029/RG020i004p00851 (1982).
[41]Z. I. Janjić, "Nonsingular implementation of the Mellor-Yamada level 2.5 scheme in the NCEP Meso model," NCEP Office Note **437**, 61 (2002).
[42]S.-Y. Hong, Y. Noh, and J. Dudhia, "A New Vertical Diffusion Package with an Explicit Treatment of Entrainment Processes," Mon. Weather Rev. **134**, 2318–2341 (2006).
[43]K. E. Taylor, "Summarizing multiple aspects of model performance in a single diagram," J. Geophys. Res.: Atmos. **106**, 7183–7192 (2001).
[44]L. Delle Monache, T. Nipen, Y. Liu, G. Roux, and R. Stull, "Kalman filter and analog schemes to postprocess numerical weather predictions," Mon. Weather Rev. **139**, 3554–3570 (2011).

TSUBAME 2.5

Compute Node

CPU:Intel Xeon X5670 (6core) × 2
GPU:NVIDIA Tesla K20X × 3

Performance: 4.08 TFLOPS
Memory: 58.0GB (CPU)
18.0GB (GPU)

Rack (30 nodes)

Performance: 122 TFLOPS
Memory: 2.28 TB

System (58 racks)

1442 nodes: 2952 CPU sockets, 4360 GPUs
Performance: 224.7 TFLOPS (CPU) ※Turbo boost
5562 TFLOPS (GPU)
Total: 5787 TFLOPS
Memory: 116 TB

Interconnect InfiniBand QDR (40Gbps) × 2 Topology: Fat-Tree
Operating System SUSE Linux Enterprise Server 11 SP3
Job Scheduler PBS Professional

Storage System

/home	/data0	/work0,1
1.2PB	2.4PB	5.9PB
cNFS	GPFS	Lustre

TSUBAMEで利用実績のあるアプリケーション

分野	アプリケーション (「*」は、GPUに対応)
分子動力学	AMBER*, CHARMM*, DesmondMD*, GROMACS*, Lammps*, NAMD*, Tinker, VSOP, etc.
量子化学	ABINIT-MP, GAMESS*, Gaussian, OpenMX, PHASE, Quantum Espresso*, VASP*, etc.
バイオ	BLAST, MEGADOCK*, etc.
流体	ANSYS Fluent*, OpenFOAM*, Particleworks*, Power Flow, Star-CCM+, etc.
構造	Abaqus*, ANSYS Mechanical*, COMSOL Multiphysics, LS-DYNA*, MSC Nastran*/Marc*, etc.
電磁界	ANSYS HFSS*, CST MW-Studio*, KeySight EMPro*, Remcom XFdtd*, etc.
その他	MATLAB*, R*, Caffe*, Chainer*, Python*, WRF, ParaView*, POV-RAY, AVS, etc.

TSUBAME共同利用サービスの利用実績

利用区分			2007年度	2008年度	2009年度	2010年度	2011年度	2012年度	2013年度	2014年度	2015年度	合計
学術利用	HPCI		-	-	-	-	-	6	5	10	14	35
	JHPCN		-	-	-	4	6	5	11	10	10	46
	有償利用		-	-	1	4	9	14	17	22	23	90
産業利用	無償利用		11	15	15	8	10	12	21	17	13	122
	有償利用	成果公開	-	-	3	6	7	9	8	10	8	51
		成果非公開	-	-	2	7	6	4	10	12	10	51
合計			11	15	21	29	38	50	72	81	78	395

お問い合わせ ● 東京工業大学 学術国際情報センター 共同利用推進室
● e-mail kyoyo@gsic.titech.ac.jp Tel. 03-5734-2085 Fax. 03-5734-3198

詳しくは **http://www.gsic.titech.ac.jp/tsubame/**

GSIC Global Scientific Information and Computing Center

201609

■ GPUの大量搭載による高性能計算ノード

計算ノードはThin、Medium、Fatの3種類のノードから構成されています。演算性能の殆どを占めるThinノードは17/2インチ幅、高さ2UのサイズにCPUを2個、KeplerコアのGPUを3個搭載するコンパクトな設計になっています。さらにQDR InfiniBand HCAを2つ接続しつつPCI Express Bus の通信帯域を確保しています。電源ユニットも3+1に多重化され、高信頼性も兼ね備えています。

Thinノード　1408ノード

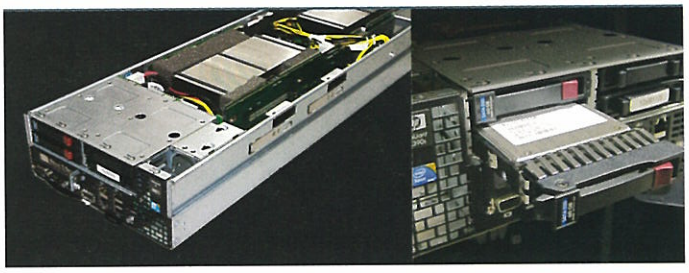

HP ProLiant SL390s G7

CPU :　Intel Xeon X5670 (Westmere-EP, 2.93GHz, 3.196GHz@Turbo boost)
　　　×2 ソケット　ソケットあたり 6 コア, ノード内合計 12 コア
GPU :　NVIDIA Tesla K20X (GK110) ×3, GPU1 個あたり 1.31TFLOPS, VRAM 6GB
Memory : 58GB DDR3 1333MHz　一部 103GB
SSD :　ノードあたり 120GB (60GB×2)　一部 240GB (120GB×2)
Network: 4X QDR InfiniBand ×2

Mediumノード　24ノード

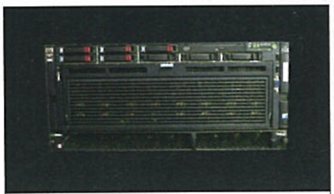

HP ProLiant DL580 G7

CPU:　Intel Xeon X7550
　(Nehalem-EX)
　2.0 GHz ×4 sockets
　(32cores/node)
GPU:　NVIDIA Tesla S1070
　(NVIDIA Tesla C1060×4) or
　NextIO vCORE Express 2070
　(NVIDIA Tesla M2070×4)
Memory:137 GB (DDR3 1066MHz)
SSD:　120GB ×4 (480GB/node)
Network: 4X QDR InfiniBand

Fatノード　10ノード

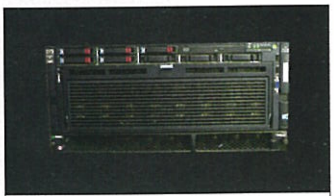

HP ProLiant DL580 G7

CPU:　Intel Xeon X7550
　(Nehalem-EX)
　2.0 GHz ×4 sockets
　(32cores/node)
GPU:　NVIDIA Tesla S1070
(NVIDIA Tesla C1060×4)
Memory:　274 GB (8 nodes) ,
　548 GB (2 nodes)
　DDR3 1066MHz
SSD:　120GB ×5 (600GB/node)
Network: 4X QDR InfiniBand

Thinノード　ブロック図

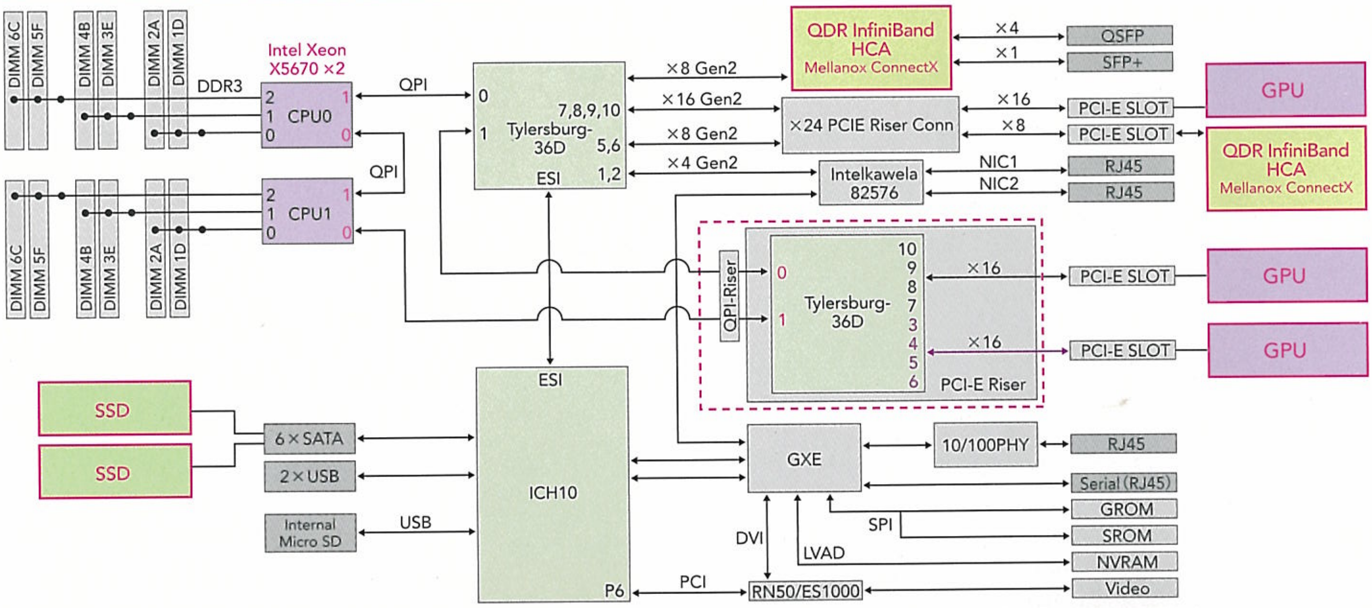

GPUの詳細

K20X Architecture (Kepler GK110 Core)

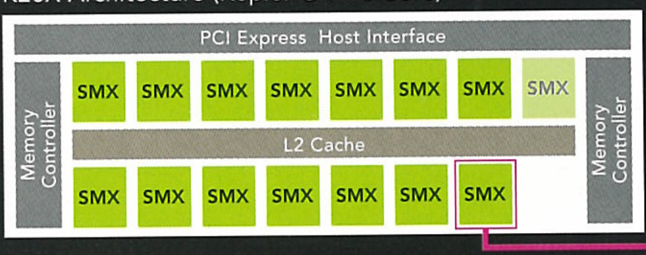

・ピーク性能：1.31 TFLOPS（倍精度）
　　　　　　　3.95 TFLOPS（単精度）
・シェーダクロック：732 MHz
・CUDA コア（SP）数：2,688 cores
・Streaming Multiprocessor（SMX）：14 SMX
・ライタブル L2 キャッシュ：1.5MB
・メモリ帯域：250GB/s
・メモリクロック：2.6GHz（GDDR5）
・ECC メモリ：内部及び外部メモリ
・オンボードメモリ：6GB

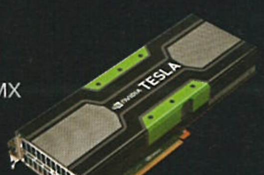

SMX の詳細

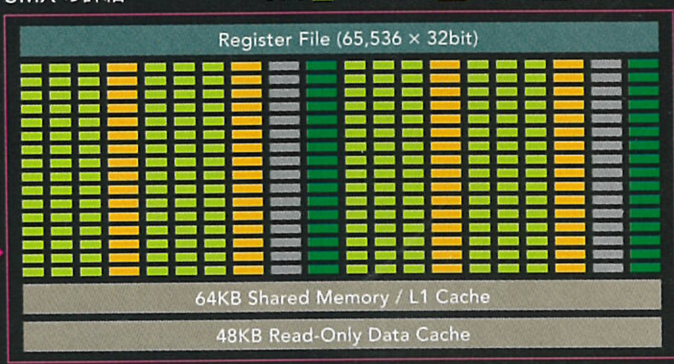

・CUDA コア（SP）/ SMX：192 cores
・DP ユニット / SMX：64　・SFU / SMX：32
・WARP スケジューラ / SMX：4 units
・シェアードメモリ / SMX：16KB or 32KB or 48KB
・ライタブル L1 キャッシュ / SMX：48KB or 32KB or 16KB
・リードオンリー・データキャッシュ / SMX：48KB

■ 高速ネットワークによる内部接続

TSUBAME2.5ネットワークはDual-Rail QDR InfiniBandをベースに構成され、計算ノード間はFat-Tree型のインターコネクションにより
フル･バイセクションバンド幅として200Tbpsを達成しています。計算ノード間End-to-Endの遅延もマイクロ秒オーダーと非常に小さく高速であり、
高信頼ストレージとも高速に接続しています。このネットワークは総計100Km, 3000本あまりの光ファイバーケーブルにより支えられています。

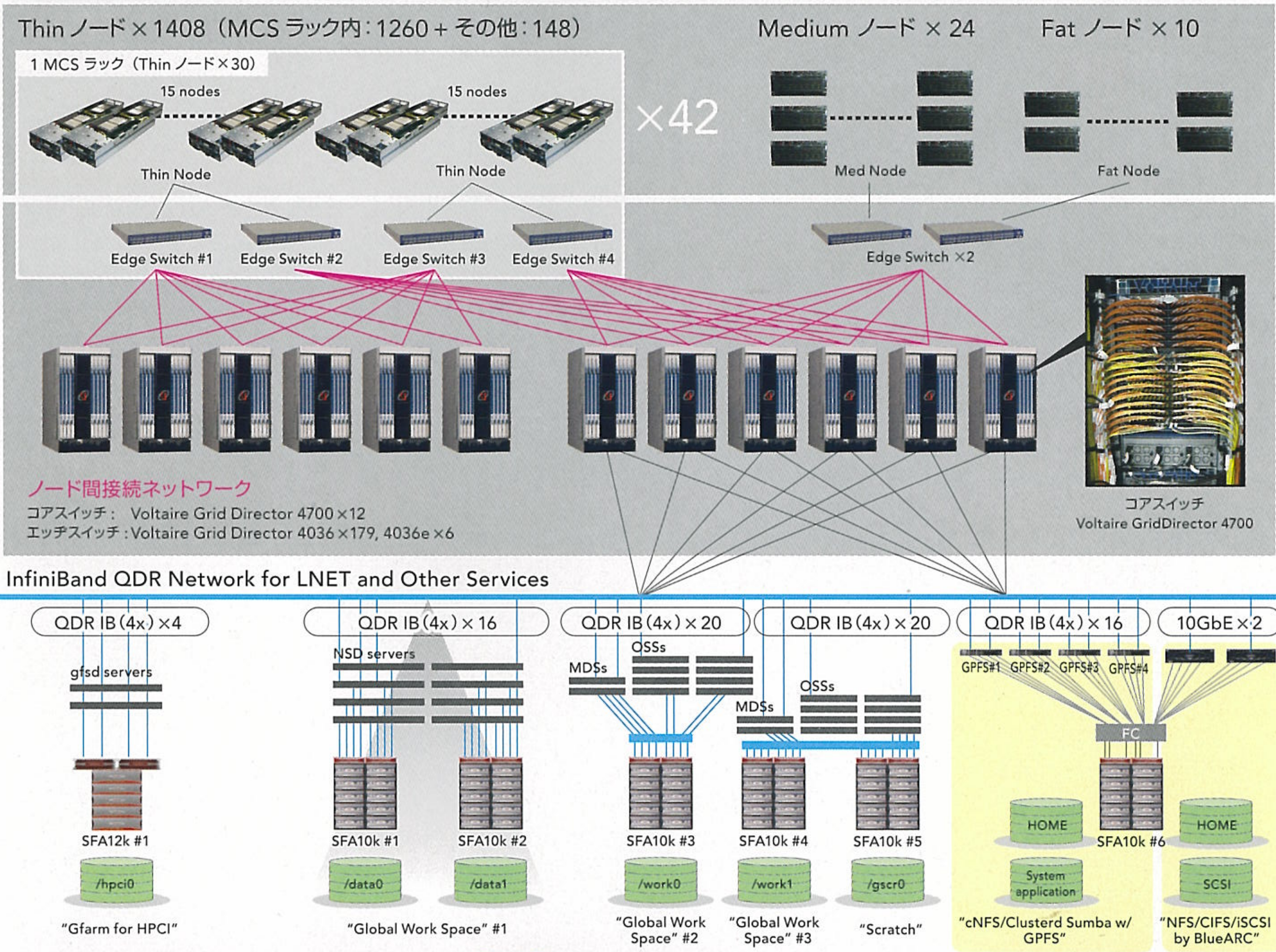

HPCI

Gfarm: ～600TB

gsfd server:
HP ProLiant DL360p Gen8 × 2
Intel XeonE5 2640 × 2,
64 GB Mem,
QDR IB (4x) × 2

Storage:
DDN SFA12k × 1
4TB SAS HDD × 155 disks

GPFS with HSM

GPFS 2.4 PB

NSD server: HP ProLiant DL380 G6 × 4
Intel Westmere EP × 2,
48GB Mem, QDR IB (4x) × 2
HP ProLiant DL360 G6 × 4
Intel Westmere EP × 2,
24GB Mem,
QDR IB (4x) × 2

Storage: DDN SFA10k × 2
2TB SATA HDD × 1180 disks
600GB SAS HDD × 20 disks

Lustre

Lustre 3.6 PB

MDS : HP ProLiant DL360 G6 × 4
Intel Westmere-EP × 2,
48GB Mem, QDR IB (4x) × 2

OSS : HP ProLiant DL360 G6 × 16
Intel Westmere-EP × 2,
24GB Mem,
QDR IB (4x) × 2

Storage: DDN SFA 10k × 3,
2TB SATA HDD × 1770 disks,
600GB SAS HDD × 30 disks

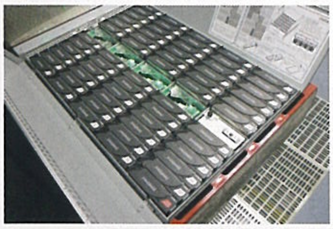

Home

Home 1.2 PB

cNFS (GridScaler)/Clustered Sumba w/ GPFS:
HP ProLiant DL380 G6 × 4
Intel Westmere EP × 2,
48GB Mem, QDR IB (4x) × 2

NFS/CIFS/iSCSI:
BlueArc Mercury 100 × 2
10Gbps × 2

Storage: DDN SFA 10k × 1
2TB SATA HDD × 600 disks

■ 高速･高信頼性ストレージ

TSUBAME2.5は、各計算ノードに備えたスクラッチ出力用の合算約190TBのSSD、高速なI/Oを行うための5.9PBのLustre、
GPFSなどの並列ファイルシステム領域、クラウドサービス用の1.2PBのホーム領域、GPFS並列ファイルシステムと連動し
階層型ストレージを構成する4PB超のテープライブラリなど、使用目的に応じて多様な計11PBもの莫大なストレージ領域を提供します。

■ 低消費電力・グリーン運用

Linpackベンチマーク電力性能：3068.71（MFLOPS/W）
システム機器ピーク消費電力：　1620（KW）
システム機器平均消費電力*：　698（KW）
システム機器アイドル消費電力：470（KW）
年間平均PUE：　1.285

「*」平均消費電力はTSUBAME 2.0実績の年間平均

冷却：Modular Cooling System

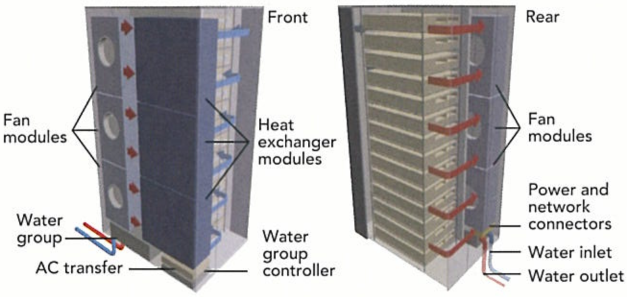

ラック内に熱交換システムを内蔵した密閉型水冷システムにより、通常のデータセンターに比べ高密度な世界トップクラス（ラックあたり最大35KW）の冷却が可能です。サーバの吸入口に均質な冷却風を提供し、ドア開閉は自動化・加湿不要となっています。完全自動温度制御による最適な消費電力点の制御を行い、95%から97%の熱を水冷で除去することが可能です。また、ポリカーボネート製のドアは大幅なノイズ削減にも貢献しています。

- 空調機器ピーク消費電力：460（KW）
- 空調機器平均消費電力*：204（KW）

グリーン運用：環境モニタリング

計算機ルームだけではなく、計算ノード、ラック毎の温度、消費電力などをリアルタイムで監視しています。

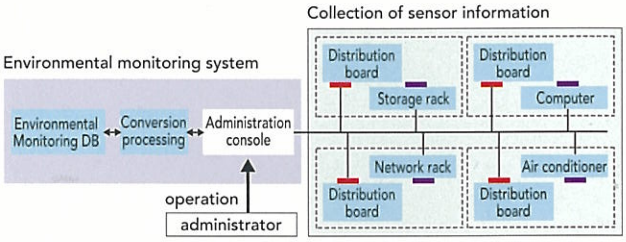

狭い設置面積

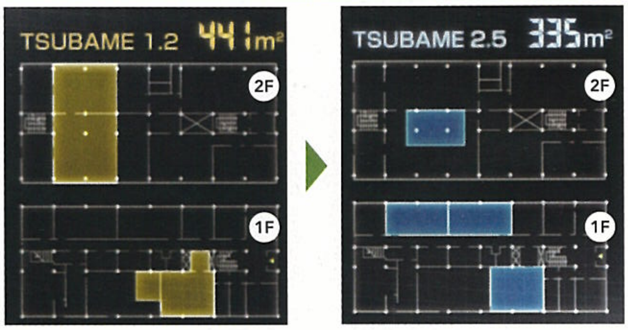

TSUBAME 1.2から性能が70倍以上向上したのに設置面積は逆に狭くなっています。

■ System Software　WindowsとLinuxを動的に切り替える“Dynamic provisioning”

ジョブ管理システムとクラスタ管理システムを連携させてユーザ環境を管理し、ノードプールから計算リソースを取り出して足りない部分に配分します。Linux用とWindows用のバッチスケジューラにより計算ノードを管理し、ノードの動的な増加・削減に対応しています。仮想マシンの実行をサポートし、それらもジョブスケジューリングの対象として管理します。

OS	SUSE Linux Enterprise Server 11 SP1 Windows HPC Server 2008 R2
バッチシステム	PBS Professional

■ ISV（commercial） Software

（「*」は GPU 対応または一部対応）（2013年11月現在）

Compilers, Debuggers and Libraries

Intel Compiler（C/C++/Fortran）
PGI Compiler*
（C/C++/Fortran, OpenACC, CUDA Fortran）
Total View Debugger*
CAPS Compiler*（HMPP, OpenACC）
CULA*（Numerical Libraries for CUDA）

Applications

ANSYS Fluent*, Workbench*
MSC Nastran*
LS-DYNA
Gaussian, Gauss View
Molpro
Scigress
MATLAB*
AVS/Express, AVS/Express PCE
ABAQUS*, ABAQUS CAE
Patran
CST STUDIO SUITE*（MW-Studio*）
AMBER*
Materials Studio, Discovery Studio
Mathematica*
Maple*
EnSight

■：全てのユーザ使用可能ライセンス　■：学内ユーザのみ使用可能ライセンス　■：産業利用のユーザのみ使用可能ライセンス

発行：東京工業大学 学術国際情報センター

〒152-8550 東京都目黒区大岡山 2-12-1　電話:03-5734-2087　FAX:03-5734-3198　E-mail:tsubame@gsic.titech.ac.jp

http://www.gsic.titech.ac.jp/

201311

みんなのスパコン TSUBAME 共同利用サービスは、ピーク性能 5.7PFlops、1400ノード、16800CPU コア、4200GPU 搭載、世界トップクラスの東京工業大学のスパコン TSUBAME 2.5 を東京工業大学以外の皆さまにもご利用いただくため の制度です。

TSUBAME 共同利用サービスの利用区分とカテゴリ

TSUBAME 共同利用サービスには「学術利用」と「産業利用」の利用区分があります。
「学術利用」は、HPCI（革新的ハイパフォーマンスコンピューティングインフラ）、JHPCN（学際大規模情報基盤共同利用・共同研究拠点）の採択により無償でご利用になれる制度と、東京工業大学学術国際情報センターが実施する有償の制度がご利用になれます。
「産業利用」は、HPCI の採択により無償でご利用になれる制度と、東京工業大学学術国際情報センターが実施する有償の制度があり、有償の制度には利用目的や利用成果を非公開とする「成果非公開」のカテゴリもあります。

TSUBAME 共同利用サービスの利用料金

TSUBAMEにおける計算資源は口数を課金単位としております。1口は3000ノード時間積で、1計算ノード（12CPUコア, 3GPU, 58GBメモリ搭載）を 3000 時間、あるいは 300 計算ノードを 10 時間というように、ご利用の用途に合わせ自由にご利用になれます。TSUBAME 共同利用サービスの利用区分・カテゴリ・利用料金を下表に示します。

利用区分	利用者	制度	募集時期	申請および審査	成果	利用料金（税別）
学術利用	他大学または研究機関等	HPCI	年1回 10月頃	HPCI 運用事務局（高度情報科学技術研究機構）	公開	無償
		JHPCN	年1回 1月頃	JHPCN 拠点事務局（東京大学 情報基盤センター）	公開	無償
		TSUBAME学術利用	随時募集中	東京工業大学 学術国際情報センター	公開	1口：120,000円
産業利用	民間企業	HPCI 実証利用	年1回 10月頃	HPCI 運用事務局（高度情報科学技術研究機構）	公開	無償
		HPCI トライアルユース	随時募集中			
		TSUBAME 産業利用	随時募集中	東京工業大学 学術国際情報センター	公開	1口：120,000円
					非公開	1口：480,000円

TSUBAME 共同利用サービスの利用申請フロー

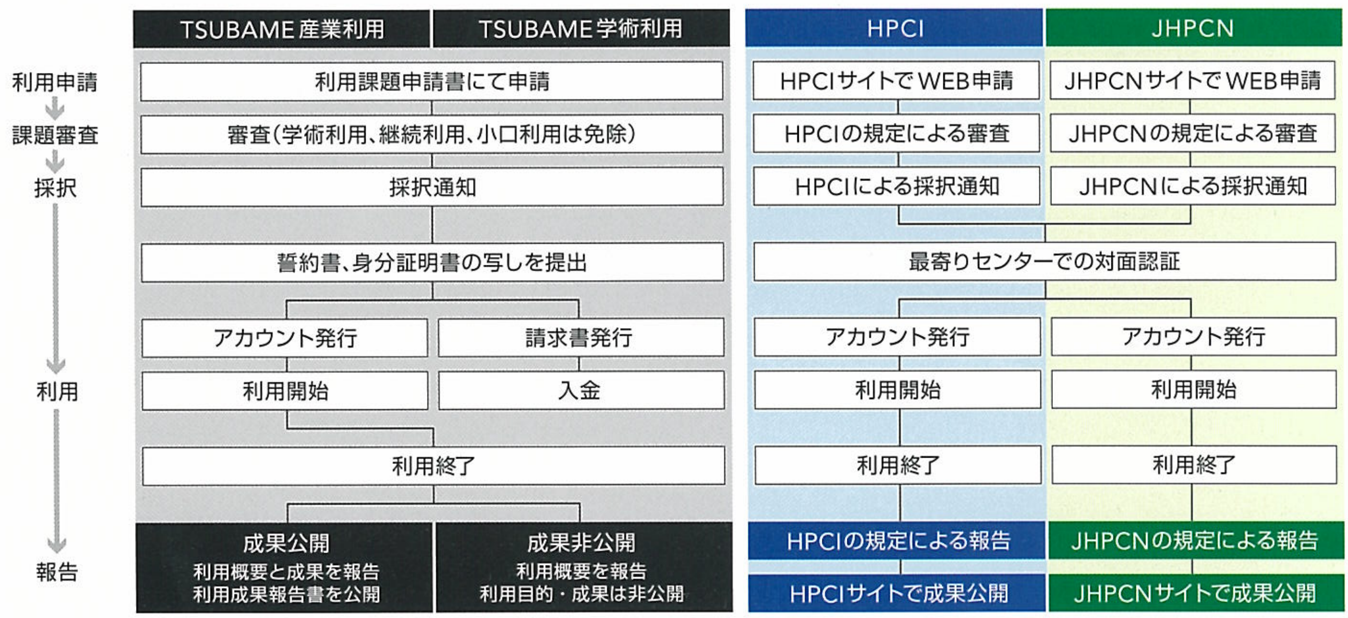

建築物の室内外環境の連成解析と
その高速化技術の開発

清水建設株式会社 技術研究所

室内外環境の連成解析モデルとその解析例

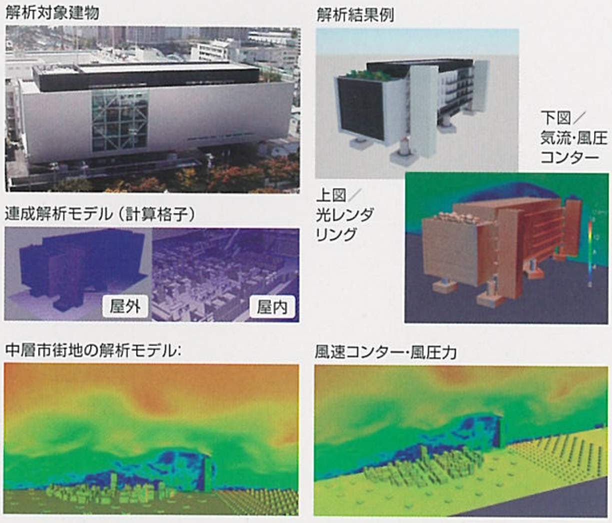

建築物の快適な室内環境の創出及び居住性の向上の他，その建築物の運用による環境への負荷を最小限に抑えるために、屋外の自然環境の活用及びその環境の変化に応じる室内設備の制御による室内外環境の連成解析の実施が必要となる。その連成解析は非常に大規模となり、通常の計算機で実施することは困難であるため、大規模計算クラスタや高速な計算方法の確立が必要となる。本件利用は、スパコンTSUBAMEの計算資源を利用することで、建築物の室内外環境の解析モデル及び連成解析システムを構築し、超並列CPU及びGPUによる数値解法を開発するとともに、大規模計算による建築物の室内外環境の評価を可能にする。

拡張アンサンブルシミュレーションによる
タンパク質とリガンドの結合構造予測法の開発

武田薬品工業株式会社 医薬研究本部 探索研究センター

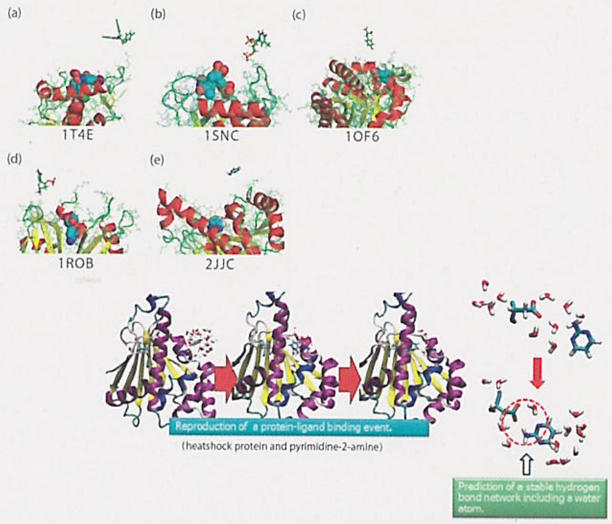

タンパク質と結合するリガンドの結合構造の予測法を開発した。我々の方法は拡張アンサンブル法の一つであるレプリカ交換アンブレラサンプリング法と、平均力ポテンシャル、主成分軸上のリガンド自由エネルギー地形解析に基づいた方法である。テストケースとして5つのタンパク質リガンド複合体系に適用したところ、タンパク質とリガンドが完全に離れた状態からシミュレーションを始めて、PDBに登録された実験構造と類似した結合構造を予測することに成功した。これは、タンパク質-リガンド結合過程におけるタンパク質、リガンド及び溶媒水のエンタルピー・エントロピー効果や結合に伴う構造変化を原子レベルで取り入れた初めての計算であり、水分子を含んだ安定な水素結合ネットワークを予測することができた。

ワイドギャップナノ構造体
精密加工のシミュレーション

日本電気株式会社 グリーンイノベーション研究所

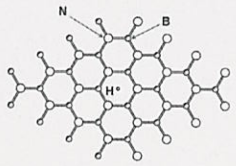

今回のシミュレーションの配置。
入射する方向より、hBN膜を見ている。
H+の位置が入射のインパクトポイント。

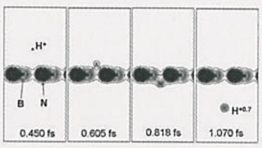

高速でプロトンが
hBNを通過する際の
全電荷分布移動の様子。
表示の時間はシミュレーション中の時間

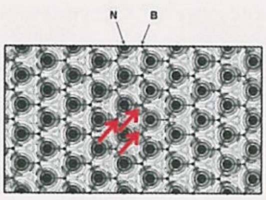

電荷分布と通常のhBNの電荷分布の差。
赤い矢印はプロトンが通過した周辺に
局在する正孔の存在を示した。

BNナノチューブを電子励起やCoulomb explosionなどで構造変化させることを、シミュレーションで調べる目的をもつ。その準備段階として、時間依存密度汎関数理論を応用して電子とイオンの運動を扱う計算コードの安定動作を、TSUBAME上にて確認した。テストケースとして、プロトンがhBN層を通過する計算を行い、hBN層内の電子集団励起によるプロトンの制動、プロトンより注入された正孔が、一瞬だけプロトンがhBN層を通過した点に局在することが観測でき、この計算コードがTSUBAME上で安定に動作し、今後予定しているさまざまな研究テーマに応用可能であることを確認した。

高層ビルの大規模非線形
地震応答解析

株式会社アライドエンジニアリング

TSUBAME16ノード
4コアを使用した
固有値解析を行った。
1次と4次モードは
短辺方向並進1次と2次、
2次と3次および5次と6次は
長辺方向並進とねじれの
連成1次と2次である。

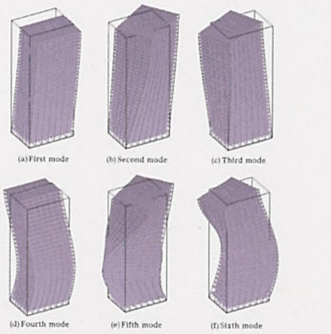

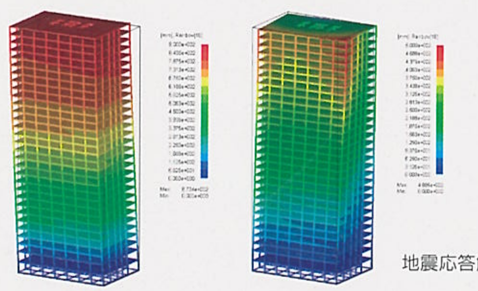

地震応答解析

建築構造物をソリッド要素を用いて標準的な有限要素法解析を行う試みは、実施者らの知り得る限り，世界的に見ても例がない。当社は，汎用並列有限要素法コードADVENTUREClusterソルバに大規模地震応答解析の機能を備えるべく開発を進めている。本課題ではTSUBAMEの並列性能を最大限引き出し大規模地震応答解析コードの実用化を目指した。

Wind energy research in INER

Lin, Yanting
Research associate
yantinglin@iner.gov.tw

Mechanical and systems engineering program

Institute of Nuclear Energy Research
Atomic energy council, ROC

Research objectives

R/D in Wind energy systems

- Small and medium scale wind turbine
  - Reliability and durability testing of 5 kW VAWT
  - System refinement and improvement of 150kW/25kW HAWT
  - Integrated system for design and analysis of wind turbine systems
- Large and offshore scale wind turbine
  - Load calculations of NREL 5MW reference wind turbine
  - Verification procedures of offshore wind turbine design
  - Development and testing of self-diagnosis system

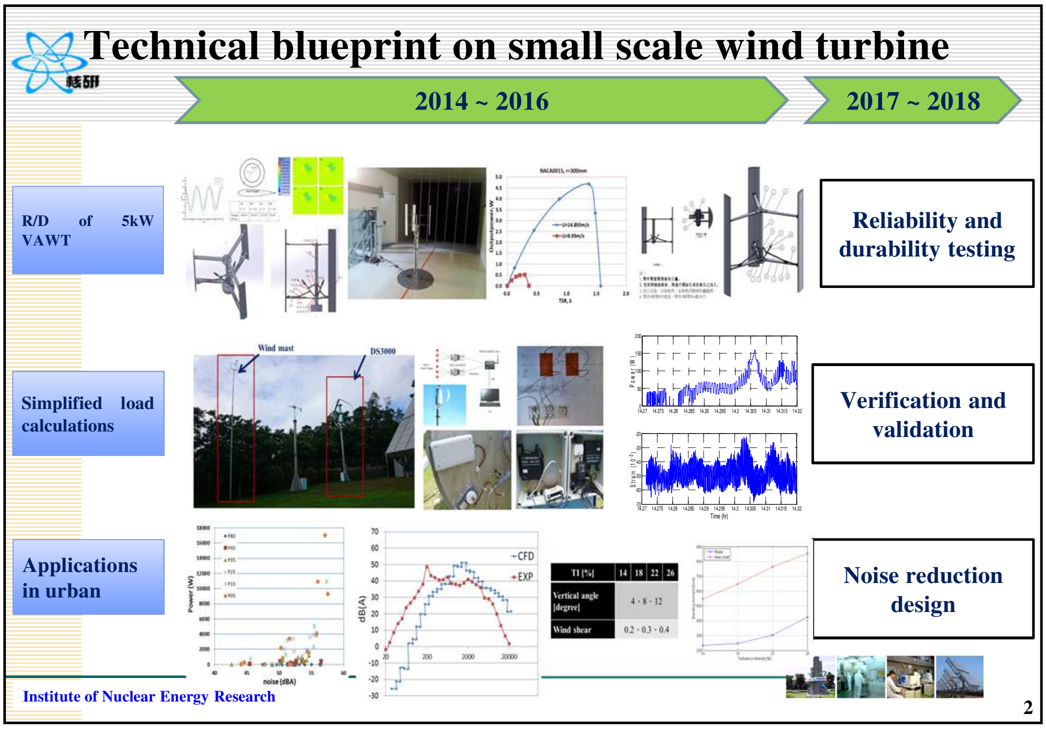
Technical blueprint on small scale wind turbine
2014 ~ 2016
2017 ~ 2018
R/D of 5kW VAWT
Reliability and durability testing
Simplified load calculations
Wind mast
DS3000
Verification and validation
Applications in urban
CFD
EXP
Noise reduction design
Institute of Nuclear Energy Research
2

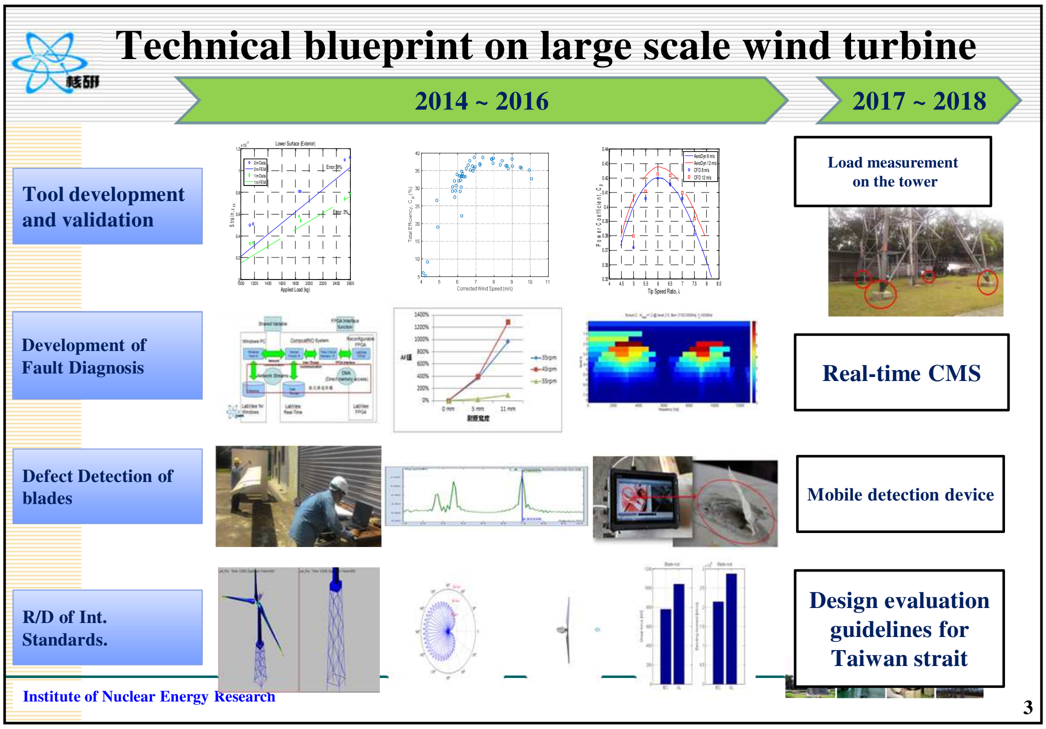
Technical blueprint on large scale wind turbine
2014 ~ 2016
2017 ~ 2018
Tool development and validation
Load measurement on the tower
Development of Fault Diagnosis
Real-time CMS
Defect Detection of blades
Mobile detection device
R/D of Int. Standards.
Design evaluation guidelines for Taiwan strait
Institute of Nuclear Energy Research
3

Testing and Verification Platform of INER 25kW and 150kW wind turbines-1/7

■ Development path of 25kW wind turbine

2005~2006	2007~2010	2011~2012	2013~now
25 kW-1st	25 kW-2nd	Modified 25 kW-2nd	Testing and Verification Platform




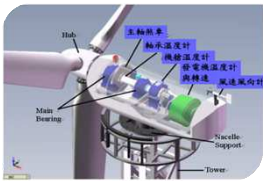

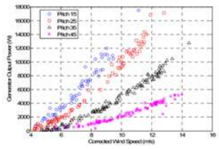
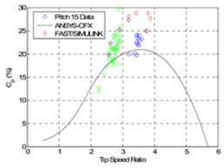

Testing and Verification Platform of INER 25kW and 150kW wind turbines-2/7

■ **25kW specification**

Standard	IEC 61400-1
IEC class	Class-IA
Blade number	3
Turbine type	Up-wind
Rated output power	25 kW
Hub height	25 m
Tower type	Monopile
Cut-in speed	4 m/s
Rated speed	12 m/s
Cut-out speed	22 m/s
Rated RPM	55~65 RPM
Pitch angle control	Active control: 0° ~ 90°
Yaw angle control	Active control: ±180°
Rotating diameter	12.46m

IEC Standard

- IEC 61400-1: Design requirements
- IEC 61400-2: Design requirements for small wind turbines
- IEC 61400-12-1: Power performance measurements of electricity producing wind turbines
- IEC TS 61400-13: Measurement of mechanical loads
- IEC 61400-22: Conformity testing and certification
- IEC TS 61400-23: Full-scale structural testing of rotor blades

GL Guideline

- Guideline for the certification of wind turbines (2010)

CNS 15176

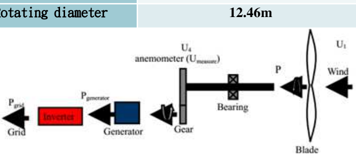

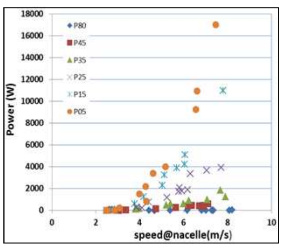

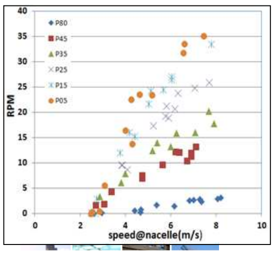

Testing and Verification Platform of INER 25kW and 150kW wind turbines-3/7

Development path of 150kW wind turbine

2005~2006 | 2007~2008 | 2009~2010 | 2011~2012 | 2013~2014

25 kW-1st

150 kW HAWT -1st

150 kW HAWT -2nd

Testing and Verification Platform of INER 25kW and 150kW wind turbines-4/7

150kW specification

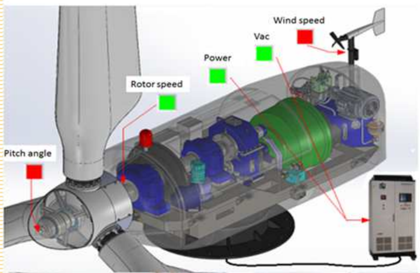

Standard	IEC 61400-1
IEC class	Class-IA
Blade number	3
Turbine type	Up-wind
Rated output power	150 kW
Hub height	50 m
Tower type	Frame
Cut-in speed	3 m/s
Rated speed	12 m/s
Cut-out speed	25 m/s
Rated RPM	45~50 RPM
Pitch angle control	Active control: 5º ~ 85º
Yaw angle control	Active control: ±180º
Rotating diameter	22.8m
Gear ratio	1 : 20
Electric generator	induction generator

Testing and Verification Platform of INER 25kW and 150kW wind turbines-5/7

■ **Measurement and Analysis of Acoustic Noise of 25kW wind turbine**

Hz	20	25	31.5	40	50	63	80	100	125	160	200
dB(A)-Pitch 05	20.9	25.3	28.7	31.4	33.8	36.4	35.4	37.8	50.2	37.7	43.2
dB(A)-Pitch 80	24.9	23.3	27.4	34.5	37.7	38.6	41.6	44.6	51.4	47.5	47.3
	total dB(A)	51.79 @Pitch 05			total dB(A)	44.48 @Pitch 80					

IEC 61400-11 & ISO 1996-2:2007 Annex D

6.3Hz to 20Hz :	18dB
25Hz to 125Hz :	15dB
160Hz to 400Hz :	8dB
500Hz to 10kHz :	6dB
12.5kHz to 20kHz :	6dB

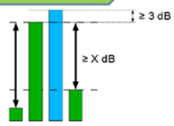

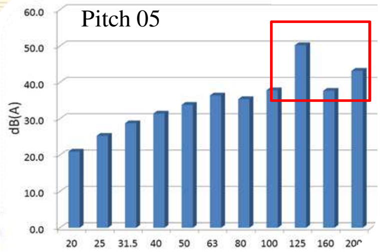

EPA Noise Regulations in low frequency (20-200Hz) and overall noise level

頻率 / 時段 / 音量 / 管制區	20Hz 至 200Hz		
	日間	晚間	夜間
第一類	39	39	36
第二類	39	39	36
第三類	44	44	41
第四類	47	47	44

overall noise level (20-20kHz) (indoor)

- **Overall in day and evening** <50dB(A)
- **Overall in night**< 40dB(A)
- **Or overall-background=-**5dB(A)

(overall=wind+back)

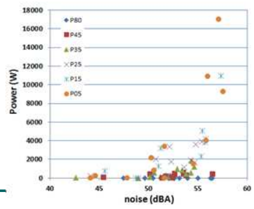

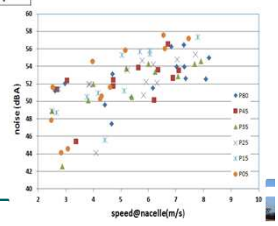

Testing and Verification Platform of INER 25kW and 150kW wind turbines-6/7

■ **Measurement and Analysis of Acoustic Noise of 25kW wind turbine**

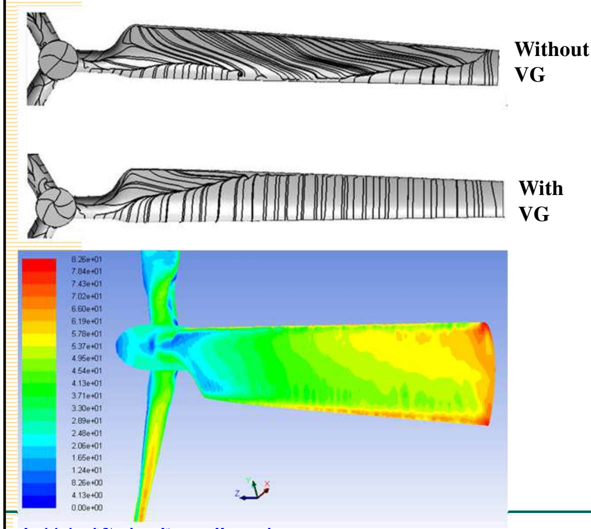

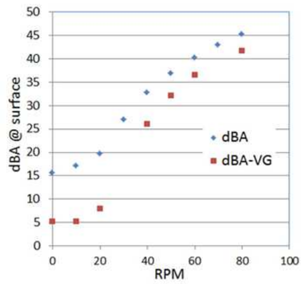

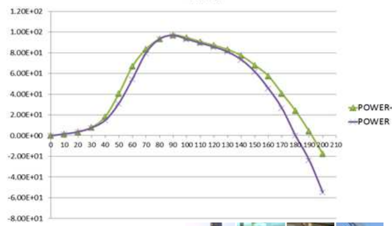

Testing and Verification Platform of INER 25kW and 150kW wind turbines-7/7

- An experimental and numerical investigation on the 150kW wind turbine

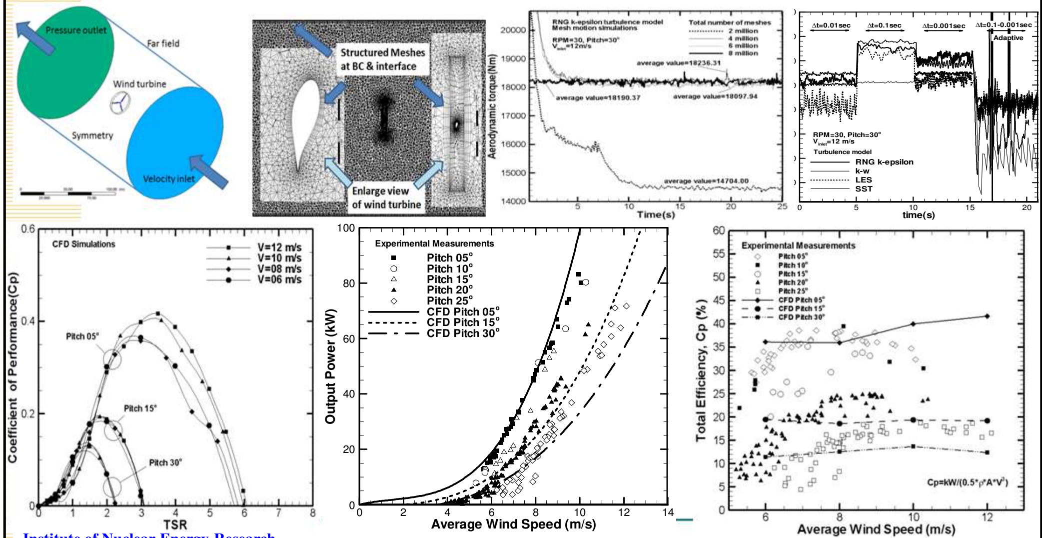

Small wind turbine design evaluation laboratory-1/4

- Path TAF laboratory

2005~2008	2008~2009	2009-2011	2011-2012	2012-2013
Team established	Evaluation of development	IEC 61400-1 and -2 design evaluation	SWTDE lab.	TAF Lab. approved

- ISO 9001、ISO 17025、ISO Guide 65➔CNS 15176-2
- ISO 17025 specifies the general requirements for the competence to carry out tests and/or calibrations, including sampling. It covers testing and calibration performed using standard methods, non-standard methods, and laboratory-developed methods.

INER, AEC
↓
Mechanical and systems engineering program
↓
SWTDE lab.
↓
Supervisor：W. Sue
↓
Quality control | Analysis group

Small wind turbine design evaluation laboratory-2/4

■ Voluntary Product Certification(VPC) by BSMI

CNS 15176-2 (2011,2013rev), -11, -12-1,
CNS 15176-2-1 (2012)

- UK BWEA(2008)
- US AWEA9.1(2009)
- Japan JSWTA(2013)
- IEC61400-2ed3(2013)

INER

Design Assessment Reports

International Certification Scheme

SWCC, MCS, JSWCC
TUV-NEL, DNV, Intertek, ClassNK….

VPC Taiwan

Type Testing Reports

Governmental Incentive Programs

Penghu test site (TERTC)

Qigu test site (MIRDC)

Small wind turbine design evaluation laboratory-3/4

■ TAF laboratory-Small wind turbine design evaluation

- TUV NORD evaluation
- DNV evaluation
- Hi-vawt Co.3kW VAWT
- EPISTAR Co. 4.8kW HAWT
- On US SWCC Consultants list

Small wind turbine design evaluation laboratory-4/4

- **Load measurements of blades on VAWT**
  - Verification of Simple load calculations
  - Strain dependence of wind speed and RPM

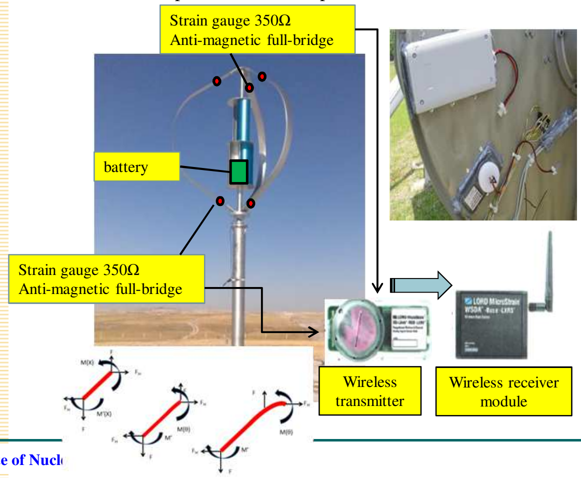

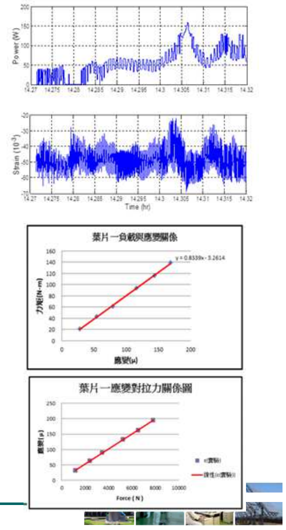

R/D of 5kW Vertical axis wind turbine-1/3

- **Joint development -Passive pitch control of VAWT**

- Simplified load calculations
- Numerical simulations
- Wind tunnel verification
- Dynamic load analysis

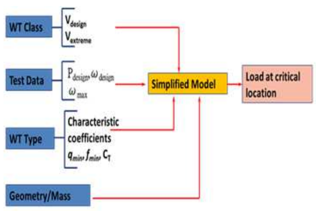

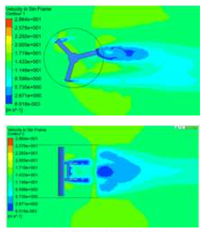

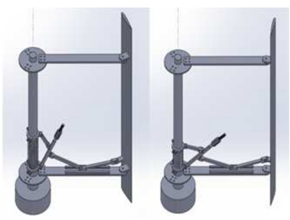

R/D of 5kW Vertical axis wind turbine-2/3

- Numerical simulations and DOE design

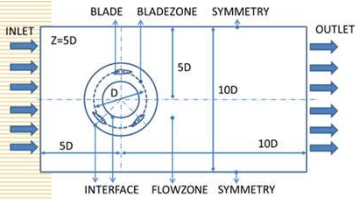

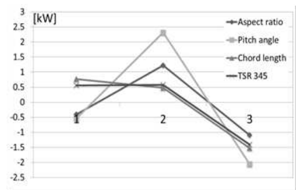

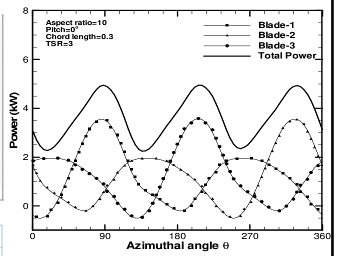

EXP	Aspect ratio	Pitch angle	Chord length	TSR
1	1	1	1	1
2	1	2	2	2
3	1	3	3	3
4	2	1	2	3
5	2	2	3	1
6	2	3	1	2
7	3	1	3	2
8	3	2	1	3
9	3	3	2	1

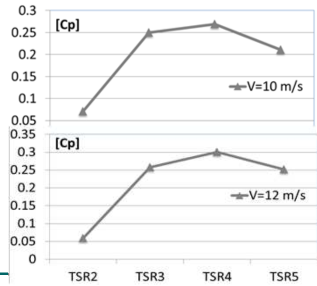

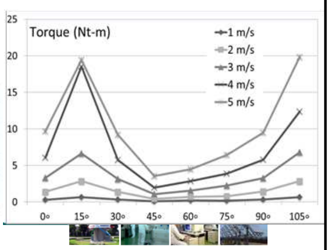

R/D of 5kW Vertical axis wind turbine-3/3

- Joint development -Passive pitch control of VAWT

Wind energy assessment-WAsP-1/2

- Micro-siting for forecasting wind energy and annual energy productionAEP

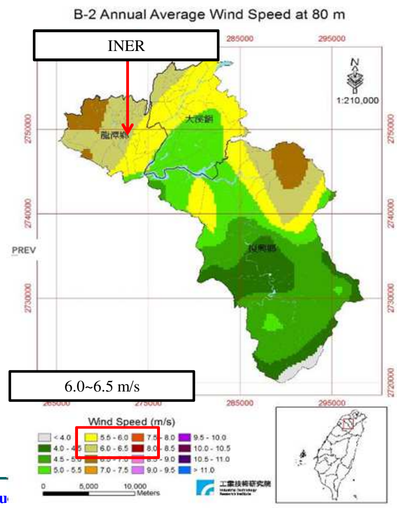

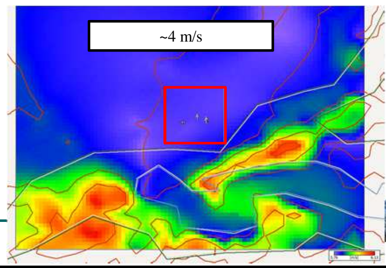

Wind energy assessment-WAsP-2/2

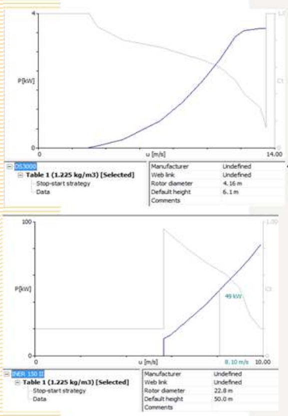

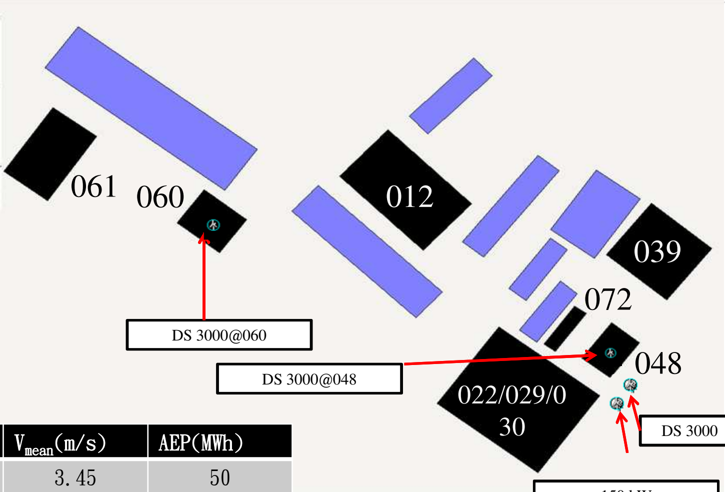

Turbine	Height (m)	V_{mean}(m/s)	AEP(MWh)
150 kW	50	3.45	50
DS3000	6.08	1.16	0.137
DS3000@048	16	1.85	0.324
DS3000@060	41	3.15	1.378

R/D of large scale wind turbine 1/2

- **Real-time CMS on 150kW wind turbine**

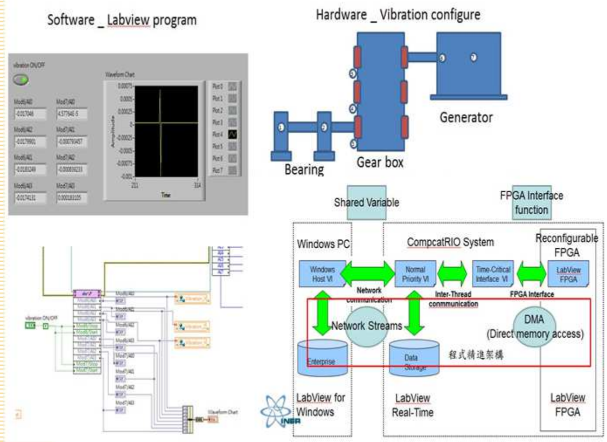

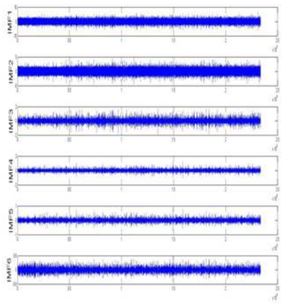

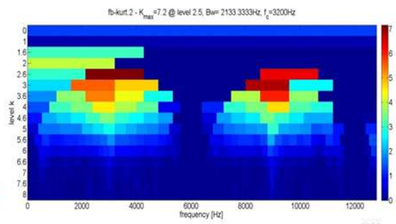

R/D of large scale wind turbine 1/2

- **Defect detection of blades**

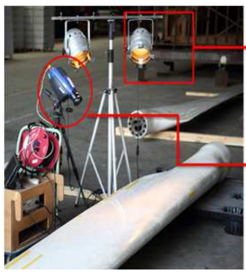

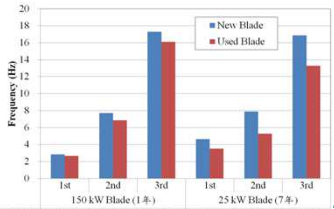

	1st	2nd	3rd	1st	2nd	3rd
New Blade	2.83	7.72	17.29	4.63	7.88	16.88
Used Blade	2.64	6.84	16.11	3.52	5.27	13.28

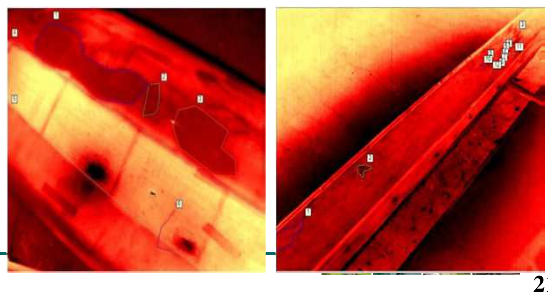

Design verification of wind turbine for Taiwan-1/2

- Equivalent Fatigue Load and Rainflow Cycle Counting

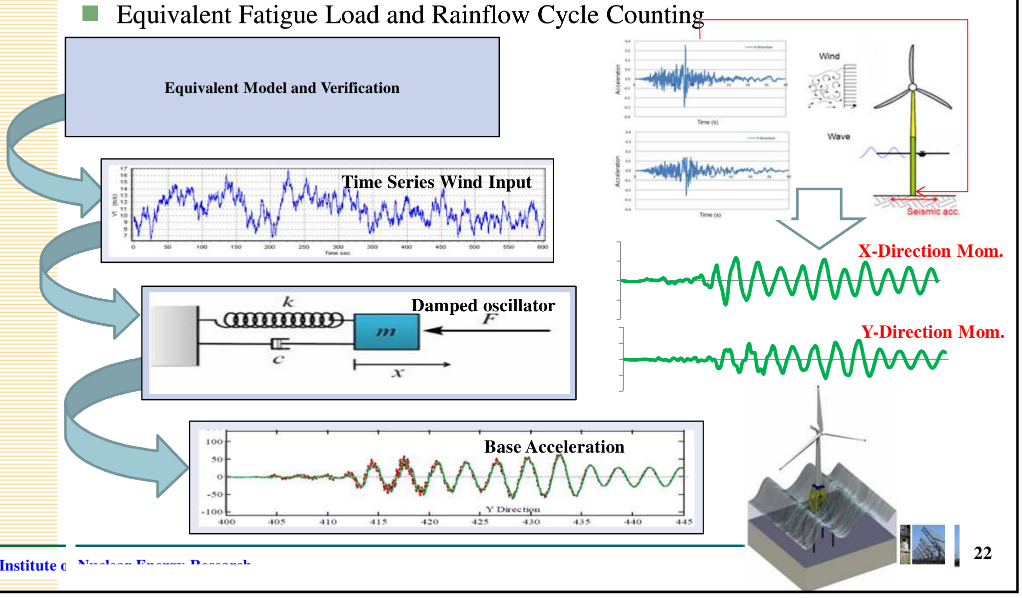

Design verification of wind turbine for Taiwan-2/2

- Design load cases of NREL 5 MW reference wind turbine


REpower 5M Wind Turbine

Gross Properties Chosen for the Baseline Turbine

Rating	5 MW
Rotor Orientation , Con figuration	Upwind , 3 Blades
Control	Variable Speed, Collective Pitch
Drivetrain	High Speed, Multiple Stage Gearbox
Rotor Diameter	126 m
Hub Height	90 m
Cut-In, Rated, Cut -Out Wind Speed	3 m/s, 11.4 m/s, 25 m/s
Cut-In, Rated Rotor Speed	6.9 rpm, 12.1 rpm
Rated Tip Speed	80 m/s
Overhang, Shaft Tilt, Precone	5 m, 5º, 2.5º
Rotor Mass	110,000 kg
Nacelle Mass	240,000 kg
Tower Mass	347,460 kg
Coordinate Location of Overall CM	(-0.2 m, 0.0 m, 64.0 m)

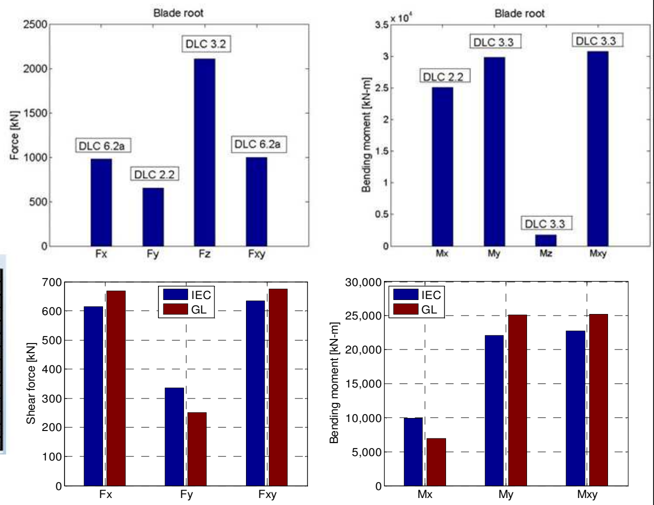

Technology Exchange

- 2016 IEA Wind Task 27 in Taiwan
- Visitor of Mr. Sasaki, ClassNK
- Workshop of small wind turbine
- Technical course by Prof. Ishihara, Uni. of Tokyo

iea wind

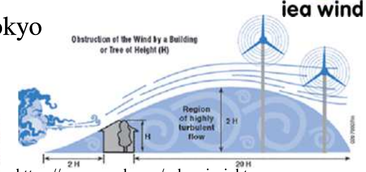

https://www.xsede.org/urban-insights

24

Thank you for being here

Institute of Nuclear Energy Research